



UNIVERSITY OF PISA

School of Graduate Studies
Fisiopatologia clinica e Scienza del Farmaco
Program in Scienze del Farmaco e delle Sostanze Bioattive
XXV ciclo

SSD BIO/15-05A1

PhD Thesis

2010-2012

**“Isolation and structural characterization of diterpenoidic compounds
and identification of their molecular targets”**

Laura Faiella

SUPERVISOR

Prof. Alessandra Braca

DIRECTOR OF THE SCHOOL

Prof. Adriano Martinelli

2013

*To those who are not afraid of distant commutes
and changes and to those who support them
with changeless and undying love*

Papers:

L. Faiella, A. Temraz, N. De Tommasi, A. Braca, Diterpenes, ionol-derived, and flavone glycosides from *Podocarpus elongatus*, *Phytochemistry*, **2012**, 76, 172-177.

L. Faiella, A. Temraz, T. Siciliano, N. De Tommasi, A., Terpenoids from the leaves of *Podocarpus gracilior*, *Phytochemistry Letters*, **2012**, 5, 297-300.

L. Faiella, F. Dal Piaz, A. Bisio, A. Tosco, N. De Tommasi, A chemical proteomics approach reveals Hsp27 as a target for proapoptotic clerodane diterpenes, *Molecular BioSystem*, **2012**, 8, 2637-2644.

Z. Rouis, N. Abid, M. Aouni, **L. Faiella**, F. Dal Piaz, N. De Tommasi, A. Braca, Benzophenone Glycosides from *Hypericum humifusum* ssp. Austral, *Journal of Natural Products*, **2013**, submitted.

Conference proceedings:

L. Faiella, A. Braca, L. Lepore, M. J. Gualtieri, N. De Tommasi, Further new steroidal glycosides from *Vernonia nigritiana* Oliv.&Hiern, XII Convegno-Scuola sulla Chimica dei Carboidrati, 2010, Certosa di Pontignano, Siena, PC-9.

F. Dal Piaz, **L. Faiella**, N. De Tommasi, Studio dell'attività biologica di sostanze naturali mediante tecniche spettroscopiche e spettrometriche, Primo Convegno Nazionale Sostanze naturali: dalla ricerca di base all'applicazione clinica, Istituto Superiore di Sanità, Rapporti ISTAN 11/19, 2011, 13-16, Roma.

A. Bader, N. De Tommasi, R. Cotugno, **L. Faiella**, N. Malafronte, A. Braca, Phenolic compounds from the roots of the Jordanian *Scorzonera judaica*, Congresso Società Italiana di Fitochimica, 2011, Roma, P21.

L. Faiella, A. Braca, A. Temraz, F. Dal Piaz, A. Tosco, N. De Tommasi, Isolation and structural characterization of diterpenes from *Podocarpus elongatus* (Aiton) L'Hér. Ex Pers. (Podocarpaceae) and identification of their molecular targets, Trends in natural products research: a Phytochemical Society of Europe young scientists' meeting, 2011, Kolymvari, Creta, Grecia, OP-24.

L. Faiella, A. Braca, A. Temraz, N. De Tommasi, Isolamento e caratterizzazione strutturale di diterpeni da *Podocarpus elongatus* (Aiton) L'Hèr. Ex Pers e *Podocarpus gracilior* Pilger (Podocarpaceae) e identificazione della loro attività biologica, Congresso interdisciplinare sulle piante medicinali, 2012, Cetraro (CS), CB7.

L. Faiella, A. Braca, , A. Temraz, N. De Tommasi, New diterpenes from *Clerodendrum Splendens* G.Don (Verbenaceae), International Congress on Natural Products Research (ICNPR 2012), the 8th Joint Meeting of AFERP, ASP, GA, PSE and SIF, 2012, New York City, USA, PI198.

Table of contents

<i>Introduction</i>	<i>1-17</i>
Chapter 1	1-17
1.1 Natural products for drug discovery.....	1
1.2 Natural compounds libraries.....	2
1.3 Diterpenes.....	5
1.3.1 Kauranes and ent-kauranes.....	6
1.3.2 Clerodanes and neo-clerodanes.....	7
1.3.3 Nagilactones.....	8
1.4 Interaction with biomolecules: potential biological activities.....	9
1.5 Target discovery strategies.....	10
1.5.1 Proteomics techniques.....	11
1.5.2 Chemical proteomics.....	11
1.5.3 Target's validation.....	14
1.6 Objectives of the project.....	15
<i>Phytochemical studies</i>	<i>18-43</i>
Chapter 2	18-43
2.1 Introduction: <i>Podocarpus</i> genus.....	18
2.2 <i>Podocarpus elongatus</i> (Aiton)L'Hèr. ex Pers.....	19
2.3 <i>Podocarpus gracilior</i> Pilger.....	20
2.4 Plant materials.....	21
2.5 Extraction and isolation.....	21
2.6 New isolated compounds.....	25
2.7 Structural elucidation.....	28
Chapter 3	44-59
3.1 Introduction: <i>Clerodendrum</i> genus.....	44
3.2 <i>Clerodendrum splendens</i> G. Don.....	45

3.3 Plant material.....	46
3.4 Extraction and isolation.....	46
3.5 New isolated compounds.....	48
3.6 Structural elucidation.....	51
Chapter 4.....	60-77
4.1 Introduction: <i>Sideritis</i> genus.....	60
4.2 <i>Sideritis pullulans</i> Vent.....	61
4.3 Plant material.....	62
4.4 Extraction and isolation.....	62
4.5 New isolated compounds.....	64
4.6 Structural elucidation.....	67
<i>An approach to discover a lead compound for drug discovery.....</i>	78-102
Chapter 5.....	78-81
5.1 Introduction.....	78
5.1.1 <i>ent</i> -Kaurane diterpenes: 15-ketoatractyligenin methyl ester.....	78
5.1.2 Starting point for a fishing for partners approach.....	81
5.2 Chemical immobilization of SR2017 on a solid support.....	81
5.3 Identification of the targets of SR2017 through a chemical proteomics method...83	
5.4 Data base search to characterize the targets.....	85
5.4 Targets validation and characterization of physical interactions.....	89
Chapter 6.....	92-102
6.1 A chemical proteomics approach to discover Hsp27 as a target for proapoptotic plerodane diterpenes.....	92
6.2 Limited proteolysis.....	95
6.3 Insuline and citrate synthase aggregation assays.....	98
6.4 Apoptosis evaluation by analysis of hypodiploid nuclei.....	99
6.5 Apoptosis evaluation by analysis of caspase 3 activity.....	100
6.6 Conclusion.....	102
<i>Experimental section.....</i>	103-109

Chapter 7.....	103-109
Chapter 8.....	110-115
Chapter 9.....	116-118
<i>Conclusions.....</i>	<i>119-123</i>
Chapter 10.....	119-123
<i>Bibliography.....</i>	<i>124-137</i>
<i>List of abbreviation.....</i>	<i>138</i>
<i>Index of figures.....</i>	<i>142</i>
<i>Index of tables.....</i>	<i>145</i>

Chapter 1

Introduction

Chapter 1

1.1 Natural products for drug discovery

Plants are the source of an almost uncountable numbers of natural compounds characterized by different chemical structures and a broad range of biological activities. Their structures are often only partially known and sometimes their synthetic pathways, mechanism of degradation and the functions in the original organism are unknown. Plant biodiversity with its richness and complexity represents the major resource of chemical diversity (Gullo *et al.*, 2006).

Human activity is often destructive so that the biodiversity of the ecosystems have been substantially stressed and threatened with the permanent loss of species, varieties, and groups (Clark, 1996; Shu, 1998).

Nowadays, the research in the field of biology, chemistry, and medicine, is directed towards the identification and structural characterization of plant secondary metabolites with pharmacological activity to discover their detailed biosynthesis pathways and as molecular targets for the industrial production or the synthesis of new drugs. Secondary metabolites are compounds nor directly involved in the primary metabolism of the plant, such as growing and reproduction, nor simple catabolic products. Experimental evidence supports their important role in the species evolution. The long-lasting experience of traditional folk medicines may facilitate the identification of novel agents from bioactive plant constituents: most of them are products of secondary metabolic pathways whose biological function is often the self-defense, for instance the protection against herbivores and various pathogens or the growth regulation. Due to these physiologic functions, secondary metabolites could have an

application in certain therapeutic areas. Database of natural products have a great number of unused scaffolds and the differences between synthetic compounds and natural products are remarkable, especially in their structural properties (Gullo *et al.*, 2006; Dobson, 2004; Rosén *et al.*, 2009). However, natural product research needs long and deep experience, particularly in taxonomy, which cannot be built up in one day (Okuda, 2002).

1.2 Natural compounds libraries

Natural compounds are a good starting point for the setting up of libraries to test for drug discovery, not only for their complex and diversified chemical space but also for their ability to interact with biomolecules. It has long been recognized that natural-product structures have the characteristics of high chemical diversity, biochemical specificity and other molecular properties. They are also rich in chiral centers, steric complexity, aromatic system, and functional groups. All these properties make them favorable as lead structures for drug discovery (Koehn and Carter, 2005).

On average, natural products incorporate fewer nitrogen, halogen, or sulfur atoms, but more oxygen atoms and are sterically more complex, with more bridgehead tetrahedral carbon atoms, and rings. The high “sterical complexity” is due to the fact that the enzymes used for biosynthesis, as well as their molecular targets, are inherently three-dimensional and chiral. Furthermore, nature has a limited palette of building blocks at its disposal, and thus has to generate novelty by branching out common intermediates into different scaffolds (Williams, 2007).

The screening of natural compounds libraries is a step to select potential lead compounds but it is true that some inconveniences using this strategy could occur. To create and to conserve a natural extract collection is very expensive and also it needs so much time. The choice of the plant materials is first step

when it is clear the kind of compounds to isolate: the plants are selected on the basis of chemotaxonomic and phylogenetic features, ethnobotanic and other literature information. Another possibility to find bioactive extracts is to make a biological screening (Figure 1.1).

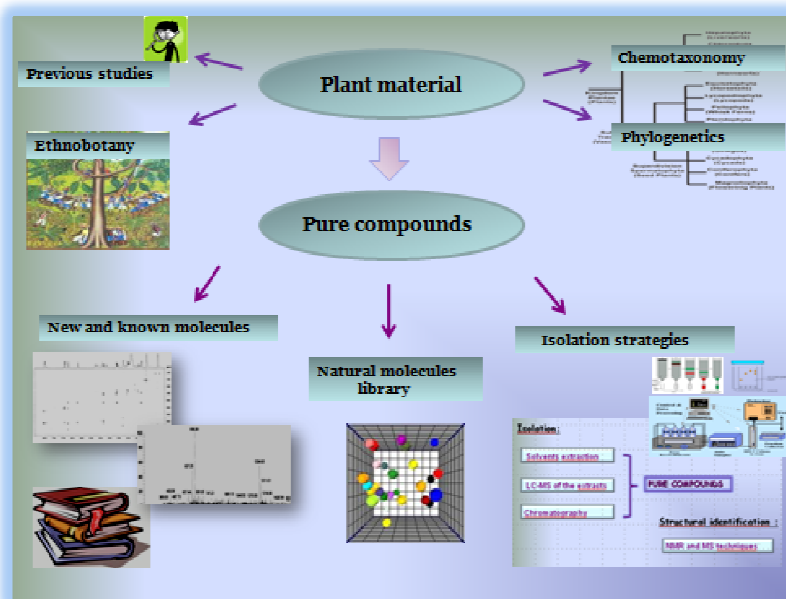


Figure 1.1: Screening of natural compounds

In both cases, when the starting point is a complex extract, it is necessary the fractionation and the identification of the bioactive component through biological assays. Later on the compound needs to be characterized.

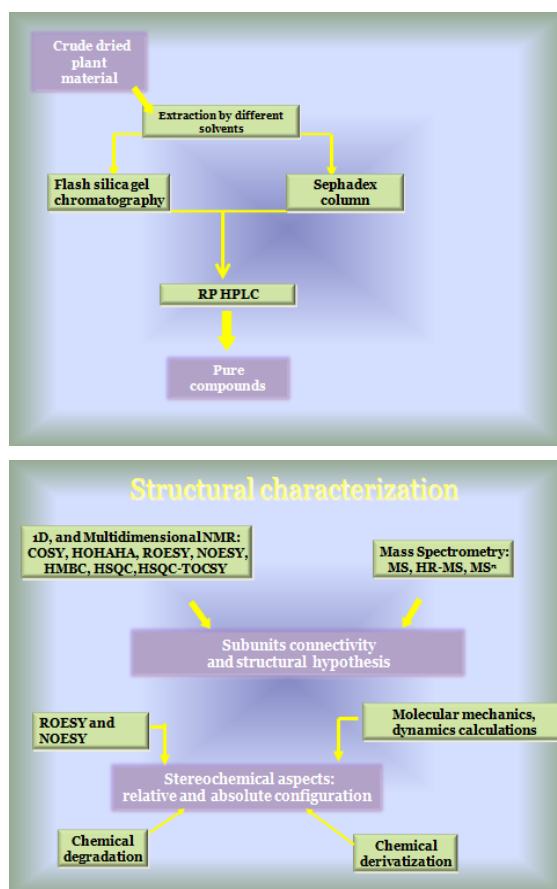


Figure 1.2: *Compounds isolation from plants and structural characterization scheme*

Anyway, natural products are often structurally complex whereby the pharmacophoric group identification and the structure-activity relationships are not very simple (Ortholand and Ganesen, 2004). The compounds isolation process from natural source is usually very complex and it needs many extraction and chromatographic processes to provide pure compounds, usually in small amount, that should be characterized by nuclear magnetic resonance (NMR) and mass spectrometry (MS) techniques. In **Figure 1.2** a method of compounds isolation from plant material and structural characterization is described.

1.3 Diterpenes

The terpenoids constitute the largest family of natural products and they play diverse functional roles in plants as hormones (gibberellins, abscisic acid), photosynthetic pigments (phytol, carotenoids), electron carriers (ubiquinone, plastoquinone), mediators of polysaccharide assembly (polyprenyl phosphates), and structural components of membranes (phytosterols).

In addition to these universal physiological, metabolic, and structural functions, many specific terpenoid compounds (commonly in the C₁₀, C₁₅, and C₂₀ families) serve in communication and defense, for example, as attractants for pollinators and seed dispersers, competitive phytochemicals, antibiotics, and herbivore repellents and toxins. In spite of the economic significance of the terpenoids and their many essential functions, relatively little is known about terpenoid metabolism and its regulation in plants.

Because all terpenoids are produced by a common biosynthetic pathway, sophisticated control mechanisms must exist to ensure the production of appropriate levels of these often structurally complex compounds in the proper metabolic, developmental, and environmental context. Pathway elucidation for highly functionalized terpenoid metabolites is not trivial, and determining the enzymology of terpenoid metabolism has proven very challenging, both because relatively little enzymatic machinery is dedicated to terpenoid metabolism and because many of the reaction types involved are unlike those of primary metabolism of carbohydrates, proteins, and lipids. The action of various prenyltransferases then generates from the precursor isopentenyl pyrophosphate (IPP) the higher order terpenoid building blocks, geranyl pyrophosphate (GPP; C₁₀), farnesyl pyrophosphate (FPP; C₁₅), and geranylgeranyl pyrophosphate (GGPP; C₂₀). These branch point intermediates may then self-condense be utilized in alkylation reactions to provide prenyl side chains of a range of nonterpenoids (including proteins), or undergo internal addition (that is,

cyclization) to create the basic parent skeletons of the various terpenoid families. Finally, oxidation, reduction, isomerization, conjugation, or other secondary transformations elaborate the unique and manifold character of the terpenoids.

Diterpenes are biosynthesized especially in plastids and an increasing number of diterpenoids are being found with skeletons that may arise by fragmentation of better known bi- and tri-cyclic systems (McGarvey and Croteau, 1995).

Diterpenoids continue to be associated with the biological activity of various plant and marine extracts. The liverworts have continued to provide a wide range of diterpenoid skeletal type. Among the uncountable shown activities there are antitumor, antimicrobial, anti-inflammatory, antioxidant, larvicidal, plant and insect growth regulation activities (Hanson, 2005).

In the following paragraphs some diterpene's classes are described.

1.3.1 Kauranes and *ent*-kauranes

Kauranes represent an important group of tetracyclic diterpenes and their structures are constituted by a perhydrophenanthrene unit (A, B and C rings) fused with a cyclopentane unit (D ring) formed by a bridge of two carbons between C-8 and C-13. Different criteria are used for the nomenclature of the kaurane diterpenes, the most frequent being the inversion of the conventional description of stereochemistry when the name is preceded by the prefix "*ent*-" (Garcia *et al.*, 2007); (**Figure 1.3**).

Kauranes and *ent*-kauranes are naturally occurring diterpenoids isolated from several families, such as Asteraceae and Lamiaceae. These compounds have attracted interest because of their structures and their biological activities as anti-tumorals, anti-HIV, and antibacterials (Bruno *et al.*, 2001).

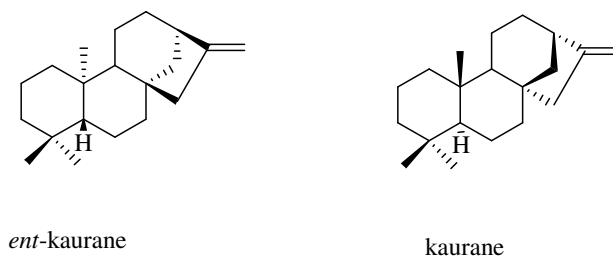


Figure 1.3: *Kauranes and ent-kauranes skeleton*

1.3.2 Clerodanes and neo-clerodanes

The clerodane diterpenoids comprise a large class of natural products which have been studied more in recent years for their wide biological activities, for instance anti-tumor and apoptotic activity against different cell lines (Coll and Tandron, 2007).

The clerodane diterpenoids belong to the group of diterpenoids with a rearranged labdane skeleton (*ent*-labdane). Sometimes substances of this type are called diterpenoids of the cascarillin group, *ent*-clerodanes, *neo*-clerodanes, and clerodanes. The name clerodanes is derived from the bitter principle isolated from *Clerodendrum infortunatum* L., clerodin I, whose structure was established in 1961. The clerodane diterpenoids belong to the bicyclic terpenoids derived from decalin. The carbon skeleton of the clerodane and *neo*-clerodane (*ent*-clerodane) diterpenoids differs from the labdane skeleton by the position of the methyl groups (Nurmukhamedova and Sidyakin); (**Figure 1.4**).

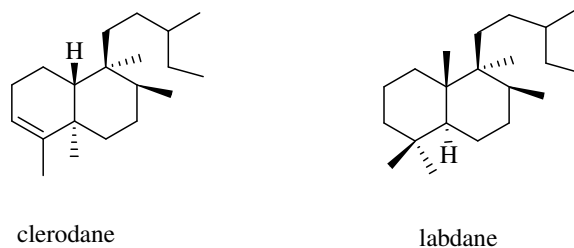


Figure 1.4: *Clerodane and labdane diterpenes skeleton*

1.3.3 Nagilactones

Nagilactones are a kind of nor and bisnorditerpene dilactones known as allelochemical and cytotoxic compounds, sometimes with antibacterial, antifungal, antifeedant activity (Hayashi *et al.*, 1972; Hayashi *et al.*, 1992; Kubo *et al.*, 1993; Kuo *et al.*, 2008); the nagilactone C is the most studied compound (**Figure 1.5**). The dilactones are classified into three major subgroups in accordance with the structure of the B/C ring part: i) α -pyrone [8(14),9(11)-dienolide] type; ii) $7\alpha,8\alpha$ -epoxy-9(11)-enolide type; iii) 7(8),9(11)-dienolide type. It should be noted that the dilactone members in each of these structural types show fine differences in their biological activity (Hayashi and Matsumoto, 1982).

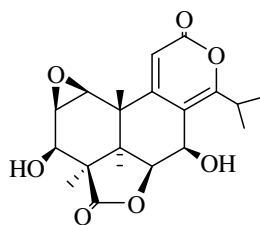


Figure 1.5: *Nagilactone C structure*

1.4 Interaction with biomolecules: potential biological activities

Over the past years there has been a rapid escalation in the discovery of molecular targets that may be applied to the discovery of novel tools for the diagnosis, prevention, and treatment of human diseases. With the sequencing of the human genome, there has been an explosion in the knowledge of the protein products associated with the constituent genes and the discovery of molecular targets associated with various disease types, such as cancer, diabetes, and obesity. Natural products research plays a highly significant role in the drug discovery and development process, through the analysis of the molecular mechanism responsible of biological activity (Chin *et al.*, 2006).

Even though natural products may not have coevolved with human proteins, they have emerged in nature to interact with biomolecules and it should be considered that varied genomes, based on similar chemistry, have spread across the Earth and human genus shares its gene families with other organisms. The production of metabolites with a certain affinity of interaction with a large variety of proteins and biological targets is improved with the evolution. Mainly the great homology between structural and functional domains of proteins from animal, vegetable or marine world allows the interaction among each other with a comparable affinity (Caporale, 2002; Koehn and Carter, 2005; Zhang, 2007).

Natural products should be able to penetrate biological barriers and make their way to certain cells or organs in which they will exert the effect. Thus, natural products are already biologically validated to reach and to bind specific proteins. Looking at all proteins and analyzing them for structural features, elements of conservatism and diversity may be found. The conservative elements are the domains: the parts that fold to compact secondary structures. Among the hundreds of thousands of human proteins, the number of distinct domains is only about 600 to 8000. Consequently, proteins that may seem altogether different are quite similar when viewed structurally, but diversity lies in the precise details

since similar domains may have very different amino acid sequences (Kirkpatrick, 2003).

1.5 Target discovery strategies

Especially for complex diseases, a lot of compounds are involved in the modulation of several targets and the exact targets of some drugs often remain unknown. The simplified “one molecule, one target” concept seems to be by now out-of date (Rix and Superti-Furga, 2009). Even if the multi-target interaction could also lead to harmful side effects, reducing the potency and efficiency of the drugs there is a possible application in multifactorial diseases (Bantscheff *et al.*, 2009).

The identification of a drug interactome followed by biological assays for the measure of its activity against the identified target proteins, is actually one of the key processes in the drug development study. Several approaches carried out in the absence of the biological context have been developed to reach this goal even if gaining only a partial coverage of the full interactome. Recent developments in analytical methods, mainly in mass spectrometry and liquid chromatography, have had an important impact in the field of target discovery. In particular, mass spectrometry-based chemical proteomics has been emerging as a powerful tool to a comprehensive characterization of a drug interactome under physiological relevant conditions. Moreover, such method enables the analysis of the drug mechanism of action, in the context of a complex proteome accelerating the difficult process of target validation and drug discovery (Jeffery and Bogyo, 2003).

1.5.1 Proteomics techniques

Proteomics, as a scientific field, is defined as the study of the protein products of the genome, and their interactions and functions. Similarly, the proteins expressed at a given time in a given environment constitute a proteome. The techniques being developed in proteomics are applicable to all areas of drug discovery, from target identification, to assessment of drug efficacy, both in pre-clinical (target selectivity) and clinical situations (patient response), to protein profiles for diagnostics.

For drug discovery, the ideal proteomics method would be one that is:

1. Sensitive enough to detect low-abundance proteins.
2. Able to detect activity over in addition to abundance.
3. Able to detect protein–protein and protein–small molecule interactions.
4. Easily implemented and performed quickly (Burbaum and Tobal, 2002).

Several proteomic techniques are based on two-dimensional gel-electrophoresis, isotope-coded affinity-tagging, “drug on-beads” immobilization, affinity chromatography.

1.5.2 Chemical proteomics

A new research field is chemical proteomics, or activity-based proteomics, that is considered a combination of affinity purification and mass spectrometric identification of a set of proteins targeted (or captured) by a small molecule. It is a multidisciplinary technique, involving different research areas such as biochemistry, cell biology, organic synthesis and mass spectrometry. This technique allows the analysis of all potential targets of a molecule in a single

experiment, leading to a complete and selective target mapping of a drug candidate. This means that the drug is able to fish out its own targets directly from the biological sample of interest.

Chemical proteomics approaches include several different experimental procedures, however three of them have emerged as most popular: (i) fishing for partners (or pull down), which employs a ligand immobilized onto a solid support, (ii) global proteomics, in which isobaric tags are used to assess changing in protein concentration upon drug treatment, and (iii) ABPP, activity-based protein profiling, which uses active site-directed probes to record variations in the activity of enzymes in a whole proteome (Sadaghiani *et al.*, 2007; Rix *et al.*, 2007).

The pull down assay is based on the non covalent and specific interactions occurring between the small molecule and its potential binders, and the following purification and mass spectrometric identification of these interacting proteins (Jeffery and Bogoy, 2003); (**Figure 1.6**).

One of the methods includes the compound of interest (with known or unknown biological activity) anchoring to a solid support through a spacer arm. This matrix is then treated with a lysate, from cells or tissue, to promote the interaction between the anchored compound and its specific binding proteins. After several washing steps, useful to reduce the amount of non-specific binding proteins, the captured proteins are eluted and subjected to either Sodium Dodecyl Sulphate Polyacrylamide gel electrophoresis (SDS PAGE), or gel free chromatography. The peptide mixtures obtained after trypsin digestion are then submitted to MS analysis and database search for the final protein identification.

The first step of the procedure is the drug on-beads immobilization: molecules containing one or more reactive sites or after synthetic modifications can be attached to a such solid support. To avoid or reduce steric interferences between the targets and the ligand-bearing matrix, the solid support is usually modified with an opportune spacer arm that provides a suitable distance between the beads

and the small molecule. The choice of the solid support is one of the most important steps of the experiment. The small molecule anchored to the solid support is then added to an opportune protein extract from a cell culture, tissue or serum, to promote ligand protein interaction. After the treatment, the matrix is washed to reduce the amount of the non-specific binding proteins and finally the elution of the retained ones is carried on. The eluted proteins are sequentially separated by gel electrophoresis, *in situ* or in solution digested with trypsin, and finally analyzed and identified by HPLC-MS/MS and data base search.

There are proteins exclusively interacted with the linker or the beads, proteins highly abundant with low affinity for the drug-support system, and proteins with high affinity for matrix with the drug.

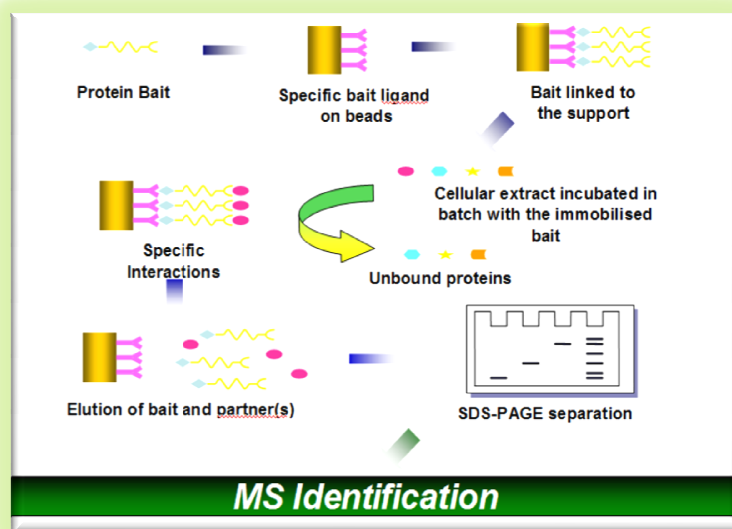


Figure 1.6: *Fishing for partners strategy*

Another key step is the protein identification: one of the procedure involves the previous enzymatic digestion of the proteins and the tandem mass spectrometric analysis of the complex peptide mixtures (Chait, 2006). The usual proteolytic enzyme used in proteomics is trypsin, a protease that cleaves peptides at C-terminus of arginine and lysine residues. The peptides originated by proteolytic cleavage have a size less than 3 kDa and a free amino group at C-terminus, and give rise to doubly and triply charged peptides, when exposed to a mass spectrometer.

The peptide mixture is subjected to liquid chromatography coupled tandem MS analysis, and the raw data are processed to give a peak list submitted to a protein search in a data base, for instance Mascot that is a web program comparing the experimental MS² spectra with theoretical fragment spectra generated “*in silico*” and needing of parameters such as peptide tolerance, proteolytic enzyme, miss cleavage and variable modifications (Perkins *et al.*, 1999).

1.5.3 Target validation

The results obtained by this technique are only indicative and useful to have an idea of the possible target of a compound but it is necessary to determine the biological relevance and the kind of the interaction.

In the first case biological assays aimed to identity enzymatic inhibition, activity ability, *in vivo* and *in vitro* effects, etc. according to the kind of the identified proteins, are necessary.

The physical interaction could be determined by measuring the quantitative binding parameters with different techniques like surface plasmon resonance (SPR), isothermic titration calorimetry (ITC), STD-NMR, and cocrystallization experiments.

1.6 Objectives of the thesis project

As part of an ongoing research program on plants biosynthesizing diterpenes, it was performed a project aimed to create a diterpenes library from different plant's species. These compounds were subjected to a chemical proteomic study as a strategy for the molecular target identification of natural bioactive compounds, setting up a method for the research of their molecular targets.

The attention was paid on plants known to be rich on diterpenes, since they are a class of natural terpenoids with a great structural variability and a wide spectrum of biological activities.

Particularly two diterpenes included in our library were considered: a semi synthetic compound 15-ketoatractyligenin methyl ester, and the hardwickiic acid.

From an experimental point of view, this work was divided into the following steps: (i) isolation and structural characterization of new and known diterpenes through a phytochemical study in order to enrich a pre-existing diterpenes library with new structures (ii) chemical proteomic approach as a strategy for the research of the molecular target of the *ent*-kaurane 15-ketoatractyligenin methyl ester (iii) validation techniques of the protein Hsp27 as a target for the clerodane diterpene hardwickiic acid.

According to the primary purpose, *Podocarpus elongatus* (Aiton) L'Hèr. ex Pers, *Podocarpus gracilior* Pilger (Podocarpaceae), *Clerodendrum splendens* G. Don. (Verbenaceae), and *Sideritis pullulans* Vent. (Lamiaceae) were selected.

In **chapters 2-4** the extraction and isolation methods and the structural characterization procedures of new and known compounds from the previously listed plants are described.

In **chapter 2** the diterpenes isolated from *P. elongatus* leaves are reported: the new diterpenes nagilactone C 7-*O*- α -L-arabinopyranosyl-(1 \rightarrow 4)- β -D-xylopyranoside, nagilactone C 7-*O*- β -D-glucopyranosyl-(1 \rightarrow 4)- β -D-xylopyranoside, nagilactone C 7-*O*- β -D-xylopyranoside, nagilactone A 7-*O*- α -L-

arabinopyranosyl-(1→4)- β -D-xylopyranoside, 2 β ,15*S*,16,17,19-pentahydroxy-isopimar-8(14)-ene 17-*O*- β -D-glucopyranoside, 2 β ,15*R*,16,17,19-pentahydroxy-isopimar-8(14)-ene 17-*O*- β -D-glucopyranoside, and the known diterpenes 4-carboxy-19-*nor*-totarol, nagilactone B, and nagilactone C. In this chapter the new diterpenes found in *P. gracilior* leaves, 2 α ,16-dihydroxy-4 β -carboxy-*O*- β -D-glucopyranosyl-19-*nor*-totarol, nagilactone K together with the known nagilactone B, nagilactone C, nagilactone D, and podolactone B are also mentioned.

In **chapter 3** 2 α -acetoxy-3 β -(2',3'-diacetoxy-2'-methyl)-butanoyloxy-14-hydro-15-hydroxyclerodin, 3 β ,15-dihydroxy-14-hydro-clerodin, 2 α ,15-dihydroxy-3 β -(2'-hydroxy-3'-acetoxy-2'-methyl)-butanoyloxy-6 α ,18-diacetoxy-4 α ,17-epoxy-clerodan-11,16-lactone, 3 β ,14*S*,15-trihydroxy-6 α ,18-diacetoxy-4 α ,17-epoxy-clerodan-11,16-lactone, and the only known 14,15-dihydroxy-3-epicariotin isolated from *C. splendens* are described.

In **chapter 4** the new diterpenes isolated from *S. pullulans*, *ent*-1 α ,3 α ,7 β ,18-tetrahydroxykaur-16-ene, *ent*-3 α ,11 α ,18-trihydroxy-17-*norkauran*-16-ene, *ent*-3 α ,7 β ,18-trihydroxy-17-*norkauran*-16-one, *ent*-3 α ,7 β -dihydroxy-18-acetyloxy-17-*norkauran*-16-one, *ent*-3 α ,7 β ,16 α ,17-tetrahydroxy-18-acetyloxy-kaurane, *ent*-7 β ,16 α ,17,18-tetrahydroxykaurane, and the known foliol, linearol, *ent*-3 α ,7 β ,17-trihydroxy-18-acetyloxy-15 α ,16 α -epoxykaurane are described.

Chapters 5 and **6** are related to studies aimed to the research of the proteic target for small molecules through chemical proteomics techniques.

In **chapter 5** a fishing for partners study as a chemical proteomics strategy to identify the proteic target of 15-ketoatractyligenin methyl ester (SR2017) is described. SR2017 is semi-synthetic *ent*-kaurane synthesized at Dipartimento di Chimica Organica, Università di Palermo (Rosselli *et al.*, 2007).

This approach revealed the heat shock protein 70 (Hsp70) and peroxisomeproliferator-activated receptor gamma (PPAR γ) as potential targets. To confirm results a SPR based binding assay was used.

In **chapter 6** the study of hardwickiic acid (HAA) and its heat shock protein 27 (Hsp27) interaction is reported. HAA is a diterpene chosen as a representative of the clerodane diterpenes library isolated from *Salvia* spp. Hsp27 was identified as potential target of HAA through a fishing for partner studies based on a chemical proteomics approach and in a previous study this was confirmed by SPR experiments.

As first step to evaluate the effect of the interaction between HAA and Hsp27 on protein structure and activity, a limited proteolysis-mass spectrometry based strategy was used.

The ability of HAA to modulate the *in vitro* chaperone activity of Hsp27 was evaluated by monitoring substrates induced aggregation in the presence of Hsp27, with or without HAA. Finally to give a cellular significance to Hsp27/HAA interaction, it was explored the pro-apoptotic activity of the small molecule in human monocytes.

Chapter 2

*Phytochemical study of Podocarpus elongatus (Aiton) L'Her. ex Pers
and Podocarpus gracilior Pilger*

Based on:“Faiella L., *et al.*, *Phytochemistry*, **2012**, 76, 172-177“; “Faiella L., *et al.*,
Phytochemistry Letters, **2012**, 5, 297-300“.

Chapter 2

2.1 Introduction: *Podocarpus* genus

Podocarpaceae is an ancient and large family of mainly Southern Hemisphere conifers, comprising about 156 species of evergreen trees and shrubs. It is especially spread in tropical and subtropical forests of the Austral Hemisphere: New Zealand, New Caledon, and Tasmania are particularly rich of genera. The Podocarpaceae family shows great diversity, both morphologically and ecologically (Eckenwalder, 2009).

Podocarpus species are important timber trees in their native areas. The timber is fine-grained, nonresinous, light, and moderately strong. Some species are used as ornamental trees, mostly for landscaping. The fruits of other species are eaten raw or cooked or used locally for jams and preserves. Other products obtained from this genus include dyes, tannins, and waxes. Some species of *Podocarpus* are used for cultural purposes in South Africa (Abdillahi *et al.*, 2010). *Podocarpus* spp. are also traditionally used in the native regions for the treatment of many diseases like fevers, asthma, coughs, cholera, arthritis, rheumatisms, and venereal diseases (Abdillahi *et al.*, 2011). The presence or absence of different compounds can be used to relate the new and the old taxa. For example, flavonoids can be a useful chemotaxonomic tool in this group of plants, since biflavonoids of the amentoflavone and hinokiflavone groups have been shown to be good taxonomic markers in the great majority of *Podocarpus* (Abdillahi *et al.*, 2010).

Phytochemical and pharmacological studies of *Podocarpus* genus led to the isolation of a number of bioactive diterpenes, including nor- and bisnor-

diterpenoid lactones (Park *et al.*, 2004; Xuan *et al.*, 1995), flavonoids (Markham *et al.*, 1985), and ecdysones (Nakanishi *et al.*, 1966). Since nor- and bis-norditerpenes are taxonomic markers of these species, the possibilities that the related taxa will have similar biological activities or bioactive compounds cannot be overruled. The nagilactone C is the most studied. It had shown an antiproliferative activity against different type of cell lines such as fibrosarcoma and murine colon carcinoma. A study on Hela cells shows that it inhibits the eukaryotic proteic synthesis, but its molecular target is unknown (Chan *et al.*, 2004; Shrestha *et al.*, 2001).

Podocarpus elongatus (Aiton) L'Her. Ex Pers. and *Podocarpus gracilior* Pilger were selected for this study mainly because of the relevant presence of diterpenes in plants belonging to this genus.

2.2 *Podocarpus elongatus* (Aiton) L'Her. ex Pers

Podocarpus elongatus (Aiton) L'Her. ex Pers (**Figure 2.1**) is a tree native to South Africa and West Cape, also known as Cape yellowwood, yellow pine, fern pine, breade river yellowwood or westelike geelhout. It is mainly used as ornamental tree mostly for landscaping. The light-brown, soft durable, moderately strong, elastic, resinous, pale yellow brown wood is used for building houses, railway sleepers, beams, planks, rafters, and furnitures (Abdillahi *et al.*, 2010).

There are only few and old previous phytochemical studies of *P. elongatus* that report the isolation of biflavones, namely amentoflavone, podocarpusflavone A, bilobetin, isoginkgetin (Prasad and Krishnamurty, 1976), hinokiflavone, and tetra-*O*-methyl-amentoflavone (Iqbal *et al.*, 1982) and abietane diterpenes, such as totarol, 16-oxytotarol, and 16-hydroxytotarol (Taylor, 1965).



Figure 2.1: *Podocarpus elongates* (Aiton) L'Her ex Pers

2.3 *Podocarpus gracilior* Pilger

Podocarpus gracilior Pilger (**Figure 2.2**) is a conifer that grows in Central and East Africa, known as African fern pine and characterized by a resistance to insect attack (Kubo *et al.*, 1984). Previous phytochemical studies on *P. gracilior* reported the isolation of diterpenes such as podolactones (Hayashi *et al.*, 1980), nagilactones C, D, and F (Kubo *et al.*, 1984), podolide (Bryan and Smith, 1975; Kupchan *et al.*, 1975), phenolic diterpenoids (Cambie *et al.*, 1983), the ecdysone ponasterone A (Kubo *et al.*, 1984) and biflavonoids such as podocarpusflavone A and dimethylamentoflavone (Kubo *et al.*, 1983; 1984).



Figure 2.2: *Podocarpus gracilior* Pilger

2.4 Plant materials

Leaves of *P. elongatus* were collected in El Zoharia Research Garden of Cairo, Egypt, on May 2008, while leaves of *P. gracilior* were collected in the same place on March 2010, both were identified by Dr. Mamdouh Shokry (El Zoharia Research Garden, Cairo, Egypt). The voucher specimens (No. 15, *P. elongatus* Ait./1 and No. 15, *P. gracilior* Pilger/1) were deposited at the Herbarium Hortii Botanici Pisani, Flora Aegyptiaca, Pisa, Italy.

2.5 Extraction and isolation

Dried powdered leaves of *P. elongatus* (800 g) and of *P. gracilior* (950 g) were successively and separately extracted for 48 h with *n*-hexane, CHCl₃,

CHCl₃-MeOH (9:1), and MeOH, by exhaustive maceration (2 l), to give 14.9, 19.7, 27.2, and 35.2 g of the respective residues for *P. elongatus* and 11.5, 17.3, 32.6, and 42.4 g of the respective residues for *P. gracilior*.

The MeOH extract of *P. elongatus* was partitioned between *n*-BuOH and H₂O, to afford a *n*-BuOH residue (15 g). Part of the *n*-BuOH fraction (6.0 g) was submitted to Sephadex LH-20 using MeOH as eluent to obtain seven major fractions (A-G) grouped by TLC. Fraction B (120 mg) was purified by RP-HPLC with MeOH-H₂O (25:75) as eluent to give pure nagilactone C 7-*O*-β-D-glucopyranosyl-(1→4)-β-D-xylopyranoside (compound **2**, 1.6 mg, *t*_R = 13 min), nagilactone C 7-*O*-α-L-arabinopyranosyl-(1→4)-β-D-xylopyranoside (compound **1**, 10.3 mg, *t*_R = 15 min), 3,4,5-trihydroxydehydro-α-ionol 9-*O*-β-D-glucopyranoside (compound **12**, 2.3 mg, *t*_R = 18 min), roseoside (compound **13**, 5.6 mg, *t*_R = 20 min), and 1-(2,6,6-trimethyl-4-hydroxycyclohexenyl)-1-hydroxybuta-1-en-3-one 4-*O*-β-D-glucopyranoside (compound **7**, 1.5 mg, *t*_R = 24 min). Fraction C (244 mg) was subjected to RP-HPLC with MeOH-H₂O (3.5:6.5) as eluent to give nagilactone A 7-*O*-α-L-arabinopyranosyl-(1→4)-β-D-xylopyranoside (compound **4**, 1.5 mg, *t*_R = 13 min), linarionoside C (compound **14**, 1.8 mg, *t*_R = 23 min), 2β,15*S*,16,17,19-pentahydroxy-*isopimar*-8(14)-ene 17-*O*-β-D-glucopyranoside (compound **5**, 2.0 mg, *t*_R = 24 min), 2β,15*R*,16,17,19-pentahydroxy-*isopimar*-8(14)-ene 17-*O*-β-D-glucopyranoside (compound **6**, 2.3 mg, *t*_R = 25 min), and 20-hydroxyecdysone (compound **15**, 8.6 mg, *t*_R = 45 min). Fraction D (300 mg) was purified over RP-HPLC with MeOH-H₂O (3:7) as eluent to yield pure *erythro*-4,7,9,9'-tetrahydroxy-3,3'-dimethoxy-8-*O*-4'-oxyneolignan 9'-*O*-β-D-glucopyranoside (compound **16**, 5.2 mg, *t*_R = 14 min), *threo*-4,7,9,9'-tetrahydroxy-3,3'-dimethoxy-8-*O*-4'-oxyneolignan 9'-*O*-β-D-glucopyranoside (compound **17**, 6.4 mg, *t*_R = 15 min), compound **13** (3.4 mg, *t*_R = 18 min), and icariside E₃ (compound **18**, 3.6 mg, *t*_R = 25 min). The CHCl₃-MeOH extract (6.0 g) was chromatographed over Sephadex LH-20 to give eight major

fractions (A-H) grouped by TLC, together with pure isoginkgetin (compound **19**, 120 mg) and bilobetin (compound **20**, 25 mg). Fractions B (123 mg) and G (163 mg) were separately purified by RP-HPLC with MeOH-H₂O (3.5:6.5) as eluent to yield blumenol C glucoside (compound **21**, 2.7 mg, $t_R = 11$ min) and compound **13** (3.1 mg, $t_R = 13$ min), from fraction B and vitexin 2''-O- β -D-(6'''-acetyl)-glucopyranoside (compound **8**, 14.4 mg, $t_R = 41$ min) from fraction G, respectively. Fraction D (60 mg) was also purified by RP-HPLC with MeOH-H₂O (3:7) as eluent to yield nagilactone C 7-O- β -D-xylopyranoside (compound **3**, 3.7 mg, $t_R = 13$ min) and compound **13** (2.0 mg, $t_R = 18$ min). Finally, fractions C (390 mg), E (185 mg), and F (220 mg) were separately subjected to RP-HPLC with MeOH-H₂O (2:3) as eluent to give compounds **18** (2.3 mg, $t_R = 20$ min) and **15** (2.8 mg, $t_R = 45$ min) from fraction C, nagilactone C (compound **22**, 2.5 mg, $t_R = 8$ min), compounds **16** (3.5 mg, $t_R = 9$ min) and **17** (2.7 mg, $t_R = 10$ min) from fraction E, and nagilactone B (compound **23**, 3.0 mg, $t_R = 9$ min) and glochidiobioside (compound **24**, 2.0 mg, $t_R = 15$ min) from fraction F, respectively.

Part of the CHCl₃ extract (10.0 g) was chromatographed over silica gel column eluting with CHCl₃ followed by increasing concentrations of MeOH in CHCl₃ (between 1% and 50%). Fractions of 25 ml were collected, analyzed by TLC (silica gel plates, in CHCl₃ or mixtures of CHCl₃-MeOH 99:1, 98:2, 97:3, 9:1, 4:1), and grouped into 10 fractions (A-L). Fraction G (290 mg) was purified by RP-HPLC with MeOH-H₂O (8.5:2.5) as eluent to obtain 4 β -carboxy-19-*nor*-totarol (compound **25**, 3.1 mg, $t_R = 10$ min).

The MeOH extract of *P. gracilior* was partitioned between *n*-BuOH and H₂O, to afford a *n*-BuOH residue (5 g) that was submitted to a Sephadex LH-20 using MeOH as eluent to obtain eight major fractions (A-H) grouped by TLC. Fraction B (372 mg) was purified by RP-HPLC with MeOH-H₂O (2.5:7.5) as eluent to give 15-hydroxy phaseic acid (compound **11**, 1.7 mg, $t_R = 10$ min), compound **22** (4.0 mg, $t_R = 19$ min), 2 α ,16-dihydroxy-4 β -carboxy-*O*- β -D-glucopyranosyl-19-

nor-totarol (compound **9**, 1.6 mg, $t_R = 38$ min), and **24** (1.2 mg, $t_R = 40$ min). Part of the CHCl_3 -MeOH extract (10.0 g) was chromatographed over Sephadex LH-20 to give ten major fractions (A-K) grouped by TLC. Fractions C (275 mg) and E (350 mg) were separately purified by RP-HPLC with MeOH- H_2O (3.5:6.5) as eluent to yield compounds **21** (1.2 mg, $t_R = 36$ min) and **15** (5.4 mg, $t_R = 38$ min) from fraction C and compounds **22** (8.4 mg, $t_R = 11$ min), nagilactone D (compound **26**, 1.8 mg, $t_R = 17$ min), **17** (3.5 mg, $t_R = 21$ min), and **18** (2.7 mg, $t_R = 24$ min) from fraction E, respectively. Fraction F (208 mg) was also purified by RP-HPLC with MeOH- H_2O (25:65) as eluent to yield pure podolactone B (compound **27**, 1.2 mg, $t_R = 15$ min), compounds **22** (4.3 mg, $t_R = 19$ min), nagilactone K (compound **10**, 1.7 mg, $t_R = 25$ min), and **26** (4.0 mg, $t_R = 42$ min).

Part of the CHCl_3 extract (10.0 g) was chromatographed over silica gel column eluting with CHCl_3 followed by increasing concentrations of MeOH in CHCl_3 (between 1% and 50%). Fractions of 25 ml were collected, analyzed by TLC (silica gel plates, in CHCl_3 or mixtures of CHCl_3 -MeOH 99:1, 98:2, 97:3, 9:1, 4:1), and grouped into 13 fractions (A-M). Fractions C (363 mg), D (100 mg) and E (182 mg) were subjected to RP-HPLC with MeOH- H_2O (3.5:6.5) as eluent to give pure compound **26** (8.9 mg, $t_R = 17$ min) from fraction C, compounds **22** (6.1 mg, $t_R = 10$ min) and **26** (5.0 mg, $t_R = 17$ min) from fraction D, and compound **23** (6.2 mg, $t_R = 11$ min) from fraction E, respectively. The structures of new compounds **1-11** are showed in **Figure 2.3** and **Figure 2.4** respectively. The structures of the diterpenes **22**, **23**, and **25** are showed in **Figure 2.5** while **26** and **27** are reported in **Figure 2.6**. The structures of the other compounds are reported in **Figure 2.7**.

2.6 New isolated compounds

Nagilactone C 7-O- α -L-arabinopyranosyl-(1 \rightarrow 4)- β -D-xylopyranoside (1)

Amorphous powder; $[\alpha]_{\text{D}}^{25}$ -10 (c 0.1, MeOH); UV (MeOH) λ_{max} (log ϵ) 285 (3.80) nm; ^1H and ^{13}C NMR, see **Table 2.1**; HRESIMS m/z 649.2122 $[\text{M}+\text{Na}]^+$ (calcd. for $\text{C}_{29}\text{H}_{38}\text{O}_{15}\text{Na}$, 649.2108); ESI-MS m/z 649 $[\text{M}+\text{Na}]^+$, 517 $[\text{M}+\text{Na}-132]^+$, 385 $[\text{M}+\text{Na}-132-132]^+$.

Nagilactone C 7-O- β -D-glucopyranosyl-(1 \rightarrow 4)- β -D-xylopyranoside (2)

Amorphous powder; $[\alpha]_{\text{D}}^{25}$ +1.6 (c 0.05, MeOH); UV (MeOH) λ_{max} (log ϵ) 290 (3.80) nm; ^1H and ^{13}C NMR, see **Table 2.1**; HRESIMS m/z 679.2261 $[\text{M}+\text{Na}]^+$ (calcd. for $\text{C}_{30}\text{H}_{40}\text{O}_{16}\text{Na}$, 679.2214); ESI-MS m/z 679 $[\text{M}+\text{Na}]^+$, 517 $[\text{M}+\text{Na}-162]^+$, 385 $[\text{M}+\text{Na}-162-132]^+$.

Nagilactone C 7-O- β -D-xylopyranoside (3)

Amorphous powder; $[\alpha]_{\text{D}}^{25}$ +5 (c 0.1, MeOH); UV (MeOH) λ_{max} (log ϵ) 280 (4.12) nm; ^1H and ^{13}C NMR, see **Table 2.1**; HRESIMS m/z 517.1712 $[\text{M}+\text{Na}]^+$ (calcd. for $\text{C}_{24}\text{H}_{30}\text{O}_{11}\text{Na}$, 517.1686); ESI-MS m/z 517 $[\text{M}+\text{Na}]^+$, 385 $[\text{M}+\text{Na}-132]^+$.

Nagilactone A 7-O- α -L-arabinopyranosyl-(1 \rightarrow 4)- β -D-xylopyranoside (4)

Amorphous powder; $[\alpha]_{\text{D}}^{25}$ -16 (c 0.1, MeOH); UV (MeOH) λ_{max} (log ϵ) 282 (4.08) nm; ^1H and ^{13}C NMR, see **Table 2.1**; HRESIMS m/z 635.2357 $[\text{M}+\text{Na}]^+$ (calcd. for $\text{C}_{29}\text{H}_{40}\text{O}_{14}\text{Na}$, 635.2316); ESI-MS m/z 635 $[\text{M}+\text{Na}]^+$, 503 $[\text{M}+\text{Na}-132]^+$.

2β,15S,16,17,19-Pentahydroxy-isopimar-8(14)-ene *17-O-β-D-glucopyranoside (5)*

Amorphous powder; $[\alpha]_D^{25} +1.3$ (c 0.08, MeOH); ^1H and ^{13}C NMR, see **Table 2.2**; HRESIMS m/z 539.2888 $[\text{M}+\text{Na}]^+$ (calcd. for $\text{C}_{26}\text{H}_{44}\text{O}_{10}\text{Na}$, 539.2832); ESI-MS m/z 515 $[\text{M}-\text{H}]^-$, 353 $[\text{M}-\text{H}-162]^-$, 293 $[\text{M}-\text{H}-162-60]^-$.

2β,15R,16,17,19-Pentahydroxy-isopimar-8(14)-ene *17-O-β-D-glucopyranoside (6)*

Amorphous powder; $[\alpha]_D^{25} +3.6$ (c 0.2, MeOH); ^1H and ^{13}C NMR, see **Table 2.2**; HRESIMS m/z 539.2895 $[\text{M}+\text{Na}]^+$ (calcd. for $\text{C}_{26}\text{H}_{44}\text{O}_{10}\text{Na}$, 539.2832); ESI-MS m/z 515 $[\text{M}-\text{H}]^-$, 353 $[\text{M}-\text{H}-162]^-$.

1-(2,6,6-Trimethyl-4-hydroxycyclohexenyl)-1-hydroxy-buta-1-en-3-one *4-O-β-D-glucopyranoside (7)*

Amorphous powder; $[\alpha]_D^{25} -42.9$ (c 0.08, MeOH); UV (MeOH) λ_{max} (log ϵ) 284 (3.78) nm; ^1H and ^{13}C NMR, see **Table 2.2**; HRESIMS m/z 409.1870 $[\text{M}+\text{Na}]^+$ (calcd. for $\text{C}_{19}\text{H}_{30}\text{O}_8\text{Na}$, 409.1839); ESI-MS m/z 409 $[\text{M}+\text{Na}]^+$, 325 $[\text{M}+\text{Na}-84]^+$.

Vitexin 2''-O-β-D-(6'''-acetyl)-glucopyranoside (8)

Amorphous powder; $[\alpha]_D^{25} -5$ (c 0.1, MeOH); UV (MeOH) λ_{max} (log ϵ) 272 (3.90), 335 (3.22) nm; ^1H and ^{13}C NMR, see **Table 2.2**; HRESIMS m/z 659.1600 $[\text{M}+\text{Na}]^+$ (calcd. for $\text{C}_{29}\text{H}_{32}\text{O}_{16}\text{Na}$, 659.1588); ESI-MS m/z 659 $[\text{M}+\text{Na}]^+$, 569 $[\text{M}+\text{Na}-90]^+$, 539 $[\text{M}+\text{Na}-120]^+$, 455 $[\text{M}+\text{Na}-204]^+$.

2 α ,16-Dihydroxy-4 β -carboxy-O- β -D-glucopyranosyl-19-nor-totarol (9)

Amorphous powder; $[\alpha]_D^{25} +50.2$ (*c* 0.05, MeOH); UV (MeOH) λ_{\max} (log ϵ) 230 (3.89), 278 (4.40) nm; ^1H and ^{13}C NMR, see **Table 2.3**; HRESIMS m/z 511.2537 $[\text{M}+\text{H}]^+$ (calcd. for $\text{C}_{26}\text{H}_{38}\text{O}_{10}$, 511.2543); ESI-MS m/z 533 $[\text{M}+\text{Na}]^+$, 371 $[\text{M}+\text{Na}-162]^+$.

Nagilactone K (10)

Amorphous powder; $[\alpha]_D^{25} +4.1$ (*c* 0.2, MeOH); UV (MeOH) λ_{\max} (log ϵ) 246 (4.03) nm; ^1H and ^{13}C NMR, see **Table 2.3**; HRESIMS m/z 319.1160 $[\text{M}-\text{H}]^-$ (calcd. for $\text{C}_{17}\text{H}_{20}\text{O}_6$, 319.1182); ESI-MS m/z 319 $[\text{M}-\text{H}]^-$, 275 $[\text{M}-\text{H}-44]^-$.

15-Hydroxy phaseic acid (11)

Amorphous powder; $[\alpha]_D^{25} +2.1$ (*c* 0.06, MeOH); UV (MeOH) λ_{\max} (log ϵ) 260 (3.95) nm; ^1H and ^{13}C NMR, see **Table 2.3**; HRESIMS m/z 297.1320 $[\text{M}-\text{H}]^-$ (calcd. for $\text{C}_{15}\text{H}_{22}\text{O}_6$, 297.1338); ESI-MS m/z 297 $[\text{M}-\text{H}]^-$, 253 $[\text{M}-\text{H}-44]^-$.

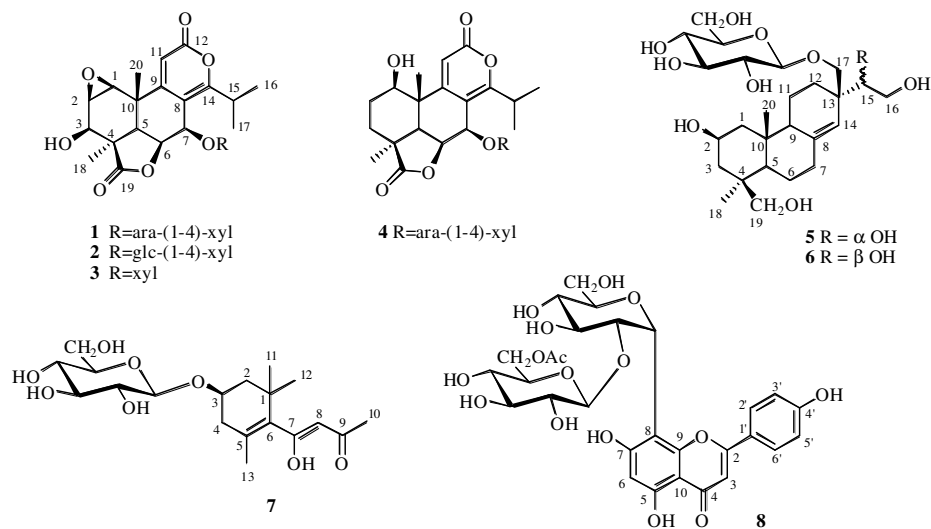


Figure 2.3: New isolated compounds from *P. elongatus*

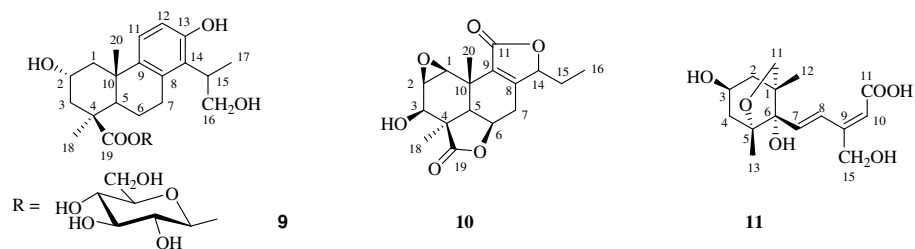


Figure 2.4: New isolated compounds from *P. gracilior*

2.7 Structural elucidation

As described before, from *P. elongatus* leaves eight new (**1–8**) and 13 known compounds were isolated. From *P. gracilior* were isolated three new compounds

(9-11) together with nine known compounds, some of which are in common with *P.elongatus*. The following known compounds were identified by comparison with published spectroscopic data: nagilactone B (Hayashi *et al.*, 1980), nagilactone C (Kubo and Ying, 1991), nagilactone D (Hayashi *et al.*, 1980), podolactone B (Hayashi *et al.*, 1980), 4 β -carboxy-19-*nor*-tatarol (Kubo and Ying, 1991), roseoside (Otsuka *et al.*, 1995), blumenol C glucoside (Pabst *et al.*, 1992), linarionoside C (Otsuka, 1994), 3,4,5-trihydroxydehydro- α -ionol 9-*O*- β -D-glucopyranoside (Rastrelli *et al.*, 1998), icariside E₃ (Kuono *et al.*, 1991), *erythro*-4,7,9,9'-tetrahydroxy-3,3'-dimethoxy-8-*O*-4'-oxyneolignan 9'-*O*- β -D-glucopyranoside (Matsuda and Kituchi, 1996), *threo*-4,7,9,9'-tetrahydroxy-3,3'-dimethoxy-8-*O*-4'-oxyneolignan 9'-*O*- β -D-glucopyranoside (Matsuda *et al.*, 1996), glochidiobioside (Takeda *et al.*, 1998), isoginkgetin (Markham *et al.*, 1987), bilobetin (Markham *et al.*, 1987), and 20-hydroxyecdysone (Miller *et al.*, 1985).

The molecular formula of compound **1** (C₂₉H₃₈O₁₅) was established by ¹³C NMR and ESIMS (*m/z* 649 [M+Na]⁺) spectra, indicating eleven degrees of unsaturation. In the ESIMS spectrum of compound **1** two ion fragments at *m/z* 517 [M+Na-132]⁺ and 385 [M+Na-132-132]⁺, due to the subsequent losses of two pentose residues, were observed. The α,β,γ -unsaturated lactone carbonyl functionality was evidenced by the presence of an ester carbonyl resonance at 164.2 ppm in the ¹³C NMR spectrum (**Table 2.1**). The ¹H NMR spectrum showed the presence of two methyls singlet at δ 1.43 (Me-18), 1.49 (Me-20), two methyl doublets at δ 1.25 (Me-16) and 1.38 (Me-17), five oxymethines at δ 3.43 (H-2), 3.59 (H-1), 4.39 (H-3), 5.12 (H-6), 5.56 (H-7), and one singlet olefinic proton at δ 6.38 (H-11) (**Table 2.1**). COSY and 1D-TOCSY measurements showing couplings between H-1—H-3, H-5—H-7, H-15—H-17 led to the assignment of the spin systems. HMBC correlations from H-11 to C-8, C-12, C-14 confirmed the assignment of α,β,γ -lactone ring carbons. Furthermore the HMBC

correlations of H-1 signal centered at δ 3.59 with C-3, C-5, and C-10 and HMBC correlations of H-2 (δ 3.43) with C-4, C-10, and Me-20 established the presence of a 1 β ,2 β -epoxide. The elucidation of the whole skeleton from the above subunits was achieved on the basis of HSQC and HMBC correlations, which also allowed the assignment of all the resonance in the ^{13}C NMR spectrum of the pertinent carbons. By this way, the aglycon moiety of **1** was characterized as nagilactone C (Kubo and Ying., 1991). 1D-TOCSY, DQF-COSY, and HSQC experiments provided evidence for the presence in the molecule of two pentose residues. On the basis of chemical shifts, multiplicity, values of the coupling constants, and magnitude in the ^1H and ^{13}C NMR spectra, the two sugar moieties were characterized as one β -xylopyranose and one α -arabinopyranose (**Table 2.1**) (De Tommasi *et al.*, 1997). The HMBC experiment provided the sugar sequence through unambiguous correlations between H-7—C-1_{xy1} and H-1_{ara}—C-4_{xy1}. The configuration of the sugar units was assigned after hydrolysis of **1** with 1N HCl and GC analysis of trimethylsilylated sugars through a chiral column. The sugar units were so determined to be D-xylopyranose and L-arabinopyranose. On the basis of the above evidences, compound **1** was identified as nagilactone C 7-*O*- α -L-arabinopyranosyl-(1 \rightarrow 4)- β -D-xylopyranoside.

The molecular formula of compound **2** ($\text{C}_{30}\text{H}_{40}\text{O}_{16}$) was established by ^{13}C NMR and ESIMS spectrum (m/z 679 for $[\text{M}+\text{Na}]^+$). In the ESIMS spectrum were also observed two main fragments at m/z 517 $[\text{M}+\text{Na}-162]^+$ and 385 $[\text{M}+\text{Na}-162-132]^+$ due to the subsequent loss of one hexose and one pentose. Its NMR spectral data (**Table 2.1**) suggested that the structure of **2** resembled that of **1**, but differed in the sugar chain. Comparison of chemical shifts of **2** with those of **1** suggested that the arabinopyranosyl residue was replaced by a β -glucopyranosyl unit. The absolute configuration of the sugar units was determined as reported for **1**. Thus, the structure of **2** was identified as nagilactone C 7-*O*- β -D-glucopyranosyl-(1 \rightarrow 4)- β -D-xylopyranoside.

The ESIMS of compound **3** (C₂₄H₃₀O₁₁) showed a main signal at m/z 517 ([M+Na]⁺) and a fragmentation pattern similar to that of **1**. Furthermore, in the MS² spectrum a fragment ion peak at m/z 385 [M+Na-132]⁺ was detected, indicating the loss of one pentose unit. Analysis of the NMR data (**Table 2.1**) of compound **3** and comparison with those of **1** revealed **3** to differ from **1** only by the absence of the terminal arabinopyranose unit. Thus, compound **3** was determined as nagilactone C 7-*O*-β-D-xylopyranoside.

Compound **4** was isolated as a colourless optically active amorphous powder, with $[\alpha]_D = -16$ ($c = 0.1$, MeOH). In the ESIMS spectrum, the [M+Na]⁺ signal was observed at m/z 635, consistent with the molecular formula C₂₉H₄₀O₁₄. A peak at m/z 503 [M+Na-132]⁺ was also observed, due to the loss of one pentose unit. The observation of signals in the ¹³C NMR spectrum (**Table 2.1**) consistent with δ-lactones and the presence of 19 carbon signals for the aglycon moiety led to the conclusion that this compound was again a norditerpene lactone glycoside (Kubo and Ying, 1991). The ¹H and ¹³C NMR data (**Table 2.1**) of **4** indicated the presence of two double bond and two hydroxyl group (δ_H 3.93, δ_C 72.0; δ_H 5.51, δ_C 65.0). An isopropyl group was clearly evident in the ¹H NMR spectrum (two methyl doublets at δ 1.25 and 1.38 and a one proton signal at δ 3.40). The absence of further coupling of the isopropyl proton at δ 3.40 indicated C-14 was fully substituted. The ¹H NMR spectral data combined with 1D TOCSY and DQF-COSY experiments suggested the sequence C-1—C-3 and C-5—C-7. Analysis of the proton coupling of the carbinolic protons allowed the remaining substitution pattern to be determined. Thus, the aglycon of compound **4** was recognized to be nagilactone A (Xuan *et al.*, 1995). Structural elucidation of the sugar moiety was performed on the basis of DQF-COSY and 1D TOCSY; starting from the well isolated anomeric signal at δ 4.45 (d, $J = 7.5$ Hz), the first sugar spin system was clarified to be β-xylose, while from the anomeric signal at δ 4.37 (d, $J = 7.0$ Hz), the other saccharide was identified as α-arabinose. The

sequence of the sugar chain could be assigned by the correlations in the HMBC spectrum between signal at δ 5.51 (H-7) and C-1_{xy1} (δ 100.8) and δ 4.37 (H-1_{ara}) and C-4_{xy1} (δ 77.0). The absolute configuration of the sugar units was determined as reported for **1**. From the foregoing evidence, the structure of **4** was established as nagilactone A 7-*O*- α -L-arabinopyranosyl-(1 \rightarrow 4)- β -D-xylopyranoside.

The molecular formula of **5** (C₂₆H₄₄O₁₀) was determined by ESIMS ([M-H]⁻ at *m/z* 515). The ¹H NMR spectrum (**Table 2.2**) showed signals for two tertiary methyl groups, two pairs of doublets centered at δ 3.05 (*J* = 11.0 Hz), 3.30 (*J* = 11.0 Hz), 3.76, and 3.85 (*J* = 12.0 Hz) for two hydroxymethylene groups, signals for protons at δ 3.79, 3.67, and 3.47 (br d, *J* = 9.0 Hz), and a hexose residue. The ¹H NMR spectral data combined with 1D TOCSY and DQF-COSY experiments suggested the sequence C-1—C-3, C-5—C-7, C-9—C-12, and C-15—C-16. The ¹³C NMR spectrum (**Table 2.2**) showed the presence of two hydroxymethines, one trisubstituted double bond, three hydroxymethylenes, and was in good agreement with that of a pimarane derivative (Nishiya *et al.*, 1991; Politi *et al.*, 2002). Structural elucidation of the glucopyranose moiety was performed on the basis of 1D TOCSY; starting from the well isolated anomeric proton signal at δ 4.28, the sugar spin system was clarified. The configuration of the glucose unit of **5** was obtained as reported before. The ¹³C NMR signals were assigned on the basis of a HSQC experiment. Location of the hydroxyl groups, the double bond, and the sugar unit was obtained by analysis of the HMBC spectrum. In fact, the signals at δ 3.47 and 3.67 (H₂-16) correlated with carbon resonances at δ 43.3 (C-13), 75.0 (C-15), and 125.3 (C-14), the signal at δ 3.79 (H-15) correlated with a signal at δ 65.5 (C-16), leading to the location of one diol group at C-15 and C-16; the signals at δ 3.76 and 3.85 (H₂-17) correlated with δ 25.7 (C-12), 43.3 (C-13), and 75.0 (C-15), establishing the location of one hydroxymethylene at C-17, and finally the signals at δ 3.05 and 3.30 (H₂-19) correlated with δ 19.2 (Me-18), 40.0 (C-4), 45.3 (C-3), 47.5 (C-5), positioning the third hydroxymethylene

function at C-19. The HMBC correlations between H-14 and C-7, C-12, and C-16 confirmed the C-8/C-14 double bond, while correlation between δ 4.28 (H-1_{glc}) and 72.6 (C-17) established the sugar location. 2D ROESY measurements supported the proposed structure and proved the relative stereochemistry at C-2, C-4, C-5, C-10, and C-13. Thus, the signal of the proton at δ 0.89 (Me-20) correlated with H-19a (δ 3.05) and H-17b signals (δ 3.85), the proton signal at δ 3.84 (H-2) affected the Me-18 (δ 0.85) signal, the proton signal at δ 1.44 (H-5) correlated with the H-9 (δ 1.90) signal, while the signal at δ 3.76 (H-17a) influenced H-12a (δ 1.36), H-19a (δ 3.05), and H-1_{glc} (δ 4.28). The absolute configuration of the 15,16-diol moiety of **5** was determined by the circular dichroism (CD) induced after in-situ complexation with dimolybdenum tetracetate in DMSO solution (Di Bari *et al.*, 2001). According to a rule proposed by Snatzke (Frelek *et al.*, 1999), the sign of the diagnostic band at about 305 nm correlated with the absolute configuration of the chiral centers in the 1,2-diol moiety. In particular a *S*-monosubstituted glycol gives rise to a positive Cotton effect at 305 nm. Thus the positive sign observed in the CD spectrum of **5** allowed us to assign the *S*-configuration to C-15. Consequently, **5** was characterized as 2 β ,15*S*,16,17,19-pentahydroxy-*isopimar*-8(14)-ene 17-*O*- β -D-glucopyranoside.

Compound **6** was assigned molecular formula C₂₆H₄₄O₁₀ (ESIMS pseudomolecular negative ion peak at m/z 515 [M-H]⁻), being an isomer of **5**. The spectral data (**Table 2.2**) of compound **6** indicated its diterpene skeleton. Comparison of its NMR spectra with those of **5** showed that **6** differed from **5** in the signals due to the 1,2-diol moiety and the ¹³C NMR resonances of C-12, C-13, C-14, and C-17. The absolute configuration of the 15,16-diol moiety of **6** was determined by the same method reported for **5**. The negative sign observed in the CD spectra of **6** led to the assignment of *R*-configuration to C-15. Thus, **6** was

identified as 2 β ,15*R*,16,17,19-pentahydroxy-*isopimar*-8(14)-ene 17-*O*- β -D-glucopyranoside.

The ESIMS spectrum of compound **7** showed a quasi molecular ion peak at m/z 409 $[M+Na]^+$ appropriate for a molecular formula $C_{19}H_{30}O_8$. The ^{13}C NMR data of **7** revealed 19 carbon signals, with 6 of them ascribable to one hexose unit and 13 to an α -ionol aglycon (**Table 2.2**) (De Tommasi *et al.*, 1996). Analysis of 1H NMR spectrum (**Table 2.2**) confirmed the presence of four methyl groups (δ_H 1.24, 1.30, 1.56, 2.23), one (δ_H 5.96) olefinic proton, and one carbinol proton (δ_H 4.16). The DQF-COSY spectrum of **7** indicated for the aglycon moiety, two spin system corresponding to the $-CH_2CHOHCH_2-$ and the $-CH_3COCH=COH-$ moieties, respectively. The three-proton singlet at δ 2.23 and the sharp one-proton singlet at δ 5.96 indicated that the side chain consisted in a β -diketone functionality present in one of the two enolized tautomeric forms. One additional tetrasubstituted double bond was apparent from the ^{13}C NMR resonances at δ 123.7 and 124.0. A HSQC experiment established the association of the protons with the corresponding carbons and HMBC spectrum led to the location of the five remaining quaternary carbons at C-1, C-5, C-6, C-7, and C-9. Definitive evidence in the compound **7** structure was derived by the HMBC spectrum, which clearly showed cross peaks between H-8 (δ 5.96) and C-1 (δ 36.0), C-6 (δ 124.0), C-9 (δ 202.0), and C-10 (δ 26.6); Me-10 (δ 2.23) and C-9 (δ 202.0); Me-13 (δ 1.56) and C-3 (δ 72.7), C-4 (δ 48.0), and C-5 (δ 123.7); H-1_{glc} (δ 4.41) and C-3 (δ 72.7). The 1H NMR and ^{13}C NMR data of the sugar portion of **7** led to conclude that the hexose moiety was β -glucopyranose. The absolute configuration of the sugar units was determined as reported for **1**. From all these data, the structure of **7** was determined as 1-(2,6,6-trimethyl-4-hydroxycyclohexenyl)-1-hydroxy-buta-1-en-3-one 4-*O*- β -D-glucopyranoside. The aglycon of **7** was previously isolated in its β -diketone form as a metabolite from the dinoflagellate *Prorocentrum minimum* (Andersen *et al.*, 1980).

The positive ESIMS of **8** showed an $[M+Na]^+$ ion at m/z 659 consistent with the molecular formula $C_{29}H_{32}O_{16}$. Major fragments at m/z 569 $[M+Na-90]^+$ and 539 $[M+Na-120]^+$ were typical of a C-glycosylflavone (Waridel *et al.*, 2001), while a fragment at m/z 455 $[M+Na-204]^+$ indicated the loss of an acylated terminal sugar. The 1H NMR spectrum (**Table 2.2**) showed an A_2B_2 spin system at δ 6.90 (2H, d, $J = 8.5$ Hz) and 8.00 (2H, d, $J = 8.5$ Hz), together with two singlet at δ 6.20 and 6.71, a sugar chain [two anomeric protons at δ 4.81 (1H, d, $J = 8.0$ Hz) and δ 4.13 (1H, d, $J = 7.8$ Hz)], and an acetyl group at δ 1.86 (3H, s). Analysis of ^{13}C NMR spectrum (**Table 2.2**) and a combination of 1D-TOCSY, DQF-COSY, and HSQC experiments suggested that **8** was a vitexin derivative and one β -glucopyranosyl unit was the additional sugar residue (Pauli and Junior, 1995; Cheng *et al.*, 2000). The exact location of the sugars and the acetyl moiety was revealed by the HMBC correlations observed between the anomeric proton signal at δ_H 4.81 (H-1_{glcI}) and C-8 (δ 105.5), C-9 (δ 158.3), and C-7 (δ 164.5) and between the anomeric proton signal at δ_H 4.13 (H-1_{glcII}) and C-2_{glcI} (δ 80.3), and by the downfield shift for H₂-6_{glcII}, indicating the occurrence of acylation at C-6_{glcII}. Therefore the structure of **8** was determined to be vitexin 2''-O- β -D-(6'''-acetyl)-glucopyranoside.

The $CHCl_3$, $CHCl_3$ -MeOH, and *n*-BuOH extracts of *P. gracilior* gave the new compounds **9-11**. The molecular formula of compound **9** ($C_{26}H_{38}O_{10}$) was established by ^{13}C NMR and HR-MS (obsd m/z 511.2537 for $[M+H]^+$ calcd m/z 511.2543) indicating eight degree of unsaturation. The NMR data (**Table 2.3**) showed that six of the elements of unsaturation were present as an aromatic ring, a hexose residue, and an esterified carboxylic group. Therefore the molecule was tricyclic. In the 1H NMR spectrum of **9**, two methyl singlets resonating at δ 1.13 and 1.42 were assigned as C-20 and C-18, respectively. One methyl doublet at δ 1.33 ($J = 6.5$ Hz, Me-17) was also present. DQF-COSY and 1D TOCSY measurement showing coupling between H-1—H-3, H-5—H-7, H-15—H-17

allowed assignment of these spin systems. Likewise, a HMBC correlation to the Me-17 resonance established the C-16 hydroxymethylene function at δ 66.0. The hydroxymethine resonance at δ_C 65.3 and δ_H 4.27 (1H, m) was assigned to C-2 by HMBC cross peaks between H-2 and C-1, Me-20 and C-1, C-2, and C-5, H₂-3 and C-1, C-5, C-18, and C-19, H-1b and C-2, C-5, and Me-20. The NMR chemical shifts in comparison to related compounds showed the presence of a carboxylic group at C-4 (δ_C 177.3). The aromatic region of the ¹H NMR spectrum showed two *ortho*-coupled doublets at δ 6.59 ($J = 8.0$ Hz) and 7.03 ($J = 8.0$ Hz) that were assigned to H-12 and H-11, respectively. Both these protons showed HMBC correlations with C-8, C-9, and C-14. The presence of a hydroxyisopropyl group was assumed from diagnostic signals of Me-17 (δ 1.33, d, $J = 6.5$ Hz), H-15 (δ 3.30, m) and H₂-16 (δ 3.91, 2H, m). According to HMBC spectrum the hydroxymethylene protons at δ 3.91 (H₂-16) showed a long range correlation with H-14 and Me-17, while the methine proton at δ 3.30 (H-15) exhibited a long range correlation with C-8 and C-13 signals, indicating a 19-*nor*-totarol derivative (Kubo and Ying, 1991). The relative stereochemistry of compound **9** was obtained on the basis of 2D-ROESY data. The α -orientation of hydroxyl group at C-2 was indicated by ROE cross peak among proton spatially related H-2 with Me-20. This was confirmed by chemical shifts of the respective carbons which matched well with those of related diterpenes (Braca *et al.*, 2004). 1D-TOCSY, DQF-COSY, and HSQC experiments provided evidence for the presence in the molecule of one hexose residue. On the basis of chemical shifts, multiplicity, values of the coupling constants, and magnitude in the ¹H and ¹³C NMR spectra, the sugar moiety was characterized as one β -glucopyranose. Its configuration was assigned after hydrolysis of **9** with 1N HCl and GC analysis of trimethylsilylated sugar through a chiral column. The sugar unit was so determined to be D-glucopyranose. The HMBC correlation between δ 5.50 (H-1_{glc}) and 177.3 (C-19) established the sugar location. Hence, compound **9** was

concluded to be 2 α ,16-dihydroxy-4 β -carboxy-*O*- β -D-glucopyranosyl-19-*nor*-totarol.

In the ESI-MS spectrum of **10** an ion at m/z 319 [M-H]⁻ and a prominent fragment due to the loss of CO₂ (m/z 275 [M-H-44]⁻) were observed. Thus, the molecular formula of **10** was C₁₇H₂₀O₆, which required a rearranged diterpenoid skeleton (HR-MS m/z 319.1160, calcd for 319.1182). The 17 carbon signals in the ¹³C NMR spectrum (Table 2.3) were established as three methyls, two methylenes, six methines, of which five were oxygenated, two quaternary carbons, two *sp*² carbons, and two lactone groups. Three spin systems were recognized from 1D TOCSY and DQF-COSY spectra: H-1—H-3, H-5—H-7, H-14—H-16. In the ¹H NMR spectrum (Table 1) two protons at δ 4.08 (d, J = 5.0 Hz) and 3.39 (dd, J = 9.0, 4.5 Hz), correlating in the HSQC spectrum with two signals at 56.4 and 50.8 ppm, respectively, allowed to establish the presence of an epoxy ring which was located at C-1/C-2 on the basis of the HMBC experiment. Key correlation peaks between H-1—C-20, H-1—C-10, H-2—C-1, H-3—C-1, H-3—C-5, H-3—C-19 were observed. In the ¹H NMR the signal at δ 5.02 (br d, J = 5.0 Hz) was attributed to an equatorial H-6. NMR data of H-6 and C-6 and HMBC correlations between H-6—C-10, H-6—C-8, H-6—C-4 and H-5—C-19, H-5—C-7, H-5—C-9, and H-5—C-10 led to establish the presence of a 6,19-olide ring. The signals at δ 172.2 was assigned to C-11 of a 14,11-olide ring by its HMBC correlations with the signals of H-7 and H-14. The DQF-COSY spectrum revealed that H-15 was coupled with H-14 which indicated that the isoethyl group of **10** was adjacent to a methine carbon not a *sp*² carbon as in the case of nagilactone C (Hayashi *et al.*, 1980) demonstrating that the C-ring was not an α -pyrone. The ROESY indicated that the protons at position 1, 2, and 3 and 5 and 6 were *syn*, relative to each other. On the basis of our spectroscopic data, the ring C resulted a five-membered α,β -unsaturated γ -lactone. From these results, the structure of compound **10** was determined and named nagilactone K.

The five-membered norditerpene dilactones are very rare in nature (Fang *et al.*, 1990; Kubo and Ying, 1991).

The composition of compound **11** was determined by HR-MS spectrometry (m/z 297.1320 [M-H]⁻) and ¹³C NMR analysis as C₁₅H₂₂O₆. The ¹H and ¹³C NMR (Table 2.3) spectra indicated that **11** was a sesquiterpenoid derivative. The carbon signals of **11** were sorted by HSQC and ¹³C NMR into two methyls, two methylenes, one hydroxymethine, two hydroxymethylenes, three quaternary carbons, two of which were hydroxylated, four olefinic carbons, and one carboxylic group. With phaseic acid used as a reference compound in the spectral analysis of **11**, close similarities were observed between spectral data of both compound ring, while their side chain provided the point of difference (Zhang *et al.*, 2010). The main differences were the absence of the signal ascribable to the methyl group linked to *sp*² C-9 and the presence of an additional hydroxymethylene group at δ_{H} 4.40 (1H, s) and δ_{C} 63.3 that was located at C-9 by HMBC correlations. Thus, **11** was determined as 15-hydroxy phaseic acid.

The present investigation of *P. elongatus* and *P. gracilior* substantiates that norditerpene lactones, biflavones, and C-glycosylflavones are characteristic constituents of the genus *Podocarpus* and could be used as chemotaxonomic markers (Abdillahi *et al.*, 2010, 2011; Markham *et al.*, 1985).

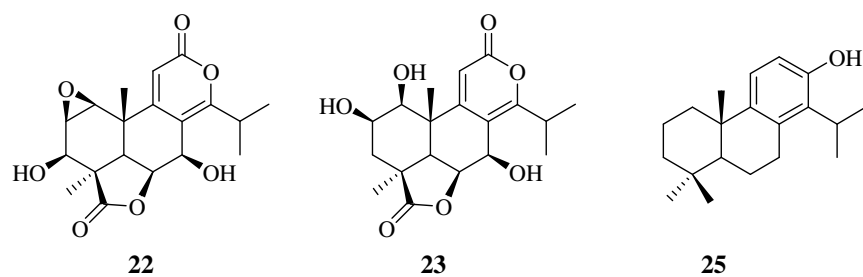


Figure 2.5: Structure of known diterpenes isolated from *P. elongatus*: compounds 22 and 23 were isolated also from *P. gracilior*

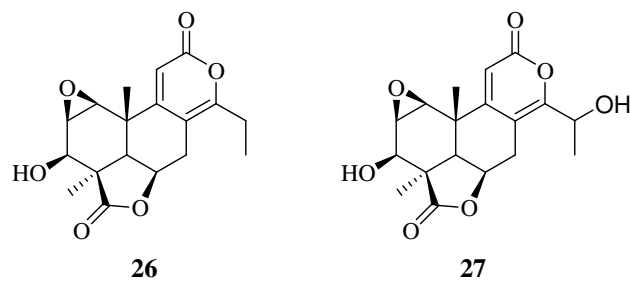


Figure 2.6: Structure of the other known diterpenes isolated from *P. gracilior*

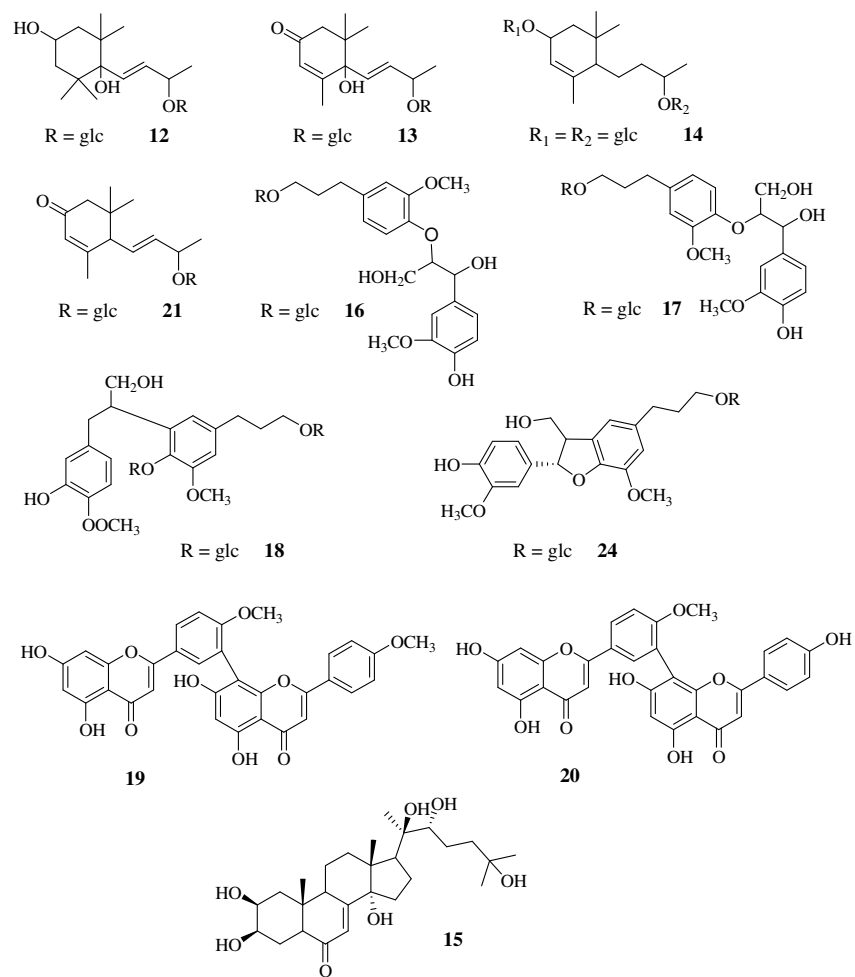


Figure 2.7: Structure of the other known compounds

Table 2.1. ^1H and ^{13}C NMR data of compounds **1-4** (CD_3OD , 600 MHz)^a

position	1		2		3		4	
	δ_{H}	δ_{C}	δ_{H}	δ_{C}	δ_{H}	δ_{C}	δ_{H}	δ_{C}
1	3.59 d (5.5)	59.0	3.60 d (5.5)	58.0	3.62 d (5.5)	59.5	3.93 dd (11.0, 5.5)	72.0
2a	3.43 dd (6.0, 5.5)	51.8	3.48 dd (6.0, 5.5)	52.0	3.40 dd (6.0, 5.5)	52.1	1.73 m	29.8
2b							1.98 m	
3	4.39 d (6.2)	68.4	4.42 d (6.0)	67.8	4.42 d (6.2)	68.8	1.55 m	28.2
4		50.1		49.5		50.3	2.27 ddd (12.0, 10.0, 4.5)	43.8
5	2.13 d (6.7)	51.6	2.14 d (6.5)	51.0	2.16 d (6.7)	51.3	1.89 d (6.5)	50.8
6	5.12 dd (6.0, 2.0)	73.6	5.14 dd (6.0, 2.0)	72.0	5.13 dd (6.5, 2.0)	73.5	5.21 dd (6.5, 2.0)	74.5
7	5.56 d (9.0)	64.7	5.57 d (9.0)	64.2	5.60 d (9.0)	64.8	5.51 d (9.0)	65.0
8		109.4		109.5		109.0		109.6
9		167.2		167.0		167.1		168.0
10		38.9		38.6		38.6		42.4
11	6.38 s	108.3	6.40 s	108.0	6.42 s	108.4	6.78 s	108.0
12		164.2		164.0		163.9		165.0
14		172.3		172.1		171.6		171.8
15	3.39 ^b	30.3	3.38 ^b	30.3	3.40 ^b	30.3	3.40 ^b	30.9
16	1.25 d (6.6)	21.7	1.28 d (6.5)	21.2	1.29 d (6.7)	21.9	1.25 d (6.7)	21.3
17	1.38 d (6.8)	20.3	1.41 d (6.6)	20.4	1.42 d (6.7)	20.7	1.38 d (6.7)	20.4
18	1.43 s	26.0	1.45 s	25.4	1.46 s	25.8	1.33 s	24.4
19		179.8		179.5		179.3		183.3
20	1.49 s	18.2	1.51 s	17.9	1.52 s	18.5	1.44 s	15.0
Xyl 1	4.43 d (7.5)	100.0	4.41 d (7.5)	100.7	4.38 d (7.5)	100.4	4.45 d (7.5)	100.8
2	3.34 dd (9.0, 7.5)	73.8	3.35 dd (9.0, 7.5)	73.5	3.29 dd (9.0, 7.5)	74.5	3.38 dd (9.0, 7.5)	73.6
3	3.51 t (9.0)	74.5	3.50 t (9.0)	75.4	3.33 t (9.0)	77.5	3.51 t (9.0)	75.0
4	3.74 m	77.5	3.78 m	77.8	3.57 m	70.8	3.93 m	77.0
5a	3.45 dd (12.0, 4.5)	64.0	3.43 dd (12.0, 4.5)	63.7	3.30 ^b	66.4	3.44 dd (12.0, 5.0)	63.8
5b	4.11 dd (12.0, 2.5)		4.17 dd (12.0, 3.0)		4.02 dd (12.0, 5.0)		4.15 dd (12.0, 3.0)	
Ara 1	4.34 d (7.0)	103.7					4.37 d (7.0)	103.5
2	3.59 dd (9.0, 7.0)	71.8					3.59 dd (9.0, 7.0)	71.6
3	3.50 dd (9.0, 2.5)	75.2					3.55 dd (9.0, 2.5)	74.0
4	3.83 m	69.6					3.84 m	69.0
5a	3.59 dd (12.0, 3.0)	67.1					3.62 dd (12.0, 3.0)	67.0
5b	3.91 dd (12.0, 2.0)						3.91 dd (12.0, 2.0)	
Glc 1			4.44 d (7.5)	102.9				
2			3.24 dd (9.2, 7.5)	74.5				
3			3.28 t (9.2)	77.3				
4			3.30 t (9.2)	70.8				
5			3.41 m	77.5				
6a			3.68 dd (12.0, 5.0)	62.8				
6b			3.88 dd (12.0, 3.0)					

^a J values are in parentheses and reported in Hz; chemical shifts are given in ppm; assignments were confirmed by DQF-COSY, 1D-TOCSY, HSQC, and HMBC experiments.

Table 2.2: ^1H and ^{13}C NMR data of compounds 5-8 (CD_3OD , 600 MHz)^a

5		6		7		8	
position	δ_{H}	δ_{C}	δ_{H}	δ_{C}	position	δ_{H}	δ_{C}
1a	1.00 t (11.0)	48.7	1.00 t (11.0)	48.7	1		36.0
1b	2.01 br d (11.0)		2.01 br d (11.0)		2a	1.58 dd (14.0, 8.0)	45.0
2	3.84 m	65.6	3.84 m	65.3	2b	2.00 dd (14.0, 4.5)	
3a	1.46 t (11.0)	45.3	1.46 t (11.0)	45.1	3	4.16 m	72.7
3b	1.60 br d (12.0)		1.60 t (12.5)		4a	1.78 m	48.0
4		40.0	-	40.2	4b	2.17 dd (13.0, 5.0)	
5	1.44 ^b	47.5	1.44 ^b	47.4	5		123.7
6a	1.30 m	22.8	1.30 m	22.6	6		124.0
6b	1.54 m		1.54 m		7		177.0
7a	2.17 m	36.6	2.17 m	36.2	8	5.96 s	102.0
7b	2.31 br d (11.0)		2.31 br d (11.0)		9		202.0
8		139.6	-	139.6	10	2.23 s	26.6
9	1.90 dd (9.0, 2.0)	52.3	1.90 dd (9.0, 2.0)	52.2	11	1.30 s	29.6
10		39.8		39.9	12	1.24 s	32.9
11a	1.55 m	19.4	1.55 m	19.4	13	1.56 s	30.6
11b	1.67 m		1.67 m		1'		
12a	1.36 m	25.7	1.36 m	24.8	2'/6'		8.00 d (8.5)
12b	1.72 m		1.72 m		3'/5'		6.90 d (8.5)
13		43.3		43.3	4'		
14	5.30 s	125.3	5.30 s	124.6	Glc I 1	4.41 d (7.5)	102.5
15	3.79 ^b	75.0	3.79 br t (6.0)	77.5	2	3.16 dd (9.5, 7.5)	74.7
16a	3.47 br d (9.0)	65.5	3.47 br d (10.0)	66.8	3	3.35 t (9.5)	77.4
16b	3.67 ^b		3.67 ^b		4	3.32 t (9.5)	71.4
17a	3.76 ^b	72.6	3.54 d (12.0)	73.1	5	3.35 m	77.4
17b	3.85 d (12.0)		4.07 d (12.0)		6a	3.67 dd (12.0, 5.0)	62.5
18	0.85 s	19.2	0.85 s	19.4	6b	3.86 dd (12.0, 3.0)	
19a	3.05 d (11.0)	71.5	3.05 d (10.5)	71.4	Glc II 1		4.13 d (7.8)
19b	3.30 d (11.0)		3.30 d (10.5)		2		2.77 ^b
20	0.89 s	16.7	0.89 s	16.7	3		2.92 t (9.5)
Glc 1	4.28 d (7.8)	104.2	4.30 d (7.5)	104.8	4		2.85 dd (4.0, 2.5)
2	3.22 dd (9.0, 7.8)	75.0	3.21 dd (9.0, 7.5)	75.0	5		2.77 ^b
3	3.38 t (9.0)	77.6	3.38 t (9.0)	77.8	6b		3.55 dd (12.0, 4.5)
4	3.29 t (9.0)	71.0	3.30 t (9.0)	71.3	6b		3.77 dd (12.0, 2.5)
5	3.29 m	77.8	3.38 m	77.7	COCH ₃		
6a	3.69 dd (12.0, 5.0)	62.5	3.68 dd (12.0, 4.5)	62.5	COCH ₃		1.86 s
6b	3.90 dd (12.0, 3.5)		3.86 dd (12.0, 3.0)				

^a *J* values are in parentheses and reported in Hz; chemical shifts are given in ppm; assignments were confirmed by DQF-COSY, 1D-TOCSY, HSQC, and HMBC experiments.

^b overlapped signal

Table 2.3: ^1H and ^{13}C NMR data of compounds **9-11** (CD_3OD , 600 MHz)^a

position	9		10		11	
	δ_{H}	δ_{C}	δ_{H}	δ_{C}	δ_{H}	δ_{C}
1a	1.20 t (12.5)	49.7	4.08 d (5.0)	56.4		48.4
1b	2.57 dd (12.5, 4.0)					
2a	4.27 m	65.3	3.39 dd (9.0, 4.5)	50.8	1.67 br d (12.5)	44.6
2b					1.87 m	
3a	1.11 t (13.0)	46.8	4.42 d (7.0)	69.7	4.11 m	65.0
3b	2.56 dd (12.5, 4.0)					
4a		45.2		48.8	1.74 dd (12.0, 3.0)	46.0
4b					2.02 dd (14.5, 7.0)	
5	1.51 br d (12.5)	53.0	2.07 d (6.0)	54.4		87.0
6a	2.04 m	22.1	5.02 br d (5.0)	74.7		83.0
6b	2.32 dd (12.5, 4.0)					
7a	2.64 m	30.9	2.77 br d (19.0)	27.2	6.42 d (16.0)	131.2
7b	3.10 dd (17.0, 5.0)		3.23 dd (19.0, 9.0)			
8		135.6		165.2	7.73 d (16.0)	129.6
9		140.3		135.7		149.1
10		40.6		34.8	6.05 br s	120.8
11	7.03 d (8.0)	125.2		172.2		170.5
12a	6.59 d (8.0)	115.3			3.71 d (7.5)	77.4
12b					3.81 d (7.5)	
13					0.95 s	16.3
14		128.3	4.98 m	84.7	1.16 s	19.7
15a	3.30 m	36.8	1.66 m	26.0	4.40 s	63.3
15b			2.04 m			
16	3.91 m	66.0	0.99 t (7.0)	8.4		
17	1.33 d (6.5)	15.2				
18	1.42 s	28.7	1.49 s	26.0		
19		177.3		180.0		
20	1.13 s	24.9	1.07 s	17.0		
Glc 1	5.50 d (7.5)	95.5				
2	3.41 dd (9.0, 7.5)	73.8				
3	3.38 t (9.0)	78.7				
4	3.39 t (9.0)	70.1				
5	3.43 m	78.0				
6a	3.70 dd (12.0, 4.5)	62.1				
6b	3.92 dd (12.0, 3.0)					

^a J values are in parentheses and reported in Hz; chemical shifts are given in ppm; assignments were confirmed by DQF-COSY, 1D-TOCSY, HSQC, and HMBC experiments.

^b overlapped signal

Chapter 3

Phytochemical study of Clerodendrum splendens G. Don.

Chapter 3

3.1 Introduction: *Clerodendrum* genus

The genus *Clerodendrum* L., Verbenaceae family, is very widely distributed in tropical and subtropical regions of the world and is comprised of small trees, shrubs, and herbs (**Figure 3.1**). The Latin name used since from the beginning is “*Clerodendrum*” while the Greek form is “*Clerodendron*” in Greek “Klero” means chance and “Dendron” means tree. Later it was readopted the Latinized name “*Clerodendrum*”, which is now commonly used by taxonomists for the classification and description of the genus and species (Moldenke 1985; Rueda 1993; Hsiao and Lin, 1995; Steane *et al.*, 1999).

Clerodendrum is a very large and diverse genus; till now 580 species have been identified and are widely distributed in Asia, Australia, Africa, and America. Many species of the genus have also been documented in traditional systems of medicine practiced in countries like India, China, Korea, Thailand, and Japan. Ethno-medical importance of various species of this genus has been reported in many indigenous systems of medicines and as folk medicines. Anti-inflammatory, antidiabetic, antimalarial, antiviral, antihypertensive, hypolipidemic, and antioxidant activities are among the major reported. It was also known the tribal use of *C. inerme* as an antidote of poisoning from fish, crabs, and toads.



Figure 3.1: *Flowers of Clerodendrum spp.*

Constituents of *Clerodendrum* genus are mainly terpenes: monoterpenes, sesquiterpenes, diterpenes, triterpenes, and iridoids. *Clerodendrum* genus is one of the major source of *neo-clerodane* diterpenoids that are a large group of naturally occurring compounds with interesting biological activities isolated mainly from Asteraceae, Lamiaceae, and Verbenaceae (Shrivastava and Patel, 2007).

3.2 *Clerodendrum splendens*

Clerodendrum splendens G. Don is a climbing evergreen brush plant with attractive red flowers (**Figure 3.2**) native to Sierra Leone (West Africa) and is used in traditional Nigerian medicine. The roots and leaves decotion are used for the treatment of skin diseases, cancer, syphilis, gonorrhea, ulcers, and various inflammatory diseases (Okwu and Uchenna, 2009).



Figure 3.2: *Clerodendrum splendens* leaves and flowers

3.3 Plant material

Leaves of *C. splendens* were collected in El Zoharia Research Garden of Cairo, Egypt, on March 2010 and identified by Dr. Mamdouh Shokry (El Zoharia Research Garden, Cairo, Egypt). The voucher specimen (No. 7191 *C. splendens* G. Don /1) was deposited at the Herbarium Hortii Botanici Pisani, Flora Aegyptiaca, Pisa, Italy.

3.4 Extraction and isolation

Dried powdered leaves of *C. splendens* (775 g) were successively and separately extracted for 48 h with *n*-hexane, CHCl_3 , CHCl_3 -MeOH (9:1), and MeOH, by exhaustive maceration (2 l), to give 15.6, 13.5, 21.7, 26.8 g of the respective residues.

The MeOH extract was partitioned between *n*-BuOH and H_2O , to afford a *n*-BuOH residue (5.7 g). The *n*-BuOH fraction was submitted to a Sephadex LH-20

using MeOH as eluent to obtain twelve major fractions (A-N) grouped by TLC. Fraction B (1.041 g) was partitioned between *n*-BuOH and H₂O, to afford a *n*-BuOH residue (780 mg) that was purified by RP-HPLC with MeOH–H₂O (2:3) as eluent to give pure phlinoside B (compound **6**, 9 mg, *t_R* =13 min), the new compound, β -(3,4-dihydroxyphenyl)ethyl-*O*- β -D-xylopyranosyl-(1 \rightarrow 2)- α -L-rhamnopyranosyl-(1 \rightarrow 3)-6-*O*-*t*-caffeoyl- β -D-glucopyranoside (compound **1**, 1.1 mg, *t_R*=20 min) and hispidulin-7-*O*-neohesperoside (compound **8**, 1 mg, *t_R* = 38 min). Fraction E (248.2 mg), fraction G (76.7 mg) and fraction I (115 mg) were directly subjected to RP-HPLC with MeOH–H₂O (2:3) as eluent to give pure compound **1** (5.6 mg), **8** (7.4 mg) and verbascoside (compound **9**, 2.4 mg, *t_R* =13 min) from fraction E, isoacteoside (compound **10**, 5.1 mg, *t_R* =20 min) from G and hispidulin-7-*O*- β -D-glucopyranoside (compound **7**, 2 mg, *t_R*=45 min) and luteolin-7-neohesperoside, (compound **11**, 2.2 mg, *t_R* =29 min) from I. Fraction N (120 mg) was purified by RP-HPLC with MeOH–H₂O (35:65) as eluent to give pure rosmarinic acid (compound **12**, 6.6 mg, *t_R* = 35 min). Part of the CHCl₃–MeOH extract (10 g) was chromatographed over Sephadex LH-20 to give twelve major fractions (A-N) grouped by TLC. Fractions F (188.5 mg) was purified by RP-HPLC with MeOH–H₂O (35:65) as eluent to yield compound **6** (11.9 mg, *t_R* = 22 min). Fraction H (70 mg) was also purified by RP-HPLC with MeOH–H₂O (2:3) as eluent to yield compound **7** (8.6 mg, *t_R* = 38 min). Part of the CHCl₃ extract (10.0 g) was chromatographed over silica gel column eluting with CHCl₃ followed by increasing concentrations of MeOH in CHCl₃ (between 1% and 50%). Fractions were grouped by TLC into 17 fractions (A-S). Fraction H-L (1.552 g) was purified by RP-HPLC with MeOH–H₂O (7:3) as eluent to yield 2 β -angeloyloxy-5 β -hydroxy-7 α ,10 β -methyl-eudesm-3-ene-1-one (compound **13**, 1.5 mg, *t_R* = 19 min). Fraction O (500 mg) was purified by RP-HPLC with MeOH–H₂O (3:2) as eluent to yield 14,15-dihydro-15-hydroxy-3-epicarioptin (compound **14**, 5.5 mg, *t_R* = 11 min) and the new compound 2 α -acetoxy-3 β -(2',3'-diacetoxy-2'-methyl)-butanoyloxy-14-hydro-15-hydroxyclerodin (compound **2**, 5.4 mg, *t_R*

= 22 min). Fractions Q (292 mg) and S (270 mg) were purified by RP-HPLC with MeOH–H₂O (2:3) as eluent to yield the new 3 β ,15-dihydroxy-14hydroclerodin (compound **3**, 1.8 mg, t_R = 27 min) from fraction Q and the new compound 3 β ,14S,15-trihydroxy-6 α ,18-diacetoxy-4 α ,17-epoxy-clerodan-11,16-lactone (compound **5**, 10.3 mg, t_R = 12 min) from fraction S. Fraction R (294 mg) was purified by RP-HPLC with MeOH–H₂O (45:55) as eluent to yield the new compound **4**, 2 α ,15-dihydroxy-3 β -(2'-hydroxy-2'-methyl-3'-acetoxy)-butanoyloxy-6 α ,18-diacetoxy-4 α ,17-epoxy-clerodan-11,16-lactone (compound **4**, 1.4 mg, t_R = 20 min). New compounds **1-5** are showed in **Figure 3.3** and **3.4**. Compounds **6-14** are reported in **Figure 3.5** and **3.6**.

3.5 New isolated compounds

β -(3,4-dihydroxyphenyl)ethyl-O- β -D-xylopyranosyl-(1 \rightarrow 2)- α -L-rhamnopyranosyl-(1 \rightarrow 3)-6-O-t-caffeoyl- β -D-glucopyranoside (1)

Brown amorphous powder; $[\alpha]_D^{25}$ -10.7 (c 0.5, MeOH); UV (MeOH) λ_{max} (log ϵ) 220sh (3.88), 288sh 3.95), 330 (4.09) nm; HRESIMS m/z 757.2637 [M+H]⁺ (calcd. for C₃₄H₄₄O₁₉, 757.2555); ESI-MS m/z 755 [M-H]⁻, 623 [M-H-132]⁻, 593 [M-H-162]⁻; 779, m/z 779 [M+Na]⁺, 647 [M+Na-132]⁺, 501 [M+Na-146]⁺; ¹H and ¹³C NMR data, see **Table 3.1**

2 α -acetoxy-3 β -(2',3'-diacetoxy-2'-methyl)-butanoyloxy-14-hydro-15-hydroxyclerodin (2)

Colorless amorphous powder; $[\alpha]_D^{25}$ -9.4 (c 0.45, MeOH); HR-ESIMS [M+H]⁺ 727.3204 (calcd. for C₃₅H₅₁O₁₆, 727.3177); ESI-MS m/z 749 [M+Na]⁺, 689

[M+Na-60]⁺, 531 [M+Na-218]⁺, 489 [M+Na-218-42]⁺, 471 [M+Na-218-60]⁺, 411 [M+Na-218-60-60]⁺. ¹H and ¹³C NMR data, see **Table 3.2**.

3β,15-dihydroxy-14hydro-clerodin (3)

Colorless amorphous powder; $[\alpha]_D^{25}$ +5.7 (*c* 0.15 MeOH); HRESIMS *m/z* 469.2500 [M+H]⁺ (calcd for C₂₄H₃₇O₉, 469.2438); ESI-MS *m/z* 467 [M-H]⁻, 425 [M-H-42]⁻, 383 [M-H-42-42]⁻; 491 [M+Na]⁺, 431 [M+Na-60]⁺, 371 [M+Na-60-60]⁺. ¹H and ¹³C NMR data, see **Table 3.2**.

2α,15-dihydroxy-3β-(2'-hydroxy-2'-methyl-3'-acetoxy-)-butanoyloxy-6α,18-diacetoxy-4α,17-epoxy-clerodan-11,16-lactone (4)

Colorless amorphous powder; $[\alpha]_D^{25}$ -5.7 (*c* 0.11, MeOH); HR-ESIMS *m/z* [M+H]⁺ 643.2899 (Calcd. for C₃₁H₄₇O₁₄, 643.2966); ESI-MS *m/z* 665 [M+Na]⁺, 605 [M+Na-60]⁺, 486 [M+Na-176]⁺. ¹H and ¹³C NMR data, see **Table 3.3**.

3β,14S,15-trihydroxy-6α,18-diacetoxy-4α,17-epoxy-clerodan-11,16-lactone (5)

Colorless amorphous powder; $[\alpha]_D^{25}$ +2.6 (*c* 0.13, MeOH); HR-ESIMS *m/z* 485.2423 [M+H]⁺, 507.2246 [M+Na]⁺ (calcd. for C₂₄H₃₇O₁₀, 485.2387, C₂₄H₃₆O₁₀Na, 507.2206); ESI-MS *m/z* 507 [M+Na]⁺, 447 [M+Na-60]⁺, 387[M+Na-60-60]⁺. ¹H and ¹³C NMR data, see **Table 3.3**.

3.5 Structural elucidation

Compound **1** molecular formula was determined as $C_{34}H_{44}O_{19}$ by high-resolution electrospray ionization (HR-ESI) mass spectrometry (m/z 757.2637 $[M+H]^+$). Its ESIMS spectrum showed a quasimolecular ion peak at m/z 779 $[M+Na]^+$; two main fragments at m/z 647 $[M+Na-132]^+$ and 501 $[M+Na-132-146]^+$ due to the loss of one pentose and one deoxyhexose moiety were also observed. The ^{13}C NMR spectrum (**Table 3.1**) of **1** displayed 34 signals, of which 17 were assigned to the aglycone moiety, including two aromatic rings and one hydroxyethyl group; the remaining 17 signals corresponded to two hexoses and one pentose sugar residues. The 1H NMR spectrum (**Table 3.1**) of **1** displayed proton signals characteristic of a *t*-caffeoyl group [three aromatic protons resonating at δ 6.80 (1H, d, $J = 8.0$ Hz), 6.90 (1H, dd, $J = 8.0, 2.0$ Hz), 7.05 (1H, d, $J = 2.0$ Hz) as an ABX system and two *trans* olefinic protons as an AB system at δ 6.30, 7.58 (1H, d, $J = 16.0$ Hz)] and 3,4-dihydroxyphenylethanol moiety [three aromatic protons at δ 6.56 (1H, dd, $J = 8.0, 2.0$ Hz), 6.64 (1H, d, $J = 2.0$ Hz), 6.70 (1H, d, $J = 8.0$ Hz) as an ABX system and an A_2B_2 system assigned to a hydroxyethyl group at δ 2.78 (2H, m), 3.76 (1H, m), 3.96 (1H, m)] (Karioti *et al.* 2003). Additionally, three signals assignable to anomeric protons indicated the presence of three sugar moieties: a doublet at δ 4.36 (1H, $J = 7.8$ Hz, H-1 of glucose), a broad singlet at δ 5.45 (1H, $J = 1.8$ Hz, H-1 of rhamnose) and one doublet at δ 4.34 (1H, $J = 7.5$ Hz, H-1 of xylose), consistent with the following C-1 configuration: β for glucose, α for rhamnose, and β for xylose. These findings matched those in the HSQC/ ^{13}C NMR spectra, where three corresponding anomeric carbons resonated at δ 104.1, 101.6, and 107.3, respectively. Other remaining 1H and ^{13}C NMR signals were assigned with the aid of 2D NMR spectra including 1D-TOCSY, DQF-COSY, HSQC, and HMBC spectra. The downfield shift of C-3' (83.8 ppm) of glucose indicated that this position was a glycosylation site. This finding was further confirmed by HMBC

experiments, where a crosspeak between H-1_{rha} (δ 5.45) and C-3_{glc} (83.8 ppm) was observed. The carbon resonances assigned to the β -xylose unit revealed no unusual chemical shifts, suggesting its terminal position. A further site of connectivity was proved to be C-2 of rhamnose, on the basis of ^1H and ^{13}C NMR spectra, as well as HMBC correlations between H-1_{xy} (δ 4.34) and C-2_{rha} (82.3 ppm). The acylation site was on C-6 of glucose as evidenced by the strong deshielding of H-6a_{glc} and H-6b_{glc} at δ 4.36 and 4.52 and the crosspeak between H-6a_{glc} and H-6b_{glc} and COO at 169.0 ppm. The configuration of the sugar units was assigned after hydrolysis of **1** with 1N HCl and GC analysis of trimethylsilylated sugar through a chiral column. On the basis of these data, compound **1** was determined to be the new phenylpropanoid glycoside β -(3,4-dihydroxyphenyl)ethyl-*O*- β -D-xylopranosyl-(1 \rightarrow 2)- α -L-rhamnopyranosyl-(1 \rightarrow 3)-6-*O*-*t*-caffeoyl- β -D-glucopyranoside.

Compound **2** molecular formula was determined as C₃₅H₅₀O₁₆ from its HRESIMS (m/z 727.3204 [M+H]⁺) and ^{13}C NMR data. The ESIMS spectrum of **2** showed a quasimolecular ion peak at m/z 749 [M+Na]⁺ and peaks at m/z 689 [M+Na-60]⁺, 531 [M+Na-218]⁺, 471 [M+Na-218-60]⁺ and 411 [M+Na-218-60-60]⁺ due to the loss of two acetyl groups and an esterified acyl group. The ^1H and ^{13}C NMR spectra (**Table 3.2**) revealed the existence of five acetoxyl signals, a methine doublet (δ 1.20, d, J = 6.5 Hz) coupled with a methyne quartet (δ 5.10, q, J = 6.5 Hz), and a methyl singlet (δ 1.58) arisen from a 2,3-diacetoxy-2-methylbutanoyloxy moiety, together with the characteristic signals of a *neo*-clerodane diterpene having a 4 α ,17-oxirane bicycle [δ_{H} 2.63, 2.91 (H₂-17), δ_{C} 41.8 (C-17); δ_{C} 64.0 (C-4)]. Analysis of 2D NMR spectra showed that compound **2** possessed a hexahydrofurofuran ring moiety typical of 14-hydroclerodin (Ohno *et al.*, 1996). In fact, protons H-11, H-15, and H-16 appeared as a pair of signals: H-11 α δ 4.04 and 4.65 (dd, J = 11.0, 6.2 Hz, 0.5 H each); H-15 δ 5.33 and 5.45 (br d, J = 5.7 Hz, 0.5 H each), and H-16 δ 5.61 and 5.65 (d, J = 5.2, 4.3 Hz, 0.5 H

each). The ^{13}C NMR spectrum of **2** was in complete agreement with the proposed structure and with the previously reported ^{13}C NMR data of other *neo*-clerodane diterpenes isolated from the genus *Clerodendrum* containing the same C-11/C-16 moiety (Pandey *et al.*, 2005). The elucidation of the whole skeleton was achieved on the basis of 1D-TOCSY, DQF-COSY, HSQC, and HMBC correlations, which also allowed the assignment of all the resonances in the ^{13}C NMR spectrum of the pertinent carbons. HMBC correlations from H-1 to C-2, C-5 and C-10, from H-3 to C-4 and C-17, from H-16 to C-11, C-13, and C-15, from H-12 to C-13, C-14, and C-16, from H-18 to C-4, C-5, C-6, and C-10, confirmed the assignment of the *neo*-clerodane ring carbons. The peak correlating signals at δ 5.46 (H-3) and 169.2 ppm and δ 4.90 (H-2) and 172.2 ppm showed that an acetoxy group and 2,3-diacetoxy-2-methylbutanoyloxy function were attached at C-2 and C-3, respectively. Elucidation of the relative stereochemistry of **2** was mostly based on the close similarities of its NMR data to those of similar compounds (Pandey *et al.*, 2005; Jannet *et al.*, 1999). Thus, compound **2** was assigned as a mixture of C-15 epimers of 2 α -acetoxy-3 β -(2',3'-diacetoxy-2'-methyl)-butanoyloxy-14-hydro-15-hydroxyclerodin.

The molecular formula of compound **3** ($\text{C}_{24}\text{H}_{36}\text{O}_9$) was established by ^{13}C NMR and HRESIMS spectrum (m/z 469.2500 for $[\text{M}+\text{H}]^+$). In the ESIMS spectrum two main fragments at m/z 425 $[\text{M}-\text{H}-42]^-$ and 383 $[\text{M}-\text{H}-42-42]^-$ due to the loss of two acetyl groups, were also observed. Its NMR spectral data (**Table 3.2**) suggested that the structure of **3** resembled that of **2**, but differed in the A ring substitutions. The observed differences in the NMR spectra of **3** and **2** were consistent with the presence in **3** of a hydroxyl group linked at C-3 instead of 2,3-diacetoxy-2-methyl-butanoyloxy group and one acetoxy group at C-2 in **2**. Thus, the structure of **3** was deduced to be a mixture of C-15 epimers of 3 β ,15-dihydroxy-14-hydroclerodin.

Compound **4** ($\text{C}_{31}\text{H}_{46}\text{O}_{14}$) showed a quasimolecular ion peak at m/z 643.2899 $[\text{M}+\text{H}]^+$ in the positive HRESIMS. The prominent fragment ion observed in the

ESIMS spectrum at m/z 486 $[M+Na-176]^+$ suggested the presence of a 2'-hydroxy-3'-acetoxy-2'-methylbutanoyl moiety in **4**. Analysis of the 1H and ^{13}C NMR spectra (**Table 3.3**) of **4** clearly indicated that it also belonged to the *neo*-clerodane diterpenoid class. Furthermore, by direct comparison of the NMR spectra of **4** with those of *neo*-clerodane derivatives isolated from *Clerodendrum* genus it was obvious that the compounds contained common functionalities. The 1H NMR spectrum showed signals due to one tertiary methyl (δ 1.02, 3H, s), one secondary methyl (δ 0.93, 3H, $J = 6.0$ Hz), three acetate residues (δ 1.91, 1.99, and 2.11, each 3H, s), and a methyl doublet (δ 1.27, d, $J = 6.5$ Hz) coupled with a methine quartet (δ 5.12, q, $J = 6.5$ Hz) and a methyl singlet (δ 1.29, s) arising from the 2'-hydroxy-3'-acetoxy-2'-methylbutanoyloxy moiety in the C-3 β position. It also showed the two AB quartets, typical of a primary carbinol methylene group at δ 4.51 and 4.65 (2H, $J = 12.0$ Hz each, H-18), an epoxide methylene group at δ 2.64 and 2.90 (2H, $J = 4.0$ Hz each, H-17), a doublet of doublets at δ 4.82 (1H, $J = 11.0, 4.5$ Hz, H-6) due to a C-6 proton, a multiplet at δ 3.64 (1H, m, H-2), and a doublet at δ 5.15 (1H, $J = 6.6$, H-3) due to C-3 proton. Signals at δ 1.80 (1H, m, H-14 a), 1.95 (1H, m, H-14b), 2.06 (1H, m, H-12a), 2.37 (1H, m, H-12b), 2.86 (1H, m, H-13), 3.67 (1H, m, H-15a), 3.72 (1H, m, H-14b) indicated the presence of a β -substituent carrying a five membered lactone ring. The structure of compound **4** was further confirmed by its ^{13}C NMR spectrum. A lowfield ^{13}C NMR resonance at 181.0 ppm suggested the presence of an 11,16-lactone. Besides the spectrum contained signals at δ 13.8 and 16.2 due to the C-19 and C-20 methyl groups, respectively. Signals attributable to the three acetate groups appeared at δ 171.5, 171.7, 172.6, and at δ 21.2 (2 signals overlapped) and 21.3, where the signals due to carbons bearing the acetate groups appeared at δ 62.5 (C-18) and 72.2 (C-6). The carbon involved in the oxirane ring formation resonated at δ 43.2 (C-17) and 64.0 (C-4). Other significant signals were observed at δ 34.3 (C-14), 39.9 (C-13), and 60.0 (C-15). The

elucidation of the whole skeleton from the above subunits was achieved on the basis of 1D-TOCSY, DQF-COSY, HSQC, and HMBC correlations, which also allowed the assignment of all the resonances in the ^{13}C NMR spectrum. The 11,16-lactone ring was confirmed by HMBC correlations between H-12, H-13, and H-14 and C-16. Consequently, **4** was characterized as $2\alpha,15$ -dihydroxy- 3β -(2'-hydroxy-2'-methyl-3'-acetoxy)-butanoyloxy- $6\alpha,18$ -diacetoxy- $4\alpha,17$ -epoxy-clerodan-11,16-lactone.

The HRESIMS of **5** showed a quasimolecular ion $[\text{M}+\text{H}]^+$ at m/z 485.2423, consistent with a molecular formula of $\text{C}_{24}\text{H}_{36}\text{O}_{10}$. In the ESIMS spectrum two fragments at m/z 447 $[\text{M}+\text{Na}-60]^+$ and 387 $[\text{M}+\text{Na}-60-60]^+$ indicated the loss of two acetoxy residues. The NMR data of **5** (Table 3.3) were similar to those of **4** differing in the values of A ring and values of H-13/C-13, H-14/C-14, H-15/C-15 (2.90/45.0 in **5** vs 2.86/39.9 in **4**, 4.06/72.6 in **5** vs 1.95, 1.89/34.3 in **4**, 3.49, 3.60/64.9 in **5** vs 3.67, 3.72/60.0 in **4**, respectively). The observed differences in the NMR spectra of **5** and **4** were consistent with the presence in **5** of a hydroxyl group linked at C-3 instead of 2-hydroxy-3-acetoxy-2-methyl-butanoyloxy group and one acetoxy group at C-2 in **4**. Another difference was the presence in **5** of a 14,15-diol moiety. The absolute configuration of the 14,15-diol moiety of **5** was determined by the circular dichroism (CD) induced after in-situ complexation with dimolybdenum tetracetate in DMSO solution (Di Bari *et al.*, 2001). According to a rule proposed by Snatzke (Frelek *et al.*, 1999), the sign of the diagnostic band at about 305 nm correlated with the absolute configuration of the chiral centers in the 1,2-diol moiety. In particular an *S*-monosubstituted glycol gives rise to a positive Cotton effect at 305 nm, while a negative sign led to the assignment of *R*-configuration. Thus the 305 nm sign observed in the CD spectrum of **5** allowed us to assign the *S*-configuration to C-14. Thus, compound **5** was assigned the structure of $3\beta,14S,15$ -trihydroxy- $6\alpha,18$ -diacetoxy- $4\alpha,17$ -epoxy-clerodan-11,16-lactone.

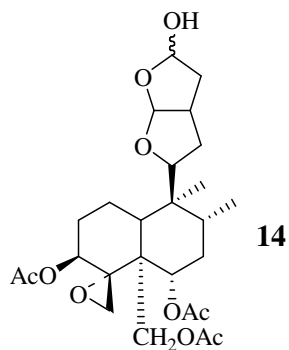


Figure 3.5: Structure of a known diterpene isolated from *C. splendens*

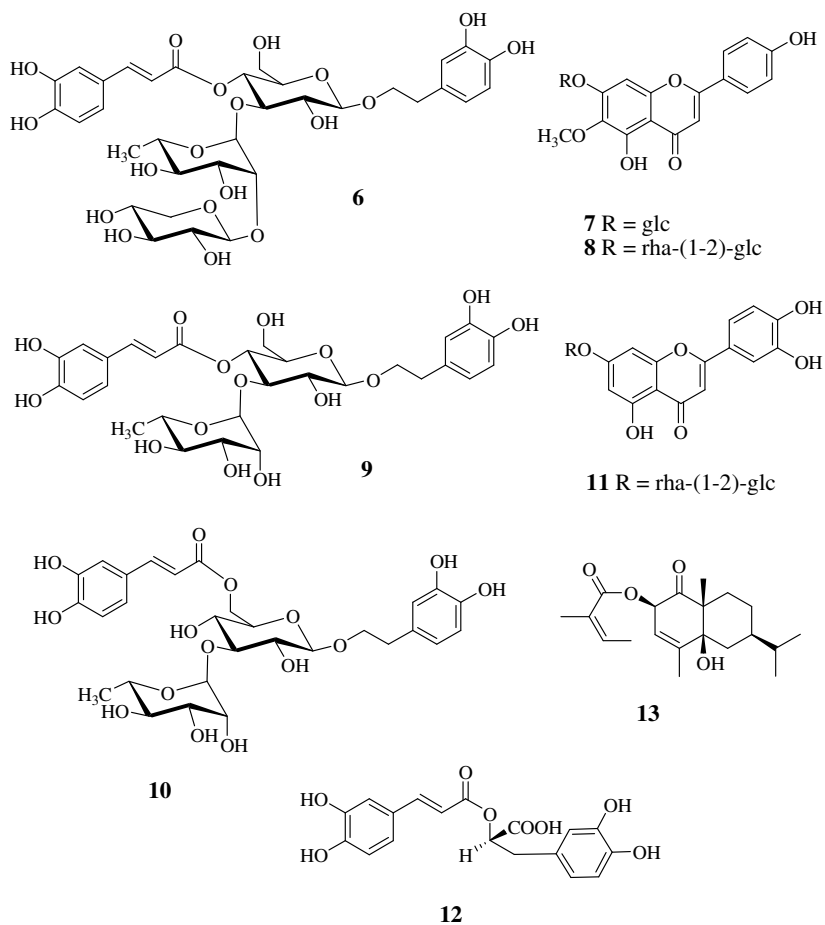


Figure 3.6: Structures of known compounds

Table 3.1: ^1H and ^{13}C NMR data of compound **1** (CD_3OD , 600 MHz)^a

1		
Position	δ_{H}	δ_{C}
1 Aglicone		130.5
2	6.64 d (2.0)	115.9
3		146.2
4		145.0
5	6.70 d (8.0)	116.8
6	6.56 dd (8.0, 2.0)	121.2
β	2.78 m	36.3
α a	3.76 m	72.1
α b	3.96 m	
1' Glc	4.36 d (7.8)	104.1
2'	3.55 dd (9.0, 7.8)	74.8
3'	3.50 t (9.0)	83.8
4'	3.45 t (9.0)	70.5
5'	3.28 m	75.0
6' a	4.52 dd (12.0, 3.0)	64.4
6' b	4.36 dd (12.0, 4.5)	
1'' Rha	5.45 d (1.8)	101.6
2''	3.99 dd (3.0, 1.8)	82.3
3''	3.77 dd (9.0, 3.0)	72.1
4''	3.38 t (9.0)	74.0
5''	3.98 m	69.7
6''	1.24 d (6.5)	17.7
1''' Xyl	4.36 d (7.5)	107.3
2'''	3.38 dd (9.0, 7.5)	74.5
3'''	3.90 t (9.0)	77.8
4'''	3.47 m	70.5
5''' a	3.22 dd (12.0, 4.5)	67.0
5''' b	3.86 dd (12.0, 3.0)	
1'''' Caffeic acid		127.8
2''''	7.05 d (2.0)	115.0
3''''		149.7
4''''		145.6
5''''	6.80 d (8.0)	116.4
6''''	6.90 dd (8.0, 2.0)	123.2
α'	6.30 (16.0)	114.7
β'	7.58 (16.0)	147.5
OCO		169.0

Table 3.2: ^1H and ^{13}C NMR data of compounds 2 and 3 (CD_3OD , 600 MHz)^a

Position	2		3	
	δ_{H}	δ_{C}	δ_{H}	δ_{C}
1 a	2.75 m	28.0	1.75 m	21.1
1 b	1.85 m		2.28 m	
2 a	4.90 ^b	71.6	1.30 m	31.3
2 b			1.82 m	
3	5.46 d (10.5)	68.3	3.98 m	65.4
4		64.0		68.0
5		47.0		49.4
6	4.87 dd (11.0, 4.5)	72.0	4.80 dd (11.0, 4.5)	71.7
7 a	1.60 m	32.4	1.70 m	33.0
7 b	1.92 m		1.42 m	
8	1.55 m	37.0	1.54 m	36.8
9		41.6		42.0
10	1.92 m	43.0	1.78	47.6
11	4.65 dd (11.0, 6.2)	84, 85.1	4.63 dd (11.0, 6.0)	84.6, 84.7
	4.04 dd (12.0, 5.0)		3.99 dd (12.0, 5.0)	
12 a	1.70 m	33.7	1.61 m	32.8
12 b	1.48 m		2.06 m	
13	3.11 m	41.0	2.97 m	40.2
14 a	2.26 m	40.6	2.07 m	49.7
14 b	1.78 m		1.78 m	
15	5.45 br d (5.7), 5.33br d (3.0)	99.3, 99.6	5.45 br d (5.0), 5.54 br d (4.6)	97.09, 98.5
16	5.61 d (5.2), 5.65 d (4.3)	108.2, 109.8	5.71 d (4.7), 5.67 d (6.2)	106.8, 108.7
17 a	2.63 (4.0)	41.8	2.84 d (3.5)	41.6
17 b	2.91 (4.0)		2.72 d (3.5)	
18 a	4.52 d (12.3)	62.7	4.91 d (12.5)	61.6
18 b	4.82 d (12.3)		4.33 d (12.5)	
19	0.96 s	15.0	0.92 d (6.5)	13.0
20	0.94 d	15.2	0.95 s	15.9
OCOCH_3	2.10, 2.10, 1.97 s	21.3, 21.3, 20.3	2.10, 1.93 s	19.7, 20.2
O^-COCH_3		172.2, 171.8, 170.0		172.8, 171.2
1'		169.2		
2'		83.5		
3'	5.10 q (6.5)	73.0		
4'	1.20 d (6.5)	15.0		
5'	1.58 s	15.2		
COCH_3	2.10, 1.92 s	21.3, 21.2		
COCH_3		171.9		
O^-COCH_3		172.2, 171.8, 170.0		

Table 3.3: ^1H and ^{13}C NMR data of compounds 4-5 (CD_3OD , 600 MHz)^a

Position	4		5	
	δ_{H}	δ_{C}	δ_{H}	δ_{C}
1 a	1.83 m	32.0	1.85 m	22.7
1 b	2.19 m			
2a	3.64 m	71.0	1.40 m	34.3
2b			2.12 br dd (11.5, 4.5)	
3	5.15 d (6.6)	74.4	4.02 dd (11.5, 5.43)	66.3
4		64.0		68.4
5		47.2		47.9
6	4.82 dd (11.6, 4.5)	72.2	4.84 t (9.0)	73.0
7 a	1.70 m	33.7	1.75 m	34.3
7 b	1.50 m		1.50 m	
8	1.67 m	35.6	1.65 m	35.5
9		42.5		48.0
10	1.95 dd	43.1	1.92 dd	43.1
11	4.70 t (9.0)	89.9	4.72 t (9.0)	88.5
12 a	2.37 br dd (13.0, 9.0)	28.4	2.31 m	23.0
12 b	2.06 m	-	2.22 m	
13	2.86 m	39.9	2.90 m	45.0
14 a	1.80 m	49.7	4.06 m	72.6
14 b	1.95 m	34.3		
15 a	3.72 m	60.0	3.49 dd (7.2, 12.0)	64.9
15 b	3.67 m		3.60 dd (6.2, 11.2)	
16		181.0		181.0
17 a	2.64 d (3.5)	43.2	2.75 d (4.5)	43.2
17 b	2.90 d (3.5)		2.90 d (4.5)	
18 a	4.51 d (11.5)	62.5	4.36 d (12.0)	62.8
18 b	4.65		4.94 d (12.0)	
19	1.02 s	13.8	1.03 s	14.0
20	0.93 d (6.0)	16.2	0.96 d (6.6)	16.4
OCOCH_3	2.11, 1.99 s	21.3, 21.2	2.12, 1.96 s	21.2, 21.4
OCOCH_3		172.6, 171.5		172.7, 171.4
1'		172.0		
2'		77.9		
3'	5.12 q (6.5)	75.0		
4'	1.27 d (6.5)	13.6		
5'	1.29 s	22.0		
OCOCH_3 '	1.91 s	21.2		
OCOCH_3 '		171.7		

^a J values for **Tables 3.1, 3.2, and 3.3** are in parentheses and reported in Hz; chemical shifts are given in ppm; assignments were confirmed by DQF-COSY, 1D-TOCSY, HSQC, and HMBC experiments.

^b overlapped signal

Chapter 4

Phytochemical study of Sideritis pullulans Vent.

Chapter 4

4.1 Introduction: *Sideritis* genus

The genus *Sideritis* belongs to Lamiaceae family and comprises more than 150 species widely distributed in temperate and tropical regions of the Northern Hemisphere. Most species are mainly found in the Mediterranean area, together with Canary and Madeira islands. It is a genus characterized by a high number of hybridizations between species. The genus name derives from the Greek word “*sideros*” in reference to the use given for these plants since ancient times to heal wounds by weapons made with this metal (González-Burgos *et al.*, 2011). The *Sideritis* species are widely used in the treatment of gastrointestinal disorders, rheumatism, cough, and they are commonly used as herbal tea in folk medicine in Mediterranean country (Guvenc *et al.*, 2010).

The aerial parts of plants from the genus, known as ‘mountain tea’, are used in popular folk medicine for gastrointestinal disorders such as stomach ache, indigestion, flatulence, to alleviate the symptoms of common colds and for tonic and diuretic effects (Erkan *et al.*, 2011). Moreover, some compounds isolated from *Sideritis* spp. have shown antiproliferative, anti-HIV or antifeedant activities. Anti-inflammatory, antioxidant, antiulcerogenic, antimicrobial, antiherpetical activities are also reported for extracts of *Sideritis* spp. Moreover, it is known that diterpenoids isolated from this genus are responsible of antifeedant, antimicrobial, and anti-inflammatory activities (González-Burgos *et al.*, 2011).

4.2 *Sideritis pullulans* Vent.

Sideritis pullulans Vent. (**Figure 4.1**) is a perennial herb of 50-80 cm with yellowish and coriaceous floral leaves. The upper part is endowed with short dense glandular hairs (Al-Eisawi, 1982). The common name of this plant is “ironwort”. Previously, only the composition of the essential oil was studied, showing a moderate antifungal activity against some phytopathogenic fungi (Abou-Jawdah *et al.*, 2004). To date no phytochemical study on *S. pullulans* is reported.



Figure 4.1: *Sideritis pullulans* Vent.

4.3 Plant material

Aerial parts and roots of *S. pullulans* were collected in As-Salt Rocky mountains, Jordan, during the flowering stage in June 2009. The plant was identified by Dr. Ammar Bader. The voucher specimen (No. Jo-It 2009/2) was deposited at the Herbarium of the Pharmacognosy Laboratory, Umm Al-Qura University, Makkah, Saudi Arabia.

4.4 Extraction and isolation

Dried powdered leaves (500 g) and roots (400 g) of *S. pullulans* were successively and separately extracted for 48 h with *n*-hexane, CHCl₃, CHCl₃-MeOH (9:1), and MeOH, by exhaustive maceration (2 l), to give 5.6, 7.2, 8.9, and 26.9 g of the respective residues for the leaves and 0.8, 1.0, 8.0, and 49.5 g of the respective residues for the roots.

Part of the aerial parts CHCl₃ extract (7 g) was chromatographed over silica gel column using an Isolera[®] Biotage[®] flash purification system, eluting with CHCl₃ followed by increasing concentrations of MeOH in CHCl₃ (between 1% and 50%). Fractions of 25 ml were collected, analyzed by TLC (silica gel plates, in CHCl₃ or mixtures of CHCl₃-MeOH 99:1, 98:2, 97:3, 9:1, 4:1), and grouped into 10 fractions (A-L). Fraction B (149 mg) was purified by RP-HPLC with MeOH-H₂O (5.5:4.5) as eluent to obtain the new diterpene, 3 α ,7 β -dihydroxy-18-acetyloxy-17-*norkauran*-16-one (compound **4**, 1.1 mg, t_R = 15 min). Fractions D (125.7 mg) and H were purified by RP-HPLC with MeOH-H₂O (3:2) as eluent to obtain the known diterpenes *ent*-3 α ,7 β ,17-trihydroxy-18-acetyloxy-15 α ,16 α -epoxykaurane (compound **9**, 1.2 mg, t_R = 10 min) and foliol or *ent*-3 α ,7 β ,18-trihydroxy-kauran-16-ene (compound **10**, 1.9 mg, t_R = 65.3 min) from fraction D and the new compounds *ent*-1 α ,3 α ,7 β ,18-tetrahydroxy-kauran-16-ene (compound **1**, 1.2 mg, t_R = 18 min) and *ent*-7 β ,16 α ,17,18-tetrahydroxykaurane (compound **6**,

1.9 mg, $t_R = 10$ min) from fraction H. Fraction E (230.9 mg), purified by RP-HPLC with MeOH-H₂O (6.5:3.5) as eluent, gave the new diterpene *ent*-3 α ,11 α ,18-trihydroxykauran-16-ene (compound **2**, 1.2 mg, $t_R = 21$ min) and compound **10** (15 mg, $t_R = 35$ min). Fractions F (125.7 mg), G (152.8 mg) and I (83.5 mg) were purified by RP-HPLC with MeOH-H₂O (4.5:5.5) as eluent to obtain syringaresinol 4'-*O*- β -D-glucopyranoside (compound **11**, 1.7 mg, $t_R = 10$ min), the new *ent*-3 α ,7 β ,18-trihydroxy-17-*nor*kauran-16-one (compound **3**, 1.8 mg, $t_R = 22$ min) and compound **9** (1.4 mg, $t_R = 24$ min) from fraction F, compound **11** (4.6 mg) and the new *ent*-3 α ,7 β ,16 α ,17-tetrahydroxy-18-acetyloxy-kaurane (compound **5**, 4.6 mg, $t_R = 19$ min) from fraction G and the iridoid 6-*O*-acetylmiosporoside (compound **12**, 4.2 mg, $t_R = 24$ min) from fraction I. Fraction L (86.4 mg), purified by RP-HPLC with MeOH-H₂O (7:3) as eluent, gave the diterpene linearol or *ent*-3 α ,7 β -dihydroxy-18-acetyloxy-kauran-16-ene (compound **13**, 3.5 mg, $t_R = 24$ min).

Part of the CHCl₃-MeOH extract (6.0 g) of the roots was chromatographed over Sephadex LH-20 to give eight major fractions (A-H) grouped by TLC. Fraction B (975 mg) was partitioned between *n*-BuOH and H₂O and the *n*-butanol portion (827 mg) was submitted to silica gel chromatography using an Isolera[®] Biotage[®] flash purification system and obtaining two major fractions (B₁-B₂). Fraction B₁ (92.5 mg) was purified by RP-HPLC with MeOH-H₂O (3.3:6.7) as eluent to give di-*O*-methylcrenatin (compound **14**, 2.8 mg, $t_R = 7$ min) and 1-hydroxy-syringaresinol-1- β -D-glucopyranoside (compound **15**, 1.8 mg; $t_R = 19$ min). Fraction B₂ (101.7 mg) was purified by RP-HPLC with MeOH-H₂O (4.5:5.5) as eluent to give leonoside A or stachyoside C (compound **16**, 3.8 mg, $t_R = 11$ min) and the new phenylpropanoid β -(3-methoxy-4-hydroxyphenyl)-ethyl-*O*- α -L-arabinopyranosyl-(1 \rightarrow 2)-L-rhamnopyranosyl-(1 \rightarrow 3)-6-*O*-feruloyl- β -D-glucopyranoside (compound **7**, 3.9 mg, $t_R = 30$ min). Fraction D (260 mg) was partitioned between *n*-BuOH and H₂O and the *n*-butanol portion (200 mg) was submitted to silica gel chromatography using an Isolera[®] Biotage[®] flash

purification system and obtaining two major fraction (D₁-D₂). Fraction D₂ (25.7 mg), purified by RP-HPLC with MeOH-H₂O (2:3) as eluent, gave the new phenylpropanoid β-(3,4-dihydroxyphenyl)-ethyl-*O*-α-L-arabinopyranosyl-(1→2)-L-rhamnopyranosyl-(1→3)-6-*O*-feruloyl-β-D-glucopyranoside (compound **8**, 3.4 mg, *t*_R = 30 min). Fraction F (272.8 mg) was purified by RP-HPLC with MeOH-H₂O (5.5:4.5) as eluent to obtain the following flavonoids isoscutellarein-7-[6'''-*O*-acetyl-β-D-allopyranosyl (1→2)]-β-D-glucopyranoside (compound **17**, 31 mg, *t*_R = 12 min), 4-methoxy-isoscutellarein-7-[6'''-*O*-acetyl-β-D-allopyranosyl (1→2)]-β-D-glucopyranoside (compound **18**, 4.6 mg, *t*_R = 23 min) and isoscutellarein-7-[6'''-*O*-acetyl-β-D-allopyranosyl-(1→2)]-6''-*O*-acetyl-β-D-glucopyranoside (compound **19**, 2.9 mg, *t*_R = 29 min). Fraction H (170.6 mg), purified by RP-HPLC with MeOH-H₂O (5.5:4.5) as eluent, gave isoacteoside (compound **20**, 3.4 mg, *t*_R = 30 min) and apigenin-7-*O*-[6'''-*O*-acetyl-β-D-allopyranosyl-(1→2)]-β-D-glucopyranoside (compound **21**, 3.4 mg, *t*_R = 30 min).

4.5 New isolated compounds

ent-1α,3α,7β,18-tetrahydroxy-kauran-16-ene (1)

Amorphous powder; $[\alpha]_{\text{D}}^{25}$ -9 (*c* 0.1, MeOH); HRESIMS *m/z* 359.3084 (calcd. for C₂₀H₃₂O₄Na, 359.2198); ESI-MS *m/z* 359 [M+Na]⁺; ¹H and ¹³C NMR, see **Tables 4.1** and **4.3**.

ent-3α,11α,18-trihydroxy-17-norkauran-16-ene (2)

Amorphous powder; $[\alpha]_{\text{D}}^{25}$ -25.3 (*c* 0.1, MeOH); HRESIMS *m/z* 343.2141 (calcd. for C₂₀H₃₂O₂Na, 343.2249); ESI-MS *m/z* 319 [M-H]⁻; ¹H and ¹³C NMR, see **Tables 4.1** and **4.3**.

ent-3 α ,7 β ,18-trihydroxy-17-norkauran-16-one (3)

Amorphous powder; $[\alpha]_{\text{D}}^{25}$ -22.3 (*c* 0.1, MeOH); HRESIMS *m/z* 345.2029 (calcd. for C₁₉H₃₀O₄Na, 345.2042); ESI-MS *m/z* 345 [M+Na]⁺; ¹H and ¹³C NMR, see **Tables 4.1** and **4.3**.

3 α ,7 β -dihydroxy-18-acetyloxy-17-norkauran-16-one (4)

Amorphous powder; $[\alpha]_{\text{D}}^{25}$ -23.3 (*c* 0.1, MeOH); HRESIMS *m/z* 387.2180 (calcd. for C₂₁H₃₂O₅Na, 387.2147), ESI-MS *m/z* 387 [M + Na]⁺; ¹H and ¹³C NMR, see **Tables 4.2** and **4.3**.

ent-3 α ,7 β ,16 α ,17-tetrahydroxy-18-acetyloxy-kaurane (5)

Amorphous powder; $[\alpha]_{\text{D}}^{25}$ -22 (*c* 0.1, MeOH); HRESIMS *m/z* 419.5332 (calcd. for C₂₂H₃₆O₆Na, 419.2410), ESI-MS *m/z* 419 [M + Na]⁺; ¹H and ¹³C NMR, see **Tables 4.2** and **4.3**.

ent-7 β ,16 α ,17,18-tetrahydroxykaurane (6)

Amorphous powder; $[\alpha]_{\text{D}}^{25}$ +16.6 (*c* 0.1, MeOH); HRESIMS *m/z* 361.2896 (calcd. for C₂₀H₃₄O₂Na, 361.2355); ESI-MS *m/z* 337 [M - H]⁻; ¹H and ¹³C NMR, see **Tables 4.2** and **4.3**.

β-(3-methoxy-4-hydroxyphenyl)-ethyl-*O*- α -L-arabinopyranosyl-(1 \rightarrow 2)-L-rhamnospyranosyl-(1 \rightarrow 3)-6-*O*-feruloyl- β -D-glucopyranoside (7)

Amorphous powder; $[\alpha]_D^{25}$ -21 (c 0.1, MeOH); UV (MeOH) λ_{\max} (log ϵ) 240 (3.95), 300sh (3.88), 329 (4.10) nm; HRESIMS m/z 807.2660 (calcd. for C₃₆H₄₈O₁₉Na, 807.2687); ESI-MS m/z 807 [M+Na]⁺, 675 [M+Na-132]⁺, 529 [M+Na-132-146]⁺; ¹H and ¹³C NMR, see **Table 4.4**.

β-(3,4-dihydroxyphenyl)-ethyl-*O*- α -L-arabinopyranosyl-(1 \rightarrow 2)-L-rhamnopyranosyl-(1 \rightarrow 3)-6-*O*-feruloyl- β -D-glucopyranoside (8)

Amorphous powder; $[\alpha]_D^{25}$ -26 (c 0.1, MeOH); UV (MeOH) λ_{\max} (log ϵ) 239 (3.85), 330 (4.01) nm; HRESIMS m/z 793.4194 (calcd. for C₃₅H₄₆O₁₉Na, 793.2531); ESI-MS m/z 793 [M+Na]⁺, 661 [M+Na-132]⁺, 515 [M+Na-132-146]⁺; ¹H and ¹³C NMR, see **Table 4.4**.

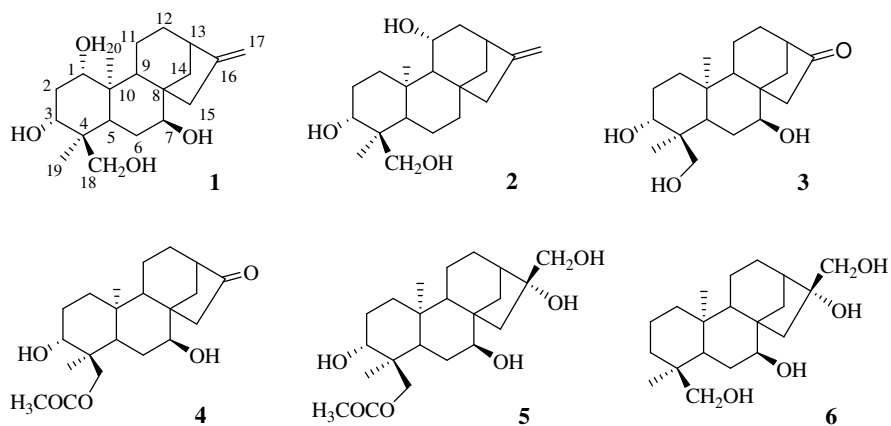


Figure 4.2: Structures of new diterpenes isolated from *S. pullulans*

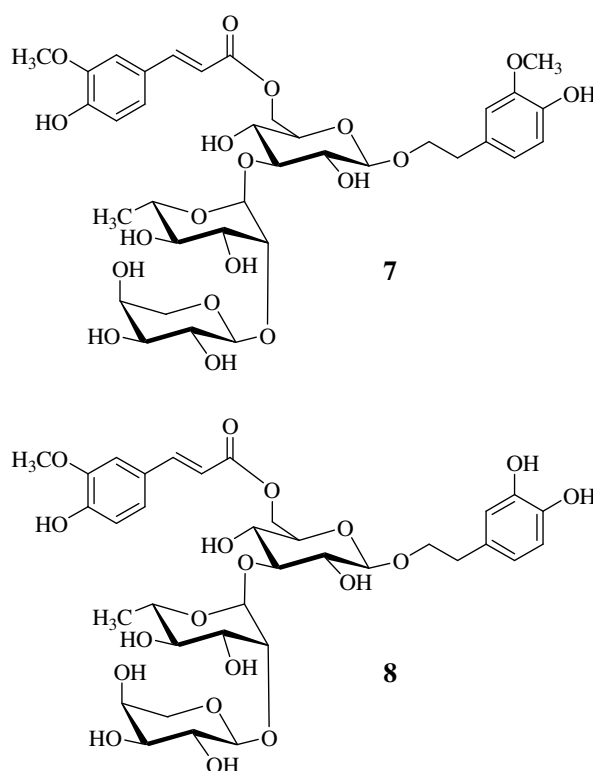


Figure 4.3: Structures of compounds 7 and 8

4.6 Structural elucidation

Compound **1** showed a molecular ion peak at m/z 359.3084 $[M+Na]^+$ in the HRESIMS. The resulting molecular formula was determined to be $C_{20}H_{32}O_4$ showing five degrees of unsaturation. The ^{13}C NMR spectrum (**Table 4.3**) confirmed the presence of twenty carbons consisting of two methyls, seven methylenes one of which hybridized sp^2 , one hydroxymethylene, three methynes, three hydroxymethynes, and four quaternary carbons. The ^{13}C NMR signals at δ_C

80.0, 71.4, 77.6 and 67.6 indicated the presence of four distinct oxygenated carbons. The signals at δ_{C} 67.2 belonged to a hydroxymethylene group. The HMBC spectrum demonstrated a correlation between δ_{C} 67.6 and Me-19 at δ 0.72 and H-5 at δ 1.80, thus the position of the primary hydroxyl group was verified to be at C-18. In the HSQC experiment the methyne signals at δ 77.6 correlated with the proton signals at δ 3.53 (1H, t, $J = 3.8$ Hz). This belonged to an equatorial proton; observation of coupling between this proton and the signals at δ_{H} 1.78 and 1.53 in the DQF-COSY spectrum indicated that the latter signals should be the C-6 methylene protons (Bruno *et al.*, 2002). 1D TOCSY experiments led us to establish the spin system H-1—H-3 showing the presence of a hydroxymethyne group at C-1 and C-3. HMBC correlations between H-3 and C-3, C-5, and Me-19; H-1 and C-5 and Me-20; Me-20 and C-1, C-5, C-8, C-9, and C-10; H-5 and C-3, C-7, C-9, C-18, and Me-19 were also observed. All other methylene and methyne proton signals extended between 1.4 and 2.6 ppm in the ^1H NMR spectrum (**Table 4.1**). The ^{13}C NMR assignments for **1** were confirmed by DQF-COSY, HSQC, and HMBC correlations. All the obtained data indicated the structure to be *ent*-1 α ,3 α ,7 β ,18-tetrahydroxykaur-16-ene for compound **1**.

Compound **2** was assigned the molecular formula $\text{C}_{20}\text{H}_{32}\text{O}_3$, as established by HRESIMS ($[\text{M}+\text{Na}]^+$ at m/z 343.2141) and ^{13}C NMR. The ^1H NMR spectrum (**Table 4.1**) displayed signals due to two tertiary methyl groups at δ 0.74 and 1.29, one hydroxymethylene group at δ 3.27 and 3.53, and one exomethylene group at δ 4.71 and 4.85. The ^{13}C NMR experiments revealed the presence of twenty carbon signals. A comparison of these carbon resonances with those of the related kaurene diterpenes suggested that **2** possessed the same skeleton (de Quesada *et al.*, 1972). The ^1H NMR spectrum of **2** combined with the observation from the 1D TOCSY and DQF-COSY experiments suggested the sequences C-1—C-3, C-5—C-7, C-9—C-14, and C-15—C-17. The location of

the functional groups were confirmed by the key correlations observed in the HMBC experiment; thus, the signal of H₂-17 correlated with C-13 and C-15, that of H-14b with C-7, C-9, C-12, C-15, and C-16, and that of H-11 with C-9, C-10, and C-13, permitting the exomethylene function to be located at C-16/C-17 and an hydroxymethyne group to be placed at C-11. The signal of H-3 correlated with C-1, C-5, and Me-19, that of H₂-18 with C-3, C-4, C-5, and Me-19 allowing a C-3 and C-18 hydroxyl groups to be established. The analysis of the coupling constants of H-3 (dd, $J = 11.6, 4.5$ Hz) and H-11 (br dd, $J = 12.0, 6.5$ Hz) showed an axial orientation, indicating therefore the α -configuration of the C-3 and C-11 hydroxyl groups. Consequently, compound **2** was established as *ent*-3 α ,11 α ,18-trihydroxykaur-16-ene.

Compound **3** (C₁₉H₃₀O₄) showed an [M+Na]⁺ peak at m/z 345.2029. Its ¹H NMR spectrum (**Table 4.1**) showed two methyl singlets at δ 0.78 and 1.19, a hydroxymethylene group at δ 3.34 and 3.55 (both d, $J = 12.0$ Hz) adjacent to a quaternary carbon, and two hydroxymethynes at δ 3.67 and 3.70. From the 1D TOCSY, DQF-COSY and HSQC spectroscopic data, the spin systems C-1—C-3, C-5—C-7, C-9—C-14 were established. The presence of a hydroxyl group at C-3 was revealed as a dd ($J = 12.0, 5.2$ Hz) and the corresponding C-3 carbon signal was observed at 74.2 ppm. This chemical shift and the doublet of doublets are characteristic signals for the α position of C-3 (Gonzalez *et al.*, 1981; Fraga *et al.*, 1987). The presence of a triplet at δ 3.70 ($J = 3.5$ Hz) was indicative of a characteristic H-7 α proton, as observed in similar kaurane diterpenes (Venturella, 1975). The ¹³C NMR spectrum of compound **3** (**Table 4.3**) showed nineteen signals whose assignments were carried out by HSQC and HMBC experiments. The cross peak signals between H-15a and C-9, C-13, and C-14, and H-13 and C-8, C-11, C-15, and C-16 indicated that a carbonyl group was situated at C-16. So, the structure of **3** was determined to be *ent*-3 α ,7 β ,18-trihydroxy-17-nor-kauran-16-one.

The NMR spectroscopic data of **4** (C₂₁H₃₂O₅; HRESIMS at m/z 387.2180 [M+Na]⁺) suggested that its structure resembled that of **3** but differed in the presence of an acetyl group. The main differences in the ¹H NMR spectrum resided in the chemical shifts of an AB system at C-18 (δ 3.87 and 4.03 in **4** versus δ 3.34 and 3.55 in **3**). Compound **4** had identical spectroscopic data that *ent*-3 α ,7 β -dihydroxy-18-acetyloxy-17-norkauran-16-one previously obtained from ozonolysis of linearol (Bruno *et al.* 2001).

Analysis of the DQF-COSY and HSQC experiments of **5** (C₂₂H₃₆O₆; HRESIMS at m/z 419.5332 [M+Na]⁺) indicated the presence of the same partial structure in rings A, B, and C, as that of **4** but showed that ring D was different. In the NMR spectra of compound **5** the presence of 16,17-diol group (a hydroxymethylene at δ 3.63 and 3.73 and a quaternary hydroxylated carbon at δ 81.8) was observed. This was confirmed by the HMBC correlations of H₂-17 and C-13, C-15, and C-16 and H-15a and C-9, C-13, and C-17. Thus, the structure of **5** was determined to be *ent*-3 α ,7 β ,16 α ,17-tetrahydroxy-18-acetyloxy-kaurane.

The HRESIMS of compound **6** (C₂₀H₃₄O₄) showed a molecular ion peak at m/z 361.2896 [M+Na]⁺. Analysis of NMR data of **6** and comparison with those of **5** exhibited that **6** differed from **5** only by the absence of the OH group at C-3 and the acetyl group at C-18 (Tables 4.2 and 4.3). This compound was previously obtained by biotransformation of candicandiol (Fraga *et al.*, 2003). Thus compound **6** was identified as *ent*-7 β ,16 α ,17,18-tetrahydroxykaurane.

Compound **7** molecular formula was determined as C₃₆H₄₈O₁₉ by high-resolution electrospray ionization mass spectrometry (HR-ESIMS) (m/z 807.2660 [M+Na]⁺). Its ESIMS spectrum showed a quasimolecular ion peak at m/z 807 [M+Na]⁺; two main fragments at m/z 675 [M+Na-132]⁺ and 529 [M+Na-132-146]⁺ due to the loss of one pentose and one deoxyhexose moiety were also observed. The ¹³C NMR spectrum (Table 4.4) of **7** displayed 36 signals, of which 19 were assigned to the aglycone moiety; the remaining 17 signals corresponded to two hexoses and one pentose sugar residues. The ¹H NMR

spectrum (**Table 4.4**) of **7** displayed proton signals characteristic of a *t*-feruloyl group (three aromatic protons resonating at δ 6.80 (1H, d, $J = 8.0$ Hz), 7.02 (1H, dd, $J = 8.0, 2.0$ Hz), 7.17 (1H, d, $J = 2.0$ Hz) as an ABX system and two *trans* olefinic protons as an AB system at δ 6.40 and 7.63 ($J = 16.0$ Hz), and 3-methoxy-4-hydroxyphenylethanol moiety [three aromatic protons at δ 6.64 (1H, dd, $J = 8.0, 2.0$ Hz), 6.66 (1H, d, $J = 2.0$ Hz), 6.69 (1H, d, $J = 8.0$ Hz) as an ABX system and an A₂B₂ system assigned to a hydroxyethyl group at δ 2.81 (2H, m), 3.78 (1H, m), 4.04 (1H, m)] (Karioti *et al.* 2003); two methoxyl groups at δ 3.75 and 3.87 were also observed. Additionally, three signals assignable to anomeric protons indicated the presence of three sugar moieties whose identification was obtained from 1D TOCSY, DQF-COSY and HSQC experiment as β -glucose, α -rhamnose, and α -arabinose. All the ¹H and ¹³C NMR signals were assigned with the aid of 2D NMR spectra including 1D-TOCSY, DQF-COSY, HSQC, and HMBC spectra. The downfield shift of C-3 (84.0 ppm) of glucose indicated that this position was a glycosylation site. This finding was further confirmed by HMBC experiment, where a crosspeak between H-1_{rha} (δ 5.49) and C-3_{glc} (84.0 ppm) was observed. The carbon resonances assigned to the α -arabinose unit suggested its terminal position. A further site of connectivity was proved to be C-2 of rhamnose, on the basis of ¹H and ¹³C NMR spectra, as well as HMBC correlations between H-1_{ara} (δ 4.33) and C-2_{rha} (82.5 ppm). The acylation site was on C-6 of glucose as evidenced by the strong deshielding of H-6_{glc} and H-6b_{glc} at δ 4.37 and 4.50 and the crosspeak between H₂-6_{glc} and COO at 169.2 ppm. The configuration of the sugar units was assigned after hydrolysis of **7** with 1N HCl and GC analysis of trimethylsilylated sugar through a chiral column. Thus, compound **7** was determined to be the new phenylpropanoid glycoside β -(3-methoxy-4-hydroxyphenyl)-ethyl-*O*- α -L-arabinopyranosyl-(1 \rightarrow 2)- α -L-rhamnopyranosyl-(1 \rightarrow 3)-6-*O*-*t*-feruloyl- β -D-glucopyranoside.

The HRESIMS of **8** (C₃₅H₄₆O₁₉) showed a sodiated molecular ion at m/z 793.4194 [M+Na]⁺. Analysis of NMR data of compound **8** and comparison with those of **7** showed **8** to differ from **7** only in the absence of a methoxyl group of the aglycon (**Table 4.4**). Therefore, the structure β -(3,4-dihydroxyphenyl)-ethyl-*O*- α -L-arabinopyranosyl-(1 \rightarrow 2)- α -L-rhamnopyranosyl-(1 \rightarrow 3)-6-*O*-*t*-feruloyl- β -D-glucopyranoside was assigned to **8**.

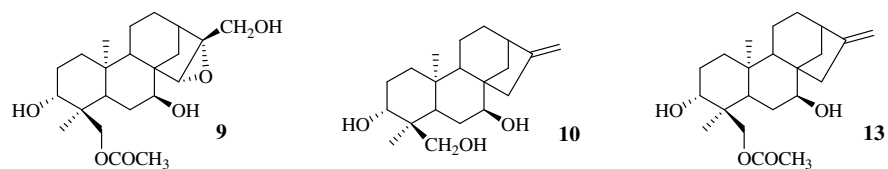


Figure 4.4: Structures of known diterpenes isolated from *S. pullulans*

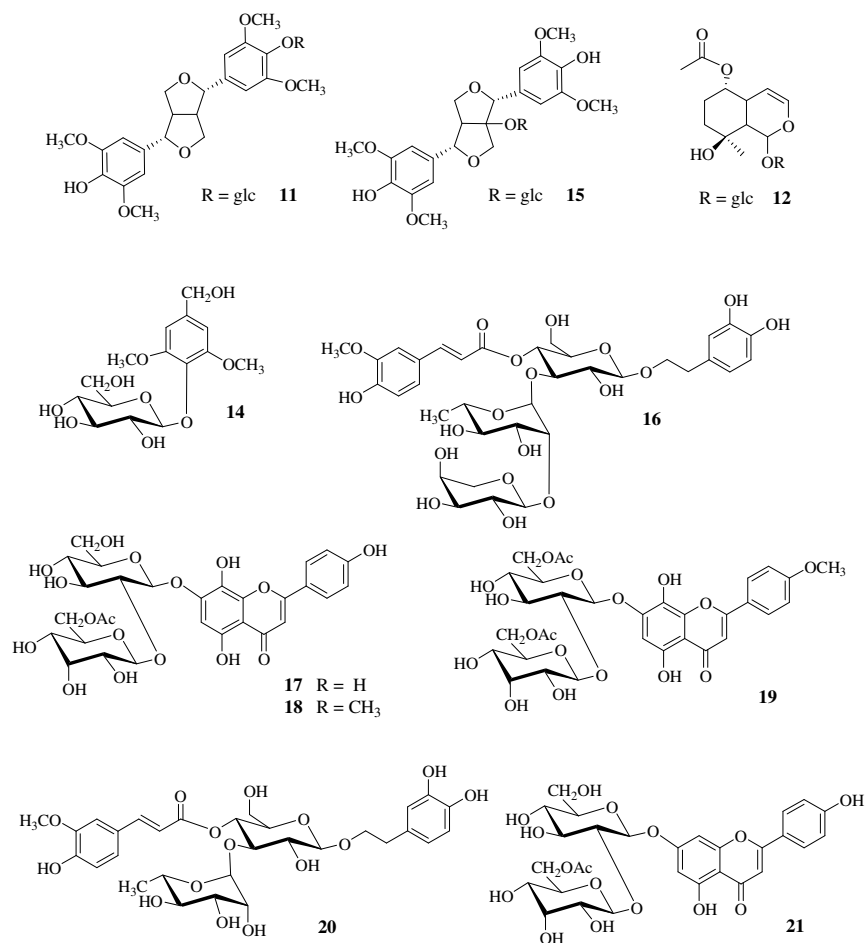


Figure 4.5: Structures of known compounds isolated from *S. pullulans*

Table 4.1: ^1H and data of **1-3** (Methanol- d_4 , 600 MHz)^a

position	1	2	3
1a	3.38 dd (12.0, 5.0)	1.14 br dd (13.0, 10.7)	1.02 ddd (14.0, 13.0, 4.0)
1b		2.77 ddd (13.4, 6.0, 2.8)	1.89 ^b
2a	1.67 m	1.65 m	1.74 ^b
2b	1.80 ^b	1.72 m	1.81 ^b
3a	3.70 dd (12.0, 5.7)	3.66 dd (11.6, 4.5)	3.67 dd (12.0, 5.2)
3b			
5	1.80 ^b	1.25 br d (10.5)	1.87 br d (11.0)
6a	1.63 ^b	1.48 ^b	1.61 ^b
6b	1.78 ^b	1.50 ^b	1.67 m
7a	3.53 t (3.8)	1.52 ^b	3.70 t (3.5)
7b		1.58 ^b	
9	1.70 dd (11.0, 5.0)	1.56 ^b	1.60 ^b
11a	1.63 ^b	4.25 br dd (12.0, 6.5)	1.52 m
11b	1.65 ^b		1.89 ^b
12a	1.43 dd (7.0, 2.0)	1.77 m	1.40 m
12b	1.77 ^b	1.90 ddd (13.0, 9.0, 1.5)	1.76 ^b
13	2.64 m	2.70 m	2.39 m
14a	1.18 m	1.07 dd (12.4, 4.5)	1.54 dd (11.8, 4.5)
14b	1.90 dd (9.0, 2.0)	2.23 br d (11.6)	2.23 br d (11.8)
15a	2.26 br s	2.01 dd (12.8, 2.0)	2.11 d (12.2)
15b		2.12 d (12.8)	2.20 d (12.2)
17a	4.76 br s	4.79 br s	
17b		4.85 br s	
18a	3.32 d (11.7)	3.27 d (11.4)	3.34 d (12.0)
18b	3.54 d (11.7)	3.53 (11.4)	3.55 (12.0)
19	0.72 s	0.74 s	0.78 s
20	1.15 s	1.29 s	1.19 s
CH ₃			

^a *J* values are in parentheses and reported in Hz; chemical shifts are given in ppm; assignments were confirmed by DQF-COSY, 1D-TOCSY, HSQC, and HMBC experiments.

Table 4.2: ^1H NMR data of **4-6** (Methanol- d_4 , 600 MHz)^a

position	4	5	6
1a	1.06 br dd (13.0, 11.0)	1.02 br dd (13.0, 11.0)	0.84 br dd (12.0, 6.0)
1b	1.91 ^b	1.92 ddd (13.5, 6.0, 2.5)	1.76 ^b
2a	1.70 m	1.34 m	1.14 m
2b	1.82 ^b	1.42 m	1.35 ^b
3a	3.65 dd (12.2, 5.0)	3.61 dd (12.0, 4.5)	1.33 ^b
3b			1.86 ^b
5	2.00 br d (12.0)	1.87 br t (13.5)	1.74 ^b
6a	1.57 ^b	1.58 ^b	1.60 ^b
6b	1.77 ^b	1.60 ^b	1.62 ^b
7a	3.67 t (2.5)	3.62 t (3.5)	3.62 t (3.0)
7b			
9	1.61 dd (11.4, 5.5)	1.46 dd (11.4, 6.0)	1.46 dd (9.0, 4.5)
11a	1.54 ^b	1.62 ^b	1.70 ^b
11b	1.84 ^b		1.80 ^b
12a	1.78 ^b	1.54 m	1.60 ^b
12b	1.89 ^b	1.63 ^b	1.70 ^b
13	2.40 m	2.08 m	2.07 m
14a	1.55 ^b	1.70 m	1.68 ^b
14b	2.22 br d (11.6)	1.83 dd (9.5, 2.0)	1.89dd (11.0, 3.0)
15a	2.14 br s	1.59 ^b	1.56 d (14.0)
15b		1.78 d (12.2)	1.75 ^b
17a		3.63 d (11.0)	3.64 d (11.5)
17b		3.73 d (11.0)	3.72 d (11.5)
18a	3.87 d (11.4)	3.86 d (11.3)	3.11 d (11.5)
18b	4.03 d (11.4)	3.99 d (11.3)	3.32 d (11.5)
19	0.78 s	0.76 s	0.81 s
20	1.19 s	1.13 s	1.14 s
CH ₃	2.07 s	2.07 s	

^a J values are in parentheses and reported in Hz; chemical shifts are given in ppm; assignments were confirmed by DQF-COSY, 1D-TOCSY, HSQC, and HMBC experiments.

^b overlapped signals

Table 4.3: ^{13}C NMR data of **1-6** (Methanol- d_4 , 600 MHz)^a

	1	2	3	4	5	6
carbon						
1	80.0	41.0	39.1	39.4	38.8	40.0
2	37.5	27.0	27.1	27.2	29.9	19.0
3	71.4	73.2	74.2	72.2	72.4	36.5
4	42.6	43.9	42.6	42.4	42.0	37.5
5	37.5	49.0	39.7	39.2	39.2	40.8
6	27.0	20.7	27.1	27.0	27.0	27.0
7	77.6	42.5	77.0	77.1	77.5	77.8
8	46.0	47.0	50.0	50.9	50.9	50.7
9	51.6	61.5	50.3	51.6	51.0	51.5
10	38.0	41.2	39.0	39.6	41.0	43.0
11	20.0	70.7	18.8	19.3	19.1	19.0
12	34.6	42.5	30.5	30.6	27.0	27.0
13	45.1	44.4	48.9	48.8	46.0	45.8
14	39.9	40.3	36.5	36.8	37.0	35.0
15	45.5	49.5	52.2	52.6	50.1	50.0
16	156.0	156.0	225.0	225.0	81.8	82.4
17	102.8	103.2			66.5	66.4
18	67.6	67.2	68.0	66.5	66.5	71.8
19	12.5	12.8	12.3	12.4	12.6	17.0
20	13.6	19.4	18.3	18.6	18.3	18.2
C=O				173.5	173.0	
CH ₃				20.9	20.5	

^a Chemical shifts are given in ppm; assignments were confirmed by HSQC and HMBC experiments.

Table 4.4: ^1H and ^{13}C NMR data of **7-8** (Methanol- d_4 , 600 MHz)^a

position	7		8	
	δ_{H}	δ_{C}	δ_{H}	δ_{C}
Aglycone				
1		131.6		130.2
2	6.66 d (2.0)	115.3	6.61 d (2.0)	116.0
3		148.8		146.2
4		145.9		145.0
5	6.69 d (8.0)	116.7	6.68 d (8.0)	117.0
6	6.64 dd (8.0, 2.0)	121.0	6.54 dd (8.0, 2.0)	120.6
α	3.78 m	72.1	3.77 m	72.0
	4.04 m		3.95 m	
β	2.81 m	36.6	2.79 m	36.7
OMe	3.75 s	56.3		
β -glucose				
1	4.34 d (7.8)	104.2	4.33 d (7.8)	104.0
2	3.54 dd (9.0, 7.8)	75.3	3.54 dd (9.0, 7.8)	75.2
3	3.49 t (9.0)	84.0	3.49 t (9.0)	84.0
4	3.41 t (9.0)	70.3	3.42 t (9.0)	70.3
5	3.34 m	75.6	3.29 m	75.4
6a	4.37 dd (12.0, 5.0)	64.4	4.35 dd (12.0, 5.0)	64.2
6b	4.50 dd (12.0, 2.5)		4.50 dd (12.0, 2.5)	
α -rhamnose				
1	5.49 d (1.8)	101.5	5.48 d (1.8)	101.4
2	3.98 dd (3.0, 1.8)	82.5	3.98 dd (3.0, 1.8)	82.4
3	3.63 dd (9.0, 3.5)	72.5	3.66 dd (9.0, 3.5)	72.5
4	3.48 t (9.0)	74.1	3.45 t (9.0)	74.1
5	4.00 m	69.6	3.98 m	69.7
6	1.24 d (6.5)	17.7	1.23 d (6.5)	17.5
α -arabinose				
1	4.33 d (7.5)	107.3	4.35 d (7.5)	107.2
2	3.65 dd (9.0, 7.5)	72.0	3.60 dd (9.0, 7.5)	72.6
3	3.50 dd (9.0, 3.0)	74.2	3.50 dd (9.0, 3.0)	74.0
4	3.79 m	69.6	3.77 m	69.7
5a	3.54 dd (12.0, 3.0)	67.2	3.54 dd (12.0, 3.0)	67.3
5b	3.87 (12.0, 2.0)		3.86 (12.0, 2.0)	
Acyl moiety				
1		127.7		128.0
2	7.17 d (2.0)	111.4	7.17 d (2.0)	111.1
3		149.4		149.5
4		150.8		150.7
5	6.80 d (8.0)	116.1	6.81 d (8.0)	116.4
6	7.02 dd (8.0, 2.0)	124.0	7.02 dd (8.0, 2.0)	124.1
α	6.40 d (16.0)	115.0	6.39 d (16.0)	115.0
β	7.63 d (16.0)	147.0	7.63 d (16.0)	147.1
CO		169.2		169.4
OMe	3.87 s	56.3	3.87 s	56.3

^a *J* values are in parentheses and reported in Hz; chemical shifts are given in ppm; assignments were confirmed by DQF-COSY, 1D-TOCSY, HSQC, and HMBC experiments.

Chapter 5

*An approach to discover a lead compound for drug discovery:
fishing for partners study*

Chapter 5

5.1 Introduction

5.1.1 *ent-Kaurane* diterpenes: 15-ketoatractyligenin methyl ester

Atractyligenin (**Figure 5.1**), is the *nor*-diterpene aglycon of the glucoside atractyloside, which occurs, together with its homologous diterpene, carboxyatractyloside, in the roots of *Atractylis gummifera* L. (Asteraceae). Atractyloside is the main compound responsible for the lethality of *A. gummifera* and *Wedelia glauca* Ort. (Asteraceae) in bovine cattle from some regions of Argentina, Brazil, and Uruguay, causing hypoglycemia, respiratory depression, nephrotoxicity, hypoxemia, and cell injury. In humans, the poisoning with this glycoside can cause renal and hepatic failure, also followed by necrosis.

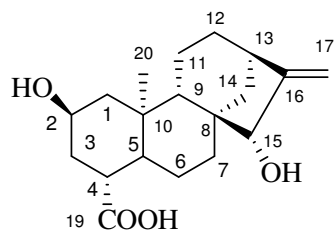


Figure 5.1: Structure of *atractyligenin*

This toxic action is due, mainly, to the inhibition of mitochondrial oxidative phosphorylation (Garcia *et al.*, 2007). Our interest in this compound was stimulated both by the high toxicity of the glucoside and by the antimicrobial and cytotoxic activities of some derivatives: atractyligenin and its derivatives showed significant cytotoxic activity against different cancer cell lines. The main structural feature for cytotoxic activity of these compounds and other natural compounds was established to be the presence of an α,β -unsaturated system, which likely serves as an alkylating center and can be part of an ester, ketone, or lactone moiety. On the basis of this information, extensive chemical work has been carried out by the research group of the Dipartimento di Chimica Organica di Palermo on the structure of atractyligenin. The 15-hydroxy group of atractyligenin was converted into a ketone in order to incorporate an α,β -unsaturated ketone into the *ent*-kaurane skeleton.

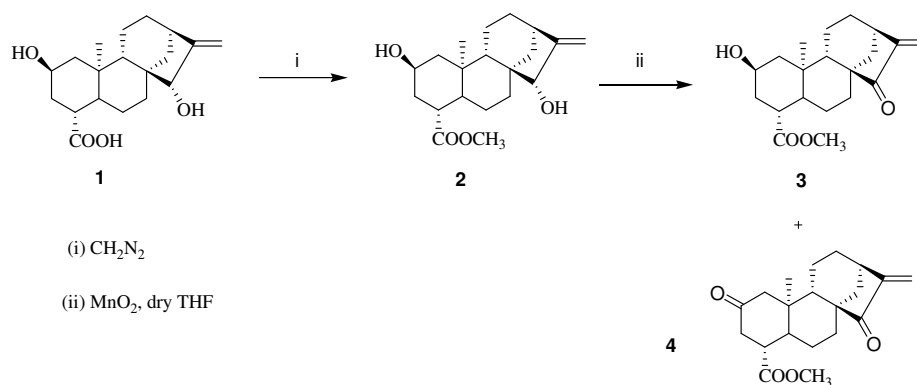


Figure 5.2: Reaction scheme of 15-ketoatractyligenin methyl ester synthesis

Atractyligenin methyl ester (2), prepared by treating atractyligenin (1) with CH_2N_2 , was reacted with MnO_2 for 3 min, obtaining 15-ketoatractyligenin

methylester (compound **3**, SR2017) as main compound and 2,15-diketoatractyligenin methyl ester as minor product (**4**, **Figure 5.2**).

Other analogues were synthesized and screened against a panel of human tumor cell lines including A549 (lung), PC-3 (prostate), 1A9 (ovarian), MCF-7 (breast), KB (nasopharyngeal), and KB-VIN (multidrug-resistant KB subline) in order to explore their cytotoxic activity and critical drug-resistance profile. Diterpenes lacking of an α,β -unsaturated ketone group were inactive.

Compound **3**, together with the analogue 2,15-ketoatractyligenin methyl ester showed cytotoxic activity against all six tested cancer cell lines and were most potent against 1A9 ovarian cancer cells with half maximal inhibitory concentration (IC₅₀) values of 0.2 and 0.3 μ M, respectively (Rosselli *et al.*, 2007). Before starting with further studies, the antitumor potential of SR2017 was also evaluated from Prof. M.A. Belisario of Dipartimento di Farmacia, Università di Salerno, using HCT-116 (colon carcinoma) Jurkat (T-cell leukemia), HepG2 (hepatoblastoma), MCF7 (breast carcinoma) tumor cell lines. SR2017 displayed strong cell growth inhibitory potency in all tested cell lines, IC₅₀ values ranging between 1.5 and 10 μ M. Leukemia-derived cells, and in particular Jurkat cells, displayed higher susceptibility to SR2017 than solid tumor-derived cell lines. Among the solid tumor-derived cell, HCT-116 were the most susceptible and so they were adopted to evaluate the antitumoral activity of SR2017 *in vivo*. After 7 days from the subcutaneous injection of HCT-116 colon carcinoma cells, treatments with daily delivery of SR2017 at 10 mg/kg in 100 μ l of vehicle for 7 days were performed. There was an inhibition of the tumor growth constant during the treatment. No evident sign of toxicity was revealed.

In the light of this information, we decided to investigate the mechanism of action of these atractyligenin derivatives researching first of all their molecular targets.

5.1.2 Starting point for a fishing for partners approach

SR2017 and 2,15-ketoatractyligenin methyl ester could be interesting new lead compounds for further investigation, so the objective was to identify the primary SR2017 partners, suitable as potential therapeutic targets.

In **chapter 1** a fishing for partner (or pull down) technique was described as a chemical proteomic approach aimed to the identification of molecular target for small molecules. This kind of study was used in the research of SR2017 targets, as reported in this chapter, and was carried out in collaboration with Prof. N. De Tomamasi team of Dipartimento di Farmacia, Università di Salerno, where I spent a training period.

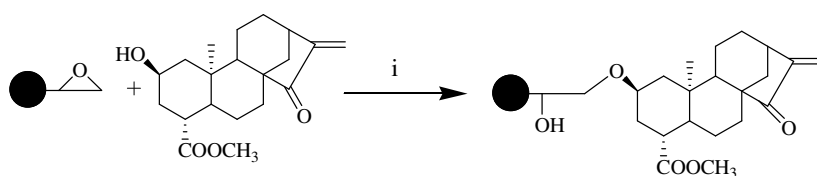
To reach this goal, a chemical proteomic strategy, using affinity chromatography coupled with mass spectrometry, has been applied. It was started a screening aimed to the identification of intracellular target(s) of SR2017 chosen as representative of a library of *ent*-kaurane diterpenes instead of 2,15-ketoatractyligenin methylester for the presence of its hydroxylic group at position 2, suitable for the successive steps of chemical immobilization on a solid support.

From an experimental point of view, this work can be divided into the following steps: (i) chemical immobilization of SR017 on a solid support; (ii) incubation of SR2017 modified beads with cell lysates; (iii) MS identification of SR2017 interactors; (iv) determination of physical interaction between SR2017 and the identified partners.

5.2 Chemical immobilization of SR2017 on a solid support

The compound-immobilized affinity chromatography is a powerful versatile method to profile cellular targets of selected drug candidates. The procedure involves immobilization of the compound on a solid support through a spacer arm and the use of this matrix as a bait to fish for interacting proteins in a cellular

lysate or tissue extract (Raida, 2011, Rix *et al.*, 2009). The chemical immobilization of a small molecule ligand is usually achieved through suitable functional group. SR2017 was anchored onto a solid support, taking advantage of its hydroxylic group at position C-2. An epoxy-activated Sepharose 6B resin, formed by reacting Sepharose 6B with 1,4-bis (2,3-epoxy-propoxy)-butane was used (**Figure 5.3**). A basic solution of 15-ketoatractylgenin was added to the swelled epoxy resin, the reaction was monitored by HPLC, and the yield was calculated by the integration of peaks relative to the SR2017 concentration in the supernatant before and after 24 h from the coupling.



(i) ACN 50%, NaHCO₃, 50 mM pH 12, 50%
24 h under stirring

Figure 5.3: Reaction's scheme of SR2017 with epoxy groups of swelled epoxy-activated Sepharose 6B resin

Each peak was also checked by ESI-MS in positive mode (**Figure 5.4**). The coupling process was completed by blocking the exceeding active epoxy groups with an ethanolamine solution. As a control, a portion of the resin was capped only with ethanolamine.

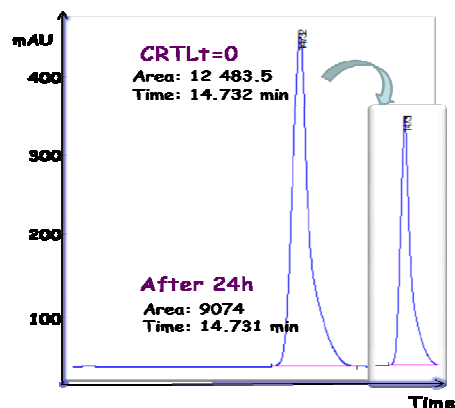


Figure 5.4: Chromatographic peaks of SR2017 at time zero and after 24 h from the coupling to the swelled resin

Before the terminal 1,4-*bis* (2,3-epoxy-propoxy)-butane group of the resin there is a spacer of 12 carbon atoms that plays an important role to avoid possible steric hindrance between the macromolecular target(s) and the immobilized ligand. For the choice of the solid support it is very crucial to evaluate the length and the hydrophilic properties of the spacer in order to minimize non-specific protein binding and maximize purification efficiency. The experimental conditions (buffer, pH, reaction time and temperature) were optimized in order to reach a final concentration of 30.12 μmol drug/mL resin, as the producer advices.

5.3 Identification of SR2017 targets through a chemical proteomic method

The crude cell extract of HCT-116 was incubated with the system SR2017-beads to promote the interaction between SR2017 and its potential partners in the cell lysate. An equal amount of cell lysate was loaded onto the covalently coupled beads and onto unmodified beads in parallel to discriminate between proteins specific interaction with SR2017 and the unspecific background. After

extensive washings, the SR2017 interacting proteins were released from the resin by elution with SDS-gel loading buffer. The protein mixtures were then resolved by SDS-PAGE and some differences were evident already by the gel visualization (**Figure 5.5**).

Since the simple gel visualization wasn't enough to establish significant differences, the gel lanes, of the SR2017 beads and control experiments were both cut in 13 pieces, digested with trypsin, and analyzed by mass spectrometry through nanoflow RP-HPLC MS/MS. Double and triple charged peptide species obtained in the conventional MS spectrum were fragmented, and all the MS/MS spectra converted into a peak list. All peak lists were then submitted to a Mascot database search for the protein identification. The experiment was done in triplicate.

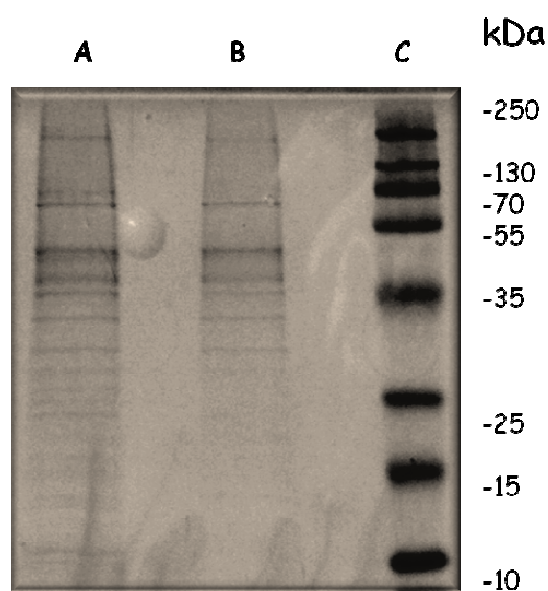


Figure 5.5: SDS PAGE analysis of the affinity purified interactome: (A) SR2017, (B) control, (C) molecular weight marker

A gel free analysis based only on affinity purification and mass spectrometry analysis of SR2017 partners was also necessary to minimize the interference of background contaminants and to increase the signals intensity of the proteic mixture and to have better results. All the steps until the incubation with the cell lysate were the same described before, but at the end the SR2017 interacting proteins were released from the resin by elution with guanidine instead of SDS-gel loading buffer. The proteins were digested by trypsin directly in solution. The tryptic digests were analyzed by mass spectrometry and the resulting peak lists were elaborated as previously described. The experiment was done in triplicate.

5.4 Database search to characterize the targets

The Mascot database search revealed the whole interactome of SR2017. A list of identified proteins, from both gel lanes (control and matrix with SR2017) and from both analytic methods (with the gel and gel-free), was obtained and compared to establish which proteins specifically interact with SR2017.

By this way three proteins were found: Heat shock protein 70 kDa (Hsp70) (**Figure 5.6**), Heat shock protein 60 kDa (Hsp60) and Peroxisomeproliferator-activated receptor gamma (PPAR γ); (**Figure 5.7**).

The Heat shock proteins (Hsp) are mainly ATP-dependent molecular chaperones. Hsp70, together with other chaperones, is essential for the folding, translocation and assembly of the proteins both in physiological situation and in stress condition (**Figure 5.7**). In stress condition they stabilize the damaged proteins in order to promote their renaturation or degradation (Mosser *et al.* 2004). Some of them are constitutively abundant while some other, like Hsp70, are over-expressed especially in many tumor cells. They seems to have a role in the regulation of cellular proliferation and apoptosis (Schmitt *et al.*, 2007).

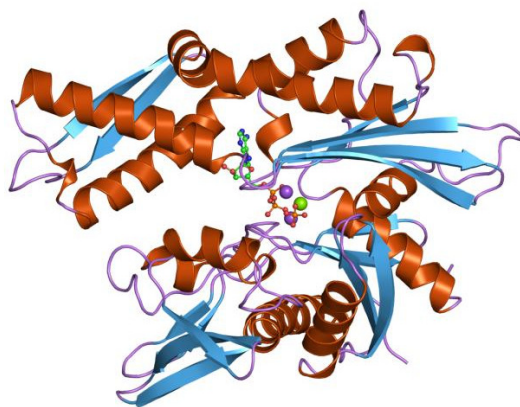


Figure 5.6: *Hsp70ATPase site* (Flaherty et al., 1990)

It is known that Hsp70 has a cytoprotective action due to anti-apoptotic effects through upstream and downstream mitochondrial signaling pathways (Didelot *et al.*, 2007). Hsp70 inhibits the caspase dependent and independent apoptosis in Jurkat cells (Creagh *et al.*, 2000). Hsp70 seems to block the caspase activation and by this way it inhibits the mitochondrial damage and the nuclear fragmentation. Furthermore the direct binding between Hsp70 and apoptosis proteases-activating factor (Apaf-1) prevents the recruitment of pro-caspase 9 of the apoptosome. Nevertheless, other studies assert that the apoptosis caspase dependent inhibition mediated by Hsp70 is related to the release of the mitochondrial cytochrome *c* through the translocation of Bax (Bcl-2-associated X protein), a pro-apoptotic protein, from cytosol to mitochondria (Mosser and Morimoto, 2004). The apoptosis caspase independent inhibition is due to the binding between Hsp70 and apoptosis-inducing factor (AIF) with the consequent inhibition of the chromatin condensation induced by AIF (Schmitt *et al.*, 2007). The pathway in which Hsp70 is involved it is very complex and this protein is an interesting target for the anti-cancer therapy.

Hsp60 is a mitochondrial chaperone that is involved in the folding of native proteins and in the intracellular proteins trafficking (Cappello *et al.*, 2008). This protein is also present in the cytosol and in tumor cells its level is high and is considered as a marker of immune system damage since it causes the activation and the maturation of dendritic cells and cytotoxic T cells (Osterloh *et al.*, 2008). Hsp60 can be found even in extracellular space where it can interact with various receptor with pro or anti-inflammatory effects (Steinhoff *et al.*, 1999). It is involved in the apoptotic process and it can explicate both pro-apoptotic than anti-apoptotic effects. It makes a complex with p53 and also stabilizes the surviving pools that usually with their degradation promote the apoptotic process (Ghosh *et al.*, 2008). An over-expression of Hsp60 together with Hsp10 leads to a decrease of anti-apoptotic factor, such as Bcl-x1 and Bcl-2, and is related to the presence of Bax, a pro-apoptotic protein (Shan *et al.*, 2003). The pro-apoptotic effect of Hsp60 is also related to caspases activation (Samali *et al.*, 1999).

Peroxisomeproliferator-activated receptors PPARs, members of the nuclear hormone receptor (NHR) family, are ligand-activated transcription factors. They were first identified as the nuclear receptors that mediate the pleiotropic effects of peroxisome proliferators. As indicated by the name, peroxisome proliferators are a collection of structurally diverse chemicals (i.e. steroids, lipids, hypolipidemic drugs, plasticizers, etc.) that cause hepatomegaly in rodents. The three known PPAR isotypes PPAR α , PPAR β/δ and PPAR γ are involved in numerous biological processes that range from lipid, glucose, and energy homeostasis to inflammation and wound repair. Following activation by ligands, PPARs heterodimerize with retinoid X receptor (RXR or NR2B), bind to the peroxisomeproliferator response element (PPRE) present in the promoter regions of target genes, recruit co-activators, and activate transcription of target genes (Mora *et al.*, 2006). Each isoform is encoded by a different gene activated by a selective ligand. PPAR α is especially expressed in liver, hearth, kidney proximal tubule cells and intestine; PPAR β/δ is expressed in many tissue and PPAR γ is

mainly found in adipocytes and it plays an important role in the adipocytes differentiation but it is also present in endothelial cells and in immune system cell (Kliwer *et al.*, 1994). They can interact with many kind of ligand and consequently they present different function. PPARs are naturally activated by lipids through diet or other biosynthetic ways and by fatty acids like prostaglandins and leukotrienes (Krey *et al.*, 1997).

PPAR γ has a molecular weight of 57.6 kDa and is involved in the lipids biosynthesis and in the carbohydrates metabolism. The activation of this receptor in diabetic patients causes a decrease of the glucose concentration. The best known therapeutic application of PPAR γ ligands is the use of thiazolidinediones (TZDs) as insulin sensitizers to treat type 2 diabetes. PPAR γ agonists have an anti-inflammatory activity with the inhibition of the production of TNF α , IL-1b and IL-6. Agonists of PPAR γ have been shown to inhibit growth and cell proliferation, promote terminal differentiation, and induce apoptosis in human breast tumor cells. A number of studies demonstrated that PPAR γ agonists of different structural classes can inhibit growth, cause terminal differentiation, and induce apoptosis of human tumor cells derived from various tissues *in vitro* and *in vivo*. Other studies suggested that PPAR γ activation may exert the opposite effect: the growth promotion (Han *et al.*, 2004; Lee *et al.*, 2006; Mora *et al.*, 2006).

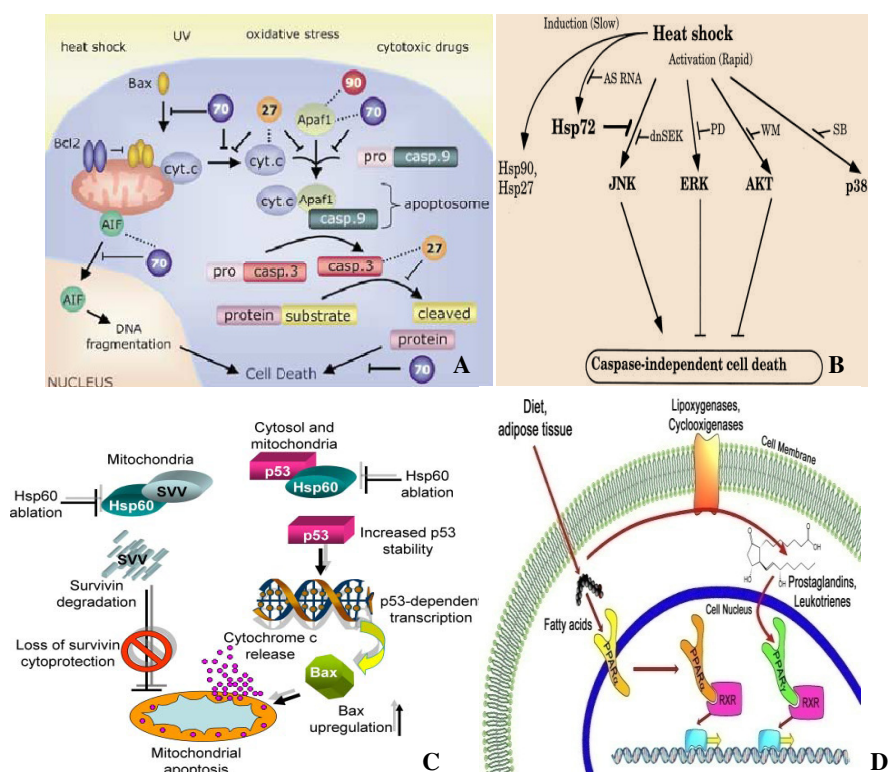


Figure 5.7: (A,B) Hsp70 involvement in cell death; (C) Hsp60 pathway (D) Peroxisome proliferator-activated receptors pathway (Mosser *et al.*, 2004; Gabai *et al.*, 2000).

5.5 Targets validation and characterization of physical interactions

Surface plasmon resonance (SPR) Biacore technology was employed to study the interactions of SR2017 with Hsp70, Hsp60, and PPAR γ . SPR is an optical technique, based on the evanescent wave phenomenon, able to measure changes in refractive index onto a sensor surface, and it is suitable for characterizing macromolecular interactions (Casper *et al.*, 2004). The binding between a compound in solution and its ligand immobilized on the sensor surface results in

a change of the refractive index, that could be monitored in real time allowing the measurement of association and dissociation rates. It is a real time biomolecular interaction analysis through which we attempted to measure the kinetic dissociation constants between SR2017 and the targets that were anchored separately onto the chip surface. This target validation method was necessary since the fishing for partners approach could give false positive results. **Figure 5.8** reported the sensorgrams detected after the binding of SR2017 and Hsp70 (**Figure 5.8 A**) and SR2017 and PPAR γ (**Figure 5.8 B**) at different protein concentrations of SR2017: 50 nM, 100 nM, 250 nM, 500 nM, 1 mM and 100 nM, 250 nM, 500 nM respectively. The increase of response units (RU) in the association phase and the slope of the dissociation phase of the complex are clearly dependent on the analyte concentration. Association and dissociation rate constants were determined, and equilibrium binding constants (KD) of 42.3 ± 8.6 nM and 89.3 ± 11.5 nM were calculated for Hsp70 and PPAR γ complex, respectively. The analysis of the sensorgram obtained by the immobilization of Hsp60 was instead negative.

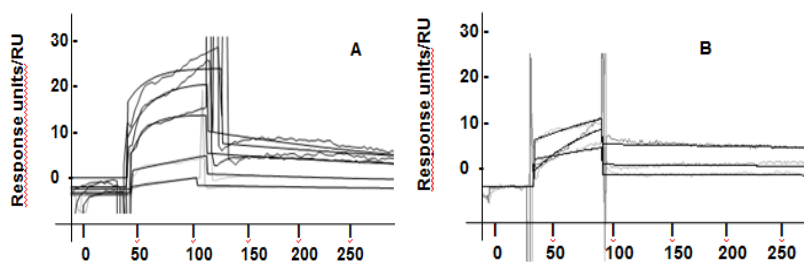


Figure 5.8: Sensorgrams obtained from immobilized Hsp 70 (A) and PPAR γ (B)

5.6 Conclusion

The results obtained for Hsp60 suggested that we could exclude this chaperone from the list of the SR2017 potential molecular targets. On the contrary, the data related to Hsp70 and PPAR γ demonstrated instead the interaction occurring between the small molecule and these proteins. Given the activities of both proteins, these information are consistent with the effects on cells showed by SR2017, especially in relation with Hsp70.

Regarding the interaction with PPAR γ , it is known that its natural ligands, such as 15-deoxy- Δ -12,14-prostaglandin J2 (15d-PGJ2) can give a Michael reaction with the cysteine 285 in the ligand-binding domain of the receptor for the presence of α,β -unsaturated keto group (Shiraki *et al.*, 2005).

However, further analysis are necessary to continue the target validation process and also biological assays are needed to clarify this molecule mechanism of action.

Chapter 6

*An approach to discover a lead compound for drug discovery:
validation of Hsp27 as molecular target of hardwickiic acid*

Based on: "Faiella *et al.*, *Molecular BioSystem*, **2012**, 8, 2637-2644".

Chapter 6

6.1 A chemical proteomics approach to discover Hsp27 as a target for proapoptotic clerodane diterpenes: summary of previous studies

Compounds isolated from members of the Lamiaceae family are traditionally used as remedies against many diseases. Within the Lamiaceae, the genus *Salvia* is worthwhile to be studied, as it is endowed with bioactive diterpenes, commonly found in the complex secretion product of these plants, whose secretory structures are widely distributed on their aerial parts. Several clerodane-type diterpenes are commonly found in the complex secretion product of plants belonging to *Salvia* genus, whose secretory structures are widely distributed on their aerial parts (Duke and Oliva, 2004) and many of them have demonstrated antimicrobial, anti-inflammatory, anti-ulcer and cytotoxic activity (Rodriguez-Hann *et al.*, 1992; Whitson *et al.*, 2010; Vieira *et al.*, 2011; Kanokmedhalkul *et al.*, 2007). Despite all these well described actions, the molecular mechanisms by which this class of compounds exerts its effects are still unclear. In this context, during my undergraduated thesis, we started a fishing for partners study aimed to the identification of intracellular target(s) of hardwickiic acid (HAA, compound **1**; **Figure 6.1**) chosen as representative of a library of clerodane diterpenes isolated from *Salvia* ssp. One of the most versatile methods to profile cellular targets of selected drug candidates is compound-immobilized affinity chromatography.

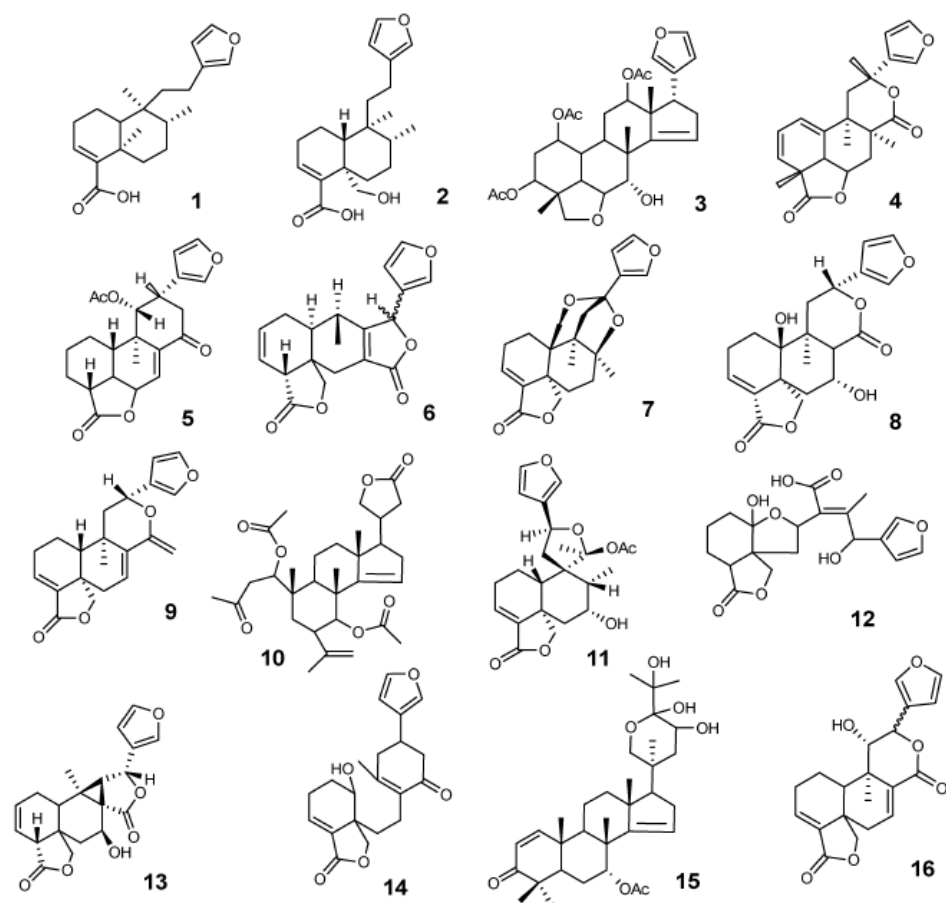


Figure 6.1: Structure of compounds 1–16

The procedure involves immobilization of the compound on a solid support through a spacer arm and the use of this matrix as a bait to fish for interacting proteins in a cellular lysate or tissue extract (Raida, 2011; Rix and Superti-Furga, 2009). The power of affinity chromatography combined with advances in protein identification by sensitive and high-throughput mass spectrometric analysis offers huge potential to find out previously unrecognized activities and potential therapeutic applications.

The diterpene HAA was selected as a testing compound from a small clerodanes library (**Figure 6.1**) because of its 4-carboxyl group, allowing us to covalently bind the compound to a solid support, an agarose matrix activated with 1,10-carbonyldiimidazole and modified by 1,12-dodecanediamine as a spacer.

Using this approach, described in **chapter 5**, we identified Heat Shock Protein 27 (Hsp27), an antiapoptotic protein characterized for its tumorigenic and metastatic properties and now referenced as a major therapeutic target in many types of cancer (Ciocca and Calderwood, 2005) as an HAA target. Hsp27 has many diverse functions including chaperone activity, mRNA stabilization, inhibition of apoptosis, cell proliferation, and modulation of actin polymerization. Hsp27 can interfere with a number of cell death pathways induced by heat shock, oxidative stress or death receptor agonist (Paul *et al.*, 2010). Expression of Hsp27 is up-regulated in numerous types of tumors and promotes unfavorable outcome (Ciocca and Calderwood, 2005). Overexpression of this protein is frequently associated with increased resistance to radiotherapy and to anti-cancer drugs, such as cisplatin, doxorubicin, and etoposide (Zhang and Shin, 2007). Targeting Hsp27 by an antisense strategy increases cancer cell death *in vitro* and *in vivo* (Aloy *et al.*, 2008). The involvement of this chaperone in many cellular processes related to apoptosis and cell proliferation (Mymrikov *et al.*, 2011; Parcellier *et al.*, 2003; Voss *et al.*, 2007) led us to further investigate the interaction of clerodane diterpenes with this target.

To confirm the binding between Hsp27 and HAA and to measure the parameters of the interaction, a Surface Plasmon Resonance (SPR) based binding assay was used obtaining a good sensogram with K_D 269 ± 35 nM, indicative of a good interaction. The same analysis was also performed using 15 terpenoids showing structural analogies with HAA (compounds **2–16** in **Figure 6.1**) in order to perform some structure–activity relationship evaluations.

Our results suggested that the interaction with Hsp27 was not affected by the dimension of the ligand while the furane ring played a critical role. During my PhD thesis, studies to evaluate the nature of the interaction between HAA and Hsp27 were performed in collaboration with the Prof. N. De Tommasi team of University of Salerno.

6.2 Limited proteolysis

In addition to SPR measurements, the validation of HAA–Hsp27 interaction was carried out by means of a panel of chemical and biological approaches, such as limited proteolysis and biochemical assays reported in this thesis work. On the basis of the previous preliminary results, a limited proteolysis-mass spectrometry based strategy was used to evaluate the effect of the interaction between HAA and Hsp27 on the protein structure and activity. This approach is based on the evidence that exposed, weakly structured, and flexible regions of a protein can be recognized by a proteolytic enzyme. The differences in the proteolytic patterns observed in the presence or in the absence of putative protein ligands can be analyzed to identify the protein regions involved in the molecular interactions (Casbarra *et al.*, 2004). Compound **16** was used as a negative control since it didn't show any interaction with Hsp27 in SPR analysis. As a first step of this study, we performed Hsp27 enzymatic digestion under strictly controlled conditions (buffer, temperature, incubation time and enzyme/substrate ratio), optimized to preserve the dimeric form of Hsp27 (protein concentration 1 mM) and the correct protein folding. Trypsin, chymotrypsin, and endoproteinase GluC were used as proteolytic agents. Digestion products were analyzed by mass spectrometry and the observed fragments were identified on the basis of their molecular weight, the selectivity of the used enzymes and their complementarities. Only the fragments released by a single hydrolytic event have been taken into account, in order to evaluate the proteolytic accessibility of the

intact protein. Under the experimental conditions used, the protein remained largely undigested. Only a limited number of fragments were released from the protein molecule, showing that its native conformation is susceptible to proteolysis at a few very specific, and probably flexible, sites (**Figure 6.2A**): most of them are located in the *N*-terminal domain of the protein, in agreement with previous observations depicting this region as poorly structured (Baranova *et al.*, 2009; 2011). Interestingly, a good agreement between the results achieved with the three enzymes was observed. When the same experiments were performed by pre-incubating Hsp27 with HAA, a different proteolytic pattern was observed (**Figure 6.2B**). Even if compounds **3** and **4** showed an affinity towards immobilized Hsp27 slightly higher than that measured for HAA, their low solubility and the small amount available led us to keep on using HAA as the testing compound. First of all, a higher amount of undigested protein was observed, regardless of the proteolytic enzyme used; besides, some of the sites prone to enzymatic hydrolysis in the *N*-terminal domain of the protein were protected following the Hsp27 interaction with HAA. In particular all the cleavage sites detected in the portion 26–36 escaped from hydrolysis in the complex, thus suggesting this region to be involved in the Hsp27 interaction with the diterpene. Experiments carried out on pre-incubating Hsp27 with compound **16** produced a proteolytic pattern superimposable to that observed for the protein. All the limited proteolysis detailed data are provided in ESI-MS.

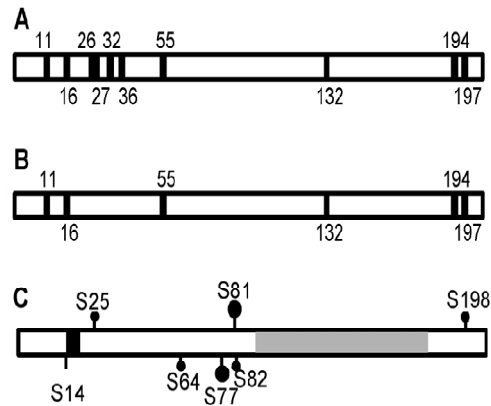


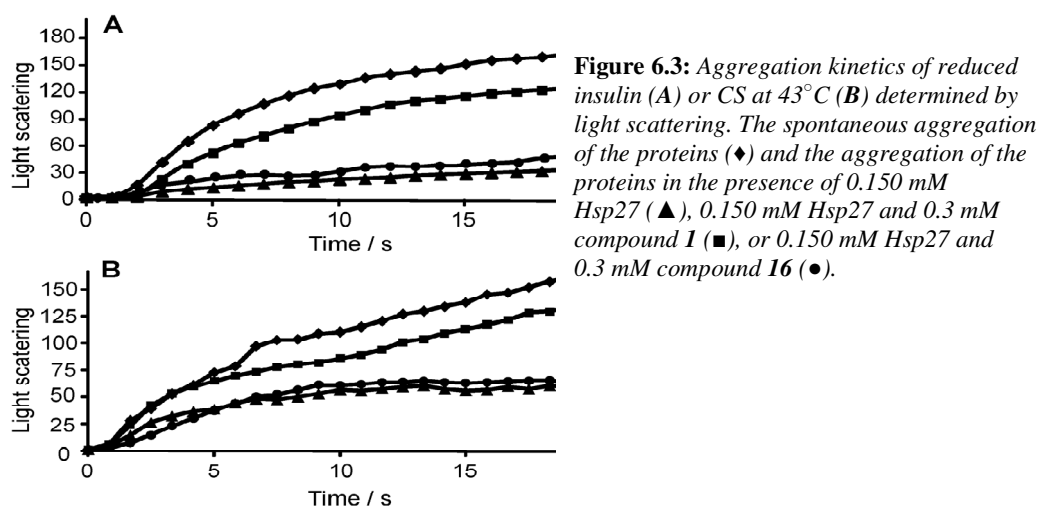
Figure 6.2: Preferential cleavage sites observed submitting to limited proteolysis Hsp27 (A) or Hsp27/I complex (B). Schematic representation of structural organization of Hsp27. (C): α -crystalline domain is underlined in grey and WDPF motif is in black. Reported and putative phosphorylation sites are indicated by large or small black circles, respectively

Hsp27 is composed of 205 aminoacids, its structure consists of *N*-terminal domain that includes the so-called WDPFmotif, the α -crystalline domain, and a short *C*-terminal sequence (**Figure 6.2C**) (Mymrikov *et al.*, 2011). Both the WDPF-motif and the α -crystalline domain seem to be important for Hsp27 oligomerization; this small heat shock protein can form variable size oligomers of up to 800 k8Da (Leji-Garolla and Mouk, 2005) and the state of oligomerization depends on many different factors such as post-translational modifications (phosphorylation and thiolation) and physical parameters (pH and temperature) (Leji-Garolla and Mouk, 2006; Rogalla *et al.*, 1999). In particular, phosphorylation leads to formation of small oligomers, while increase in the temperature or decrease in the pH leads to large oligomers. Ser26 is a putative phosphorylation site that stands just at the beginning of the interaction region between the protein and the HAA, suggesting that the small molecule could influence the posttranslational modification of this residue. But, more probably,

the binding with the diterpene clerodane could provoke a conformational change of Hsp27 influencing the interaction with its protein targets.

6.3 Insuline and citrate synthase aggregation assays

The ability of HAA to modulate the *in vitro* chaperone activity of Hsp27 was evaluated by monitoring the insulin dithiothreitol (DTT) induced (Leji-Garolla and Mouk, 2006) and the citrate synthase (CS) thermal induced (Rogalla *et al.*, 1999) aggregation in the presence of Hsp27, with or without HAA or compound **16**, used as a negative control. The molecular chaperone activity of small heat shock proteins is often evaluated by DTT reduction of insulin. Reduction breaks the disulfide bonds holding together insulin chains A and B whereupon chain B aggregates but this aggregation can be prevented by adding stoichiometric amounts of Hsp27 (**Figure 6.3A**). When a 4-fold molar excess of HAA was added to this mixture, the slope of the curve became comparable to that observed without the chaperone, suggesting the inhibition of Hsp27 chaperone activity by this compound. Conversely, the presence of compound **16** did not perturb the Hsp27 antiaggregation effect. Similar results were achieved by evaluating the effects of Hsp27 on CS thermal induced aggregation. Upon incubation at elevated temperatures, CS underwent quantitative protein aggregation but the presence of stoichiometric amounts of Hsp27 changed the aggregation kinetics significantly (**Figure 6.3B**). Again, adding a 4-fold molar excess of HAA the anti-aggregation effect of Hsp27 was substantially reverted, whereas the same amount of compound **16** did not produce any sensible effect. These results demonstrate that when HAA binds to the small heat shock protein it influences the ability of Hsp27 to interact with denatured proteins *in vitro*.



6.4 Apoptosis evaluation by analysis of hypodiploid nuclei

In the effort to give a cellular significance to Hsp27–HAA interaction, it was decided to explore the pro-apoptotic activity of the small molecule in human monocytes. Hsp27 has recently been shown to be highly and constitutively expressed in human monocytic leukemia cells (Voss *et al.*, 2007). Apoptosis was evaluated by analysing the percentage of hypodiploid nuclei by propidium iodide incorporation with the collaboration of Dr. Alessandra Tosco, Dipartimento di Farmacia, Università di Salerno.

U937 cells were incubated with different concentrations of HAA (50, 100, and 200 mM) and 200 mM of compound **16**, after 24 hours cells were harvested and analyzed for apoptosis.

Figure 6.4 shows an increasing ability of HAA to induce apoptosis. Compound **16** was used as negative control.

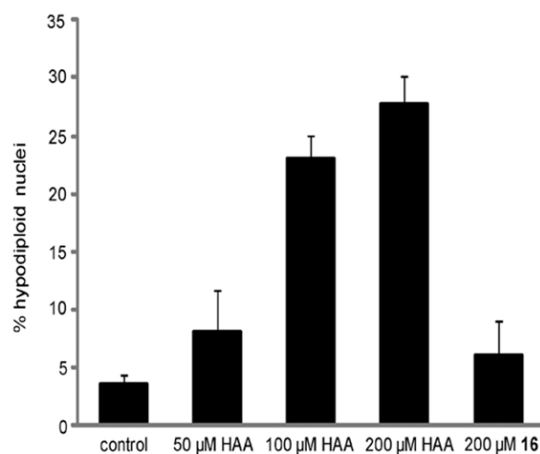


Figure 6.4: Apoptosis evaluation by analysis of hypodiploid nuclei percentage in U937 cells incubated with different concentrations of HAA and compound 16

6.5 Apoptosis evaluation by analysis of caspase-3 activity

High levels of Hsp27 seem to block apoptosis induced by chemotherapeutic drugs through the binding of caspase-3 prodomain, which provides a protection against the proteolytic cleavage necessary for caspase-3 activation (**Figure 6.5A**).

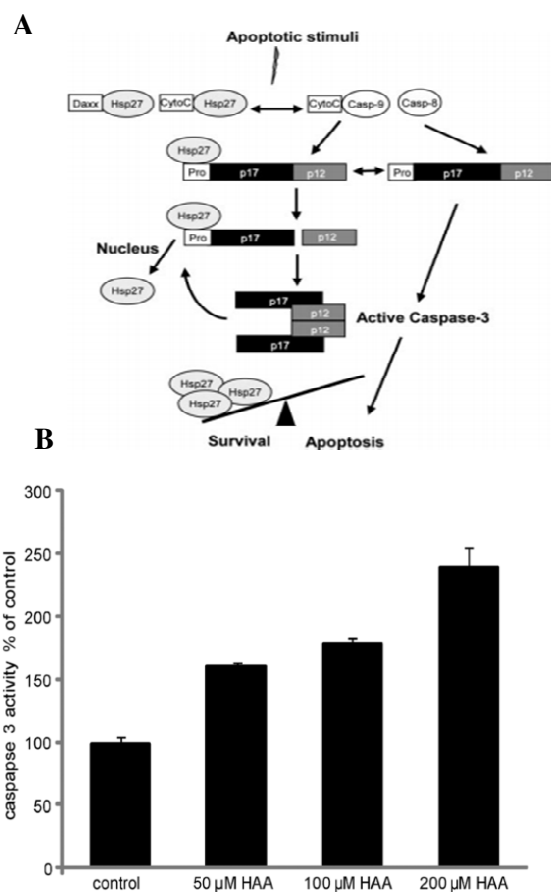


Figure 6.5: (A) Scheme of the Hsp27 protection from the proteolytic cleavage necessary for caspase-3 activation; (B) Apoptosis evaluation by analysis of caspase-3 activity measurements by fluorimetric assays in U937 cells incubated with different concentrations of HAA.

Caspase-3 activity was measured by a fluorimetric assay based on the proteolytic cleavage of the 7-amido-4-methylcoumarin (AMC)-derived substrate which yields a fluorescent product. U937 cells were treated with different concentrations of HAA for 24 h. **Figure 6.5B** shows the results of the caspase-3 activity measurements in cell lysates, demonstrating a concurring increase in the executioner caspase activation.

6.6 Conclusion

Since the previous studies were aimed at the identification of the molecular target(s) of clerodane diterpenes this further investigation suggested that these compounds can interact with Hsp27, modulating its biological activity.

Chemical proteomic approaches, used in this study resulted efficient and reliable, allowing us to identify the possible molecular target responsible for the observed effect of clerodane diterpenes on certain cancer cells proliferation and survey.

The multidisciplinary approach used to validate the chemical proteomics results confirmed the affinity of these molecules towards the chaperone, also suggesting the protein region involved in the interaction, and permitted to demonstrate the inhibitory effects of such interaction on Hsp27 chaperon activity. At the cellular level, this inhibition resulted in a concentration dependent activation of caspase-3 determining the observed pro-apoptotic effect.

Despite the increasing interest towards small heat shock proteins because of their emerging role in different physiological and pathological processes, few compounds capable of modulating their biological activity have been actually described.

However, such molecules could represent a useful tool both to design new therapeutic agents and as probes to investigate the structure and function of these chaperones. In this light, HAA and related compounds could be promising in the development of optimized compounds.

Experimental section

Chapter 7

Phytochemical methods

Chapter 7

7.1 Chromatography techniques

7.1.1 Thin Layer Chromatography (TLC)

TLC was performed on precoated kieselgel 60 F₂₅₄ plates (Merck), 0.25 mm thick, with glass or aluminium as support. The spots were revealed using UV detection with lamp at 254 or 366 nm and successively using a specific spray reagent, allowing to the development of typical colouring that can give information about the nature of examined compounds. As eluting solvents in the TLC analyses, some mixtures of solvents were mainly used: CHCl₃:MeOH (99:1), CHCl₃:MeOH (98:2), CHCl₃:MeOH (97:3), CHCl₃:MeOH (95:5), CHCl₃:MeOH (9:1), CHCl₃:MeOH:H₂O (40:9:1), CHCl₃:MeOH:H₂O (70:30:3), *n*-BuOH:AcOH:H₂O (60:15:25).

CeSO₄/H₂SO₄, a general reactive, was used to reveal all compounds contained in mixtures. It is a saturated solution of cerium sulphate in 65% sulphuric acid. Heating at 120°C for 15 min is needed to reveal the spots.

7.1.2 Column Chromatography (CC)

7.1.2.1 Gel Filtration Chromatography

Gel filtration chromatography was performed over Sephadex LH-20 (25-100 μm, Pharmacia Fine Chemicals) using columns 3 x 100 cm, for 2-4 g of extract,

and 5 x 100 cm for 5-10 g of material, and a peristaltic pump Pharmacia Fine Chemicals P1. The eluent was always methanol, at constant flow rate (0.8 mL/min).

7.1.2.2 Flash Chromatography

Flash chromatography (**Figure 7.1**) was performed over Silica gel 60 (230-410 μm , Merck), eluting with CHCl_3 containing an increasing amount of MeOH. Compressed air was used maintaining a constant flow rate at 20 mL/min. Columns size, related to the quantity of mixtures charged, are illustrated in **Table 7.1**.

Table 7.1: Flash chromatography parameter

Diameter (mm)	Length (mm)	Material (mg)
10	160	40-100
20	160	160-400
30	160	400-900
40	160	800-1600
100	160	5000



Figure 7.1: Flash chromatography column

Some purification were carried out with Biotage® Isolera® Spektra four flash purification system to improve fractions and compound purity with λ detection and PDA spectral analysis at 254 and 320 nm. Cartridge size, related to the quantity of the mixture charged, is reported in **Table 7.2**.

Table 7.2: Biotage® Isolera® parameters

Cartridge (g)	Load capacity (mg)	Flow rate (ml/min)
10	100-500	10-20
25	250-1250	15-40
50	500-2500	30-50
100	1000-5000	30-50
340	3400-17000	65-120

7.1.2.3 Solid Phase Extraction (SPE) Chromatography

SPE chromatography was conducted over silica gel 60 RP-18 (40-63 μm , Merck) using H_2O containing an increasing amount of MeOH. Columns size, related to the quantity of mixtures charged, are illustrated in **Figure 7.2**.






1 mL	3 mL	6 (8 mL)	12 (15 mL)	20 (25 mL)
				
Sorbent weight				
50 mg 100 mg	200 mg 500 mg	1 g 2 g	3 g	5 g

Figure 7.2: SPE chromatography parameters

7.1.2.4 High Performance Liquid Chromatography (HPLC)

Reverse-phase HPLC separations (**Figure 7.3**) were conducted on a Shimadzu LC-8A series pumping system equipped with a Shimadzu RID-10A refractive index detector and Shimadzu injector on a C₁₈ μ -Bondapak column (30 cm x 7.8 mm, 10 μ m Waters, flow rate 2.0 ml/min). MeOH:H₂O mixtures were used as mobile phases.



Figure 7.3: HPLC system

7.1.2.5 Gas Chromatography (GC)

Gas chromatography analyses were performed using a Dani GC 1000 instrument on a L-CP-Chirasil-Val column (0.32 mm x 25 m).

7.2 Nuclear Magnetic Resonance analyses (NMR)

NMR experiments were performed on Advance Bruker 250 spectrometer (**Figure 7.5**) and Bruker DRX-600 spectrometer at 300 K. All the 2D NMR spectra were acquired in CD₃OD or in DMSO-*d*₆ in the phase-sensitive mode with the transmitter set at the solvent resonance and TPPI (Time Proportional

Phase Increment) used to achieve frequency discrimination in the ω_1 dimension. Standard pulse sequences and phase cycling were used for DQF-COSY, TOCSY, HSQC, HMBC, and ROESY experiments. NMR data were processed on Topsin software and Silicon Graphic Indigo2 Workstation using UXNMR software. Chemical shifts were expressed in δ (parts per million) referenced to the solvent peaks δ_{H} 3.34 and δ_{C} 49.0 for CD_3OD and δ_{H} 2.49 and δ_{C} 39.5 for $\text{DMSO}-d_6$.



Figure 7.4: Advance Bruker 250 NMR spectrometer

7.3 Mass Spectrometry analyses (MS)

MS and MS^n analyses (positive and negative mode) were obtained using a LCQ Advantage spectrometer (Thermo Finnigan, San Jose, CA, USA) equipped with an ion trap analyzer and Xcalibur 3.1 software (**Figure 7.5**). All the analyzed molecules were dissolved in MeOH and then diluted to 10-20 $\mu\text{m}/\text{mL}$. Samples were injected into the spectrometer at a flow rate of 5 $\mu\text{L}/\text{min}$ using an external syringe pump. HRESIMS were achieved using a nano LC-MS/MS system, with a nanoAcquity UPLC module and a Q-TOF premiere spectrometer

equipped with a nanoelectrospray ion source (Waters-Milford, MA, USA), and provided with a lock-mass apparatus to perform a real-time calibration correction.



Figure 7.5: *LCQ Advantage ion trap mass spectrometer*

7.4 Optical Rotations analyses

Optical rotations analyses were measured on a Perkin–Elmer 241 polarimeter equipped with a sodium lamp (589 nm) and a 1 dm microcell.

7.5 Ultraviolet-Visible (UV) Spectroscopy

UV spectra were recorded on a Perkin–Elmer–Lambda Spectrophotometer. Samples were dissolved in MeOH.

7.6 Circular Dichroism (CD) Spectroscopy

CD spectra were measured on a JASCO J-810 spectropolarimeter with a 0.1 cm cell in DMSO at room temperature under the following conditions: speed 50 nm/min, time constant 1 s, bandwidth 2.0 nm.

7.7 Determination of absolute configuration of the 15,16-diol moiety using Snatzke's method

Dimolybdenum tetracetate was purchased from Sigma–Aldrich. According to the published procedure (Di Bari *et al.*, 2001), about 1:1 diol-to-molybdenum mixtures were prepared using 0.5 mg/ml of each compound. Soon after mixing, the first CD spectrum was recorded and its evolution monitored until stationary (30–60 min). The sign of the diagnostic band at 305 nm is correlated to the absolute configuration of the 15,16-diol moiety.

7.8 Acid hydrolysis

A solution of each compound (2.0 mg) in 1 N HCl (1 ml) was stirred at 80 °C in a stoppered reaction vial for 4 h. After cooling, the solution was evaporated under a stream of N₂. The residue was dissolved in 1-(trimethylsilyl)imidazole and pyridine (0.2 ml), and the solution was stirred at 60 °C for 5 min. After drying the solution, the residue was partitioned between H₂O and CHCl₃. The CHCl₃ layer was analyzed by GC using a L-CP-Chirasil-Val column (0.32 mm x 25 m). Temperatures of both the injector and detector was 200 °C. A temperature gradient system was used for the oven, starting at 100 °C for 1 min and increasing up to 180 °C at a rate of 5 °C/min. Peaks of the hydrolysate were detected by comparison with retention times of authentic samples of D-xylose, L-arabinose, L-rhamnose, and D-glucose (Sigma–Aldrich) after treatment with 1-(trimethylsilyl)imidazole in pyridine.

Chapter 8

*Chemical proteomics applied to 15-ketoatractiligenin methyl ester
target discovery*

Chapter 8

8.1 Material

Epoxy-Activated Sepharose 6B[®] support and the protease inhibitor cocktail were purchased from Sigma Aldrich. Hsp 60, Hsp 70 and PPAR γ were obtained from Tebu-Bio. HTC-116 cell line pellets were obtained on kind concession of Dr. S. De Falco, Istituto di Genetica Molecolare, CNR, Napoli. Biacore 3000, CM5 sensor chip, and coupling reagents [*N*-ethyl-*N'*-(3-dimethylaminopropyl) carbodiimide (EDC), *N*-hydroxy-succinimide (NHS), and ethanolamine-HCl] were purchased from GE Healthcare (United Kingdom).

8.2 Chemical immobilization of 15-ketoatractyligenin methyl ester

The *Epoxy-Activated Sepharose 6B*[®] resin was treated as specified from the company before the use. 8.57 mg of the previously swelled resin was treated with 1.1 mg of SR 2017, dissolved in 60% of CH₃CN and 40% of 50 mM sodium bicarbonate (NaHCO₃) at pH 8 for 24 h at 35 °C under continuous shaking. Final volume was 200 μ l.

The amount of immobilized SR2017 was calculated integrating the peaks relative to free SR2017 after HPLC injections of supernatants at $t = 0$ h and $t = 24$ h. An Agilent 1100 Series chromatograph (Figure 8.1), binary pump (G-1312A), autosampler (G1329A), DAD (G-1315D) was used on a C₁₂ Jupiter 4 μ PROTEO (150 x 2.00 mm) column at flow rate of 0.3 ml/min. The gradient

(solution A: H₂O 1% HCOOH, solution B: CH₃CN) started at 30% and ended at 95% B after 25 min (**Table 8.1**).



Figure 8.1: HPLC-DAD Agilent

Table 8.1: HPLC gradient used to quantify SR2017 immobilization yield

Time	% B
0	30
5	30
20	60
21	70
23	95
25	95

The residual epoxy groups were blocked by consecutive washing steps with 50 mM NaHCO₃ pH 8 and the final addition of 50 µl of 1 M ethanolamine at pH

8 for 16 h at 45 °C. The ethanolamine exceeding was removed with consecutive and alternate washing steps 0.1 M CH₃COONa (sodium acetate), 0.5 M Sodium chloride (NaCl) at pH 4 and 0.1 M tris(hydroxymethyl)aminomethane hydrochloride (Tris HCl), 0.5 M NaCl at pH 8. PBS was used for a final washing. The same procedure was used to obtain the control matrix.

8.3 Purification of Proteic SR2017 Targets by Affinity Chromatography

Cell pellets were lysed in PBS 1X (50 mM sodium Phosphate, 150 mM NaCl), 0.1% Igepal. Protease inhibitor cocktail was added and the mixture was stored in ice for 30 min and then clarified by centrifugation 12000 g, 4 °C for 15 min. Protein concentration was determined by Bradford assay (Bradford, 1976; Van Kley and Hale, 1977) and adjusted to 1 mg/ml.

SR2017-fixed beads (50 µl dry volume) and the control beads (50 µl dry volume) were separately mixed with 500 µl of crude cell extract (1 mg/ml) and incubated at 4 °C for 16 h on a rotating wheel. After three washing with PBS 1% glycerol and two with PBS, the bound proteins were eluted with SDS-PAGE sample buffer (60 mM Tris HCl pH 6.8, 2% SDS, 0.001% bromophenol blue, 10% glicerol, 2% 2-mercaptoethanol).

Eluted samples were loaded on a monodimensional 12% SDS-PAGE, and separated proteins were stained with Brilliant Blue G-Colloidal (Sigma Aldrich). In gel trypsin digestions were performed as described (Shevchenko *et al.*, 2006). Briefly, Coomassie-stained protein bands were excised from the polyacrylamide gel, reduced, alkylated using iodoacetamide, and digested by trypsin. The resulting fragments were extracted and analyzed by LC/MS/MS using a Q-TOF premier instrument (**Figure 8.2**) (Waters, Milford, USA) equipped with a nano-ESI source coupled with a nano-Acquity capillary UPLC (Waters): peptide separation was performed on a capillary BEH C₁₈ column (0.075 mm x 100 mm,

1.7 mm, Waters) using aqueous 0.1% HCOOH (A) and CH₃CN containing 0.1% HCOOH (B) as mobile phases. Peptides were eluted by means of linear gradient from 5% to 50% of B in 45 min and a 300 nL/min flow rate. Capillary ion source voltage was set at 2.5 kV, cone voltage at 35 V, and extractor voltage at 3 V.

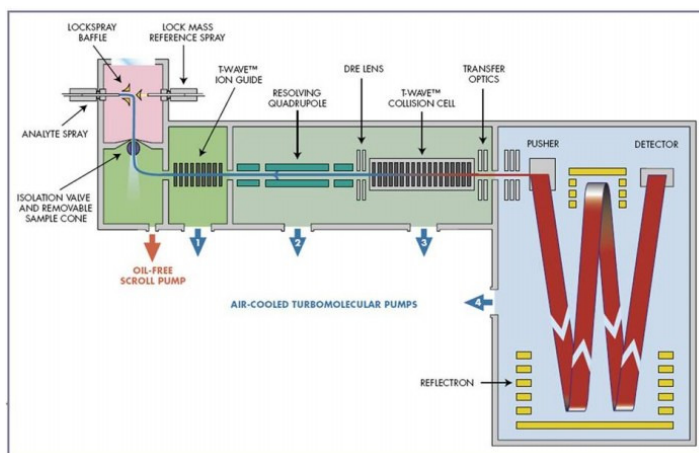


Figure 8.2: *Q-TOF instrument*

Peptide fragmentation was achieved using argon as collision gas and a collision cell energy of 25 eV. Mass spectra were acquired in an m/z range from 400 to 1800, and MS/MS spectra in a 25–2000 range. Mass and MS/MS spectra calibration was performed using a mixture of angiotensin and insulin as an external standard and [Glu]-Fibrinopeptide B human as a lock mass standard.

A gel-free approach was also used: proteins were eluted from the resin using guanidine hydrochloride 6 M, dithiothreitol 20 mM, Tris-HCl 50 mM solution, pH 7.8. After a 30 min incubation with iodoacetamide, the protein mixtures underwent trypsin digestion. Resulting peptides were analyzed by the previously

described LC/MS/MS apparatus, using for the chromatographic separation a linear gradient from 3% to 55% of B in 90 min. MS and MS/MS conditions were identical to those described above. In both experiments, doubly and triply charged peptide-ions were automatically chosen by the MassLynx software and fragmented. MS data were automatically processed and peaklists for protein identifications by database searches were generated by the ProteinLynx software. MS and MS/MS data were used by Mascot (Matrix Science) to interrogate the Swiss Prot non-redundant protein database. Settings were as follows: mass accuracy window for parent ion, 50 ppm; mass accuracy window for fragment ions, 200 millimass units; fixed modification, carbamidomethylation of cysteines; variable modifications, oxidation of methionine. Proteins with more than 2 peptides and program scores >75 were considered as reliable proteins. Protein Prospector software was eventually used to confirm protein identification; setting parameters included selection of trypsin with up to 2 missed cleavage sites, fixed modification, carbamidomethylation of cysteines; variable modifications, oxidation of methionine.

8.4 Surface Plasmon Resonance (SPR)

To perform SPR studies optical biosensor BIACORE 3000 (GE Healthcare) was used. Hsp 60 and Hsp 70 solutions 1 μ M in 50 mM sodium acetate at pH 4 were prepared. Human recombinant PPAR γ solution 1 μ M in sodium acetate 100 mM at pH 4.5 was prepared. Each protein was separately immobilized on a CM5 sensor chip (**Figure 3**). The carboxylic groups of the chip were previously activated by EDC 0.2 M and NHS 0.05 M. The exceeding active groups were inactivated with ethanolamine 1 M. SR2017 was dissolved in 100% DMSO to obtain a 4 mM solution, and then diluted 1:1000 (v/v) in PBS (10 mM NaH₂PO₄, 150 mM NaCl, pH 7.4) to a final DMSO concentration of 0.1%. For PPAR γ it

was used HBS-EP buffer instead of PBS. HBS is made up of 0.01 M 4-(2-hydroxyethyl)piperazine-1-ethanesulfonic acid (HEPES) pH 7.4, 0.15 M NaCl, 3 mM ethylenediaminetetraacetic acid (EDTA) and Surfactant P₂₀ 0.005%. A concentration series of SR2017 was prepared as twofold dilutions into running buffer: the complete binding study was performed using a six-point concentration series, typically spanning 0.025–1 mM, and triplicate aliquots of the sample's concentration were dispensed into single-use vials.

Multiple blank samples of running buffer alone were included in each analysis. Binding experiments were performed at 25 °C, using a flow rate of 50 mL min⁻¹. The dissociation time was set at 600 seconds. Rate constants for association (k_a) dissociation (k_d) and the dissociation constant (K_D) were obtained by globally fitting data from all the injection of different concentration of the sample, using the simple 1:1 Langmuir binding model. Simple interactions were adequately fit to a single-site bimolecular interaction model ($A + B = AB$), yielding a single K_D. Sensorgram elaborations were performed using the BIAevaluation software provided by GE Healthcare. The procedure was repeated for each SR2017 injection series on each immobilized protein.

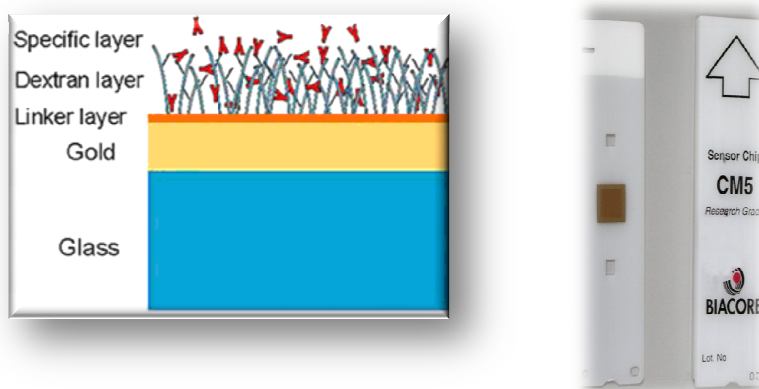


Figure 8.3: Sensor chip CM5

Chapter 9

Methods to validate Hsp27 as target of HAA

Chapter 9

9.1 HAA/Hsp27 interaction: limited proteolysis

Limited proteolysis experiments were performed at 37 °C in PBS, 0.1% DMSO, and 20 mM DTT, using trypsin, endoproteinase GluC (V8) or chymotrypsin as proteolytic agents; 30 mL of a 2 mM Hsp27 solution were used for each experiment. Binary complex Hsp27/hardwickiic acid was formed by incubating the protein with a 5:1 molar excess of the compound at 37 °C for 15 min prior to proteolytic enzyme addition. Both protein and the complex were digested using a 1:100 (w/w) enzyme to substrate ratio. The extent of the reactions was monitored on a time-course basis by sampling the incubation mixture after 5, 15, and 30 min of digestion. Samples were desalted by ziptip C₄ (Merk Millipore) and the proteolytic fragments were analyzed by MALDITOF/MS (**Figure 9.1**) using a MALDI micro MX (Waters). In order to optimize the sensitivity and accuracy of the mass measurements, two different m/z ranges were explored for each sample: a first range, from m/z 500 to 3500 was analyzed in reflector mode; the other range, from m/z 3500 to 25000 was analyzed in linear mode. Each m/z range was calibrated using a suitable peptide or protein mixture. Mass data were elaborated using the Masslynx software (Waters). Preferential hydrolysis sites on Hsp27 under different conditions were identified on the basis of the fragments released during the enzymatic digestions. When comparative experiments were carried out on Hsp27 in the presence or absence of HAA, differences in the susceptibility of specific cleavage sites were detected, from which protein regions involved in the conformational changes could be inferred.



Figure 9.1: MALDI-TOF instrument

9.2 Insulin and citrate synthase (CS) aggregation assays

The ability of HAA to modulate the chaperone activity of Hsp27 was evaluated by monitoring the insulin DTT induced and the citrate synthase (CS) thermal induced aggregation in the presence of stoichiometric amounts of Hsp27, and with or without a 4-fold molar excess of HAA. The aggregation process was monitored by right angle light scattering measurements, using a Perkin Elmer LS 50B fluorimeter with a Perkin Elmer PTP-1 controlled water bath in stirred and thermostated quartz cells. Both the emission and excitation wavelengths were set at 500 nm, and the band pass was 5 nm. Kinetics traces reported here are the averages of two measurements. Insulin aggregation was initiated incubating 0.57 nmol of the polypeptide with 0.1 M DTT in PBS, pH 7.4 at 37 °C. CS aggregation was initiated by submitting the protein (0.075 mM) to an incubation in 40 mM HEPES–KOH, pH 7.5 at 43 °C. To eliminate the exceeding citrate before the analyses, CS was dialyzed against Tris–HCl, 50 mM, and EDTA, 2 mM, at pH 8 using a 500 mL cut-off 10 000 Da filter.

9.3 Apoptosis evaluation

U937 cells were seeded in 48-well plastic plates, 250 μ L per well at 2×10^5 cells mL^{-1} and HAA or compound **16** was added at different concentrations (50, 100 and 200 μ M) for 24 h. At the end of the treatments 250 μ L of a hypotonic buffer (0.1% sodium citrate, 0.1% Triton X-100 and 50 μ g mL^{-1} propidium iodide) was added to cell suspensions. Apoptosis was evaluated by analysing the percentage of hypodiploid nuclei by propidium iodide incorporation. Samples were analysed by a FACS-Calibur flow cytometer using the Cell Quest software (Becton Dickinson, North Ryde, NSW, Australia). All the experiments were performed at least in triplicate.

9.4 Analysis of caspase-3 activity

Caspase-3 activity was measured by a fluorimetric assay based on the proteolytic cleavage of the 7-amido-4-methylcoumarin (AMC)-derived substrate (Ac-DEVD-AMC, Sigma-Aldrich), which yields a fluorescent product. U937 cells were treated with different concentrations of HAA for 24 h, then harvested and washed three times with PBS 1X. Pellets were lysed with caspase-3 reaction buffer (50 mM HEPES pH 7.5, 0.1 mM EDTA, 0.1% Nonidet P-40, 0.1% CHAPS, 1 mM DTT) incubated for 30 min on ice and clarified by centrifugation for 15 min at 15000 g at 4 °C. Assays were performed in 96-well plates by incubating 10 μ g of protein extracts with 20 μ M Ac-DEVD-AMC in 200 μ L of assay buffer at 37 °C for 3 h. Samples were analyzed using a micro-plate reader (L55 Fluorescence Spectrometer Perkin Elmer Instruments; excitation: 360 nm, emission: 460 nm).

Chapter 10

Conclusions

Conclusions

This thesis work reported an approach to investigate the activities of diterpenoids isolated from natural source in order to find for them an interesting application (**Figure 10.1**).



Figure 10.1: Work scheme

The starting point was the selection of some plants known as rich in diterpenes: *Podocarpus elongatus*, *Podocarpus gracilior*, *Clerodendrum*

splendens, and *Sideritis pullulans*. The following step was their phytochemical study with the aim to isolate pure compounds. Chromatographic separation led to the isolation and structural characterization of 27 diterpenes of which 18 were new natural compounds (**Figure 10.2-10.7**). These compounds were introduced in our diterpenes library (**Chapters 2-4**).

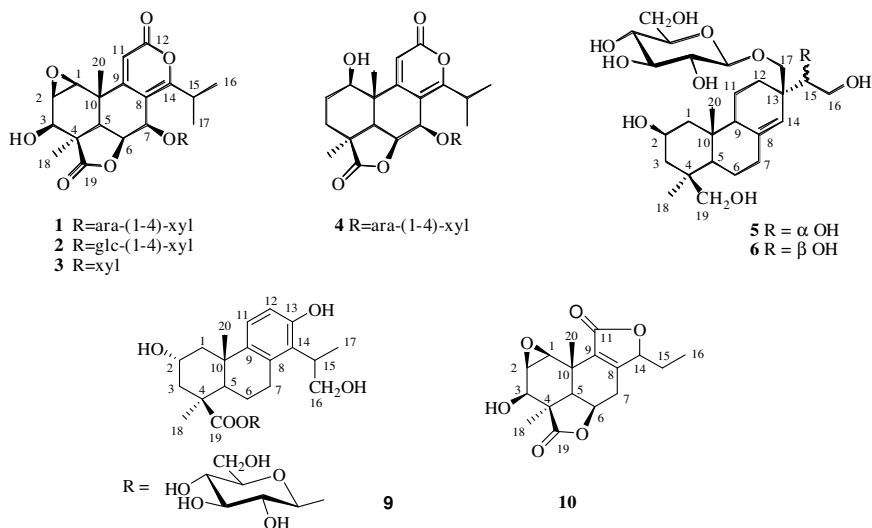


Figure 10.2: New diterpenes isolated from *Podocarpus* spp., see **Chapter 2**

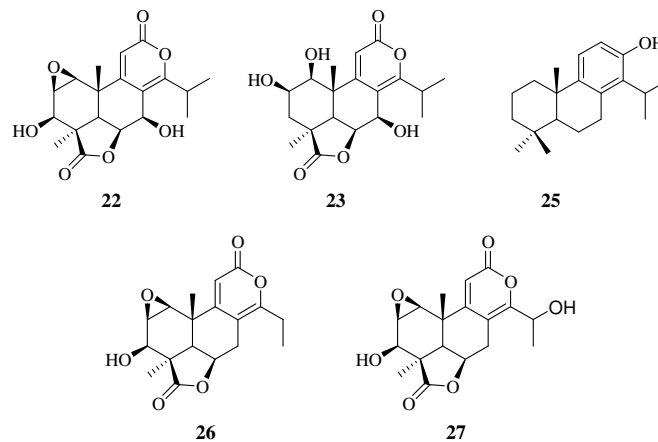


Figure 10.3: Structures of known diterpenes from *Podocarpus* spp., see Chapter 2

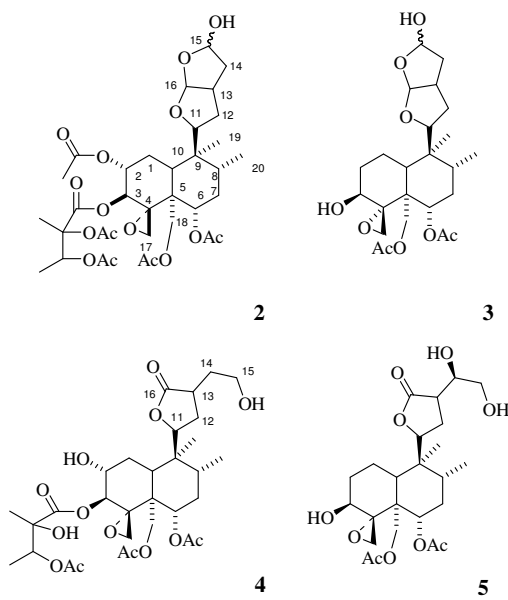


Figure 10.4: New clerodanes from *C. splendens*, see Chapter 3

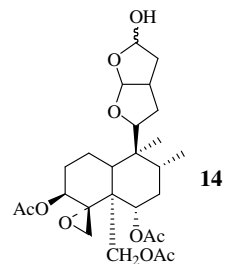


Figure 10.5: Known clerodanes from *C. splendens*, see Chapter 3

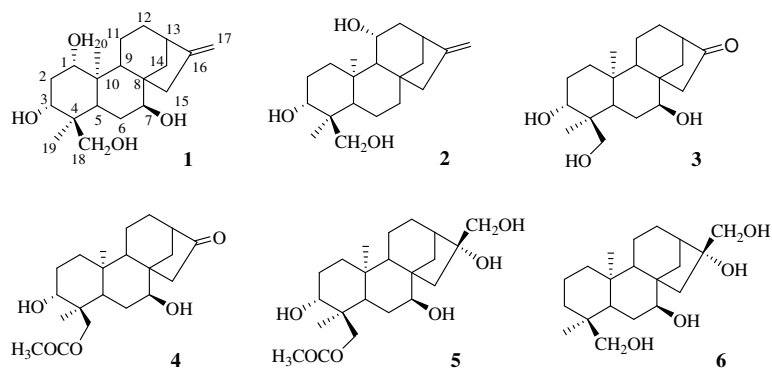


Figure 10.6: New diterpenes from *S. pullulans*, see Chapter 4

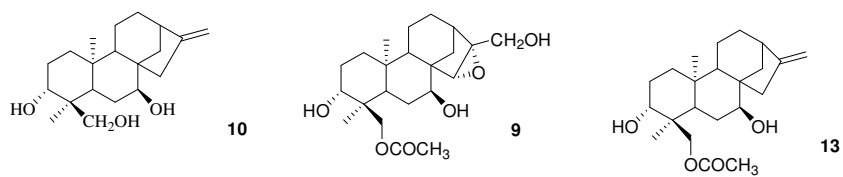


Figure 10.7: Known diterpenes from *S. pullulans*, see Chapter 4

The importance of natural compounds libraries was described in **Chapter 1** and in **Chapter 5** a method for the research of the molecular targets for small molecules library was described: the fishing for partners study. Using this chemical proteomics approach, Hsp70 and PPAR γ were recognized as potential proteic targets for the semi-synthetic derivative of atractyligenin, 15-ketoatractyligenin methyl ester, an *ent*-kaurane selected from our library. The power of the chemical proteomics was clear in this investigation since it could be applied when the information about the proteic targets are lacking. The targets of bioactive molecules are often unknown even if the biological effects are quite known like in our case. Further studies will be necessary to validate these two targets and also to explain the relationships between the interactions of the atractyligenin derivative and the two proteins and the effects that were observed in cancer cell lines.

In **Chapter 6** some methods to validate Hsp27 as molecular target for HAA were reported. HAA induced a conformational change in *N*-terminal domain of the protein and enhanced the chaperone function. Very few information about ligand of the small heat shock proteins are available and HAA together with the other clerodanes of our library could be a useful tool both to design new therapeutic agents and as probes to investigate the structure and function of these chaperones.

Bibliography

Abdillahi, H.S., Finnie, J.F., Van Staden J., *Journal of Ethnopharmacology*, **2011**, *136*, 496-503.

Abdillahi, H.S., Stafford, G.I., Finnie, J.F., Van Staden, J., *African Journal of Botany*, **2010**, *76*, 1-24.

Abou-Jawdah, Y., Wardan, R., Sobh, H., Salameh, A., *Phytopathologia Mediterranea*, **2004**, *43*, 377-386.

Al-Eisawi, D.M., *Mitteilungen der Botanischen Staatssammlung München*, **1982**, *18*, 179-182.

Aloy, T., Hadchity, E., Bionda, C., Diaz-Latoud, C., Claude, L., Rousson, R., Arrigo, A.P., Rodriguez-Lafrasse, C., *International Journal of Radiation Oncology Biology Physics*, **2008**, *70*, 543-553.

Andersen, R.J., Le Blanc, M.J., Sum, F.W., *Journal of Organic Chemistry*, **1980**, *45*, 1169-1170.

Bantscheff, M., Scholten, A., Heck, A.J., *Drug Discovery Today*, **2009**, *14*, 1021-1029

Baranova, E. V. Weeks, S.D., Beelen, S., Bukach, O.V., Gusev, N.B., Strelkov, S.V., *Journal of Molecular Biology*, **2011**, *411*, 110-122.

Baranova, E.V., Beelen, S., Gusev, N.B., Strelkov, S.V., *Acta Crystallographica, Section F: Structural Biology and Crystallization Communications*, **2009**, *65*, 1277-1281.

Braca, A., Armenise, A., Morelli, I., Mendez, J., Mi, Q., Chai, H., Swanson, S.M., Kinghorn, A.D., De Tommasi, N., *Planta Medica*, **2004**, *70*, 540-550.

Bradford, N.M., *Analytical Biochemistry*, **1976**, *72*, 248-254.

Bruno, M., Rosselli, S., Pibiri, I., Piozzi, F., Bond, M.L., Simmonds, M.S.J., *Phytochemistry*, **2001**, *58*, 463-474.

Bruno, M., Rosselli, S., Pibiri, I., Kilgore, N., Lee, K.H., *Journal of Natural Products*, **2002**, *65*, 1594-1597.

Bryan, R.F.; Smith, P.M., *Journal of Chemical Society, Perkin Transactions 2: Physical Organic Chemistry*, **1975**, *14*, 1482-6.

Burbaum, J., Tobal G.M., *Current Opinion in Chemical Biology*, **2002**, *6*, 427-433.

Cambie, R.C., Cox, R.E., Croft, K.D., Sidwell, D., *Phytochemistry*, **1983**, *22*, 1163-1166.

Caporale, L., *Darwin In the Genome: Molecular Strategies in Biological Evolution*, New York, Mc Graw Hill Companies, **2002**, 9-18.

Cappello, F., Conway de Macario, E., Marasà, L., Zummo, G., Macario, A.J.L., *Cancer Biology and Theraphy*, **2008**, *7*, 801-809.

Casbarra, A., Birolo, L., Infusini, G., Dal Piaz, F., Svensson, M., Pucci, P., Svanborg, C., Marino, G., *Protein Science*, **2004**, *13*, 1322-1330.

Casper, D., Bukhtiyarova, M., Springman, E.B., *Analytical Biochemistry*, **2004**, *325*, 126-136.

Chait., B.T., *Science*, **2006**, *314*, 65-66.

Chan, J., Khan, S.N., Harvey, I., Merrik, W., Pellettier, J., *RNA*, **2004**, *10*, 528-543.

Cheng, G., Bai, Y., Zhao, Y., Tao, J., Liu, Y., Tu, G., Ma, L., Liaoc, N., Xuc, X., *Tetrahedron*, **2000**, *56*, 8915-8920.

Chin, Y., Baluna,s M., Chai, H.B., Kinghorn, A.D., *The AAPS Journal*, **2006**, *8*, 28.

Ciocca, D.R., Calderwood, S.K., *Cell Stress Chaperones*, **2005**, *10*, 86-103.

Clark, A.M., *Pharmaceutical Research*, **1996**, *13*, 1133-1138.

Coll, J., Tandron, Y.A., *Phytochemistry Reviews*, **2007**, *7*, 25-49.

Creagh, E.M., Carmody, R.J., Cotter, T.G., *Experimental Cellular Research*, **2000**, *257*, 58-66.

De Tommasi, N., Piacente, S., De Simone, F., Pizza, C., *Journal of Agricultural and Food Chemistry*, **1996**, *44*, 1676-1680.

De Tommasi N., Pizza C., Bellino, A., Venturella P., *Journal of Natural Products*, **1997**, *60*, 663-668.

De Quesada, T., Rodriguez, B., Valverde, S., Huneck, S., *Tetrahedron Letters*, **1972**, 2187.

Di Bari, L., Pescitelli, G., Pratelli, C., Pini, D., Salvadori, P., *Journal of Organic Chemistry*, **2001**, *66*, 4819-4825.

Didelot, C., Lanneau, D., Brunet, M., Joly, A.L., De Thonel, A., Chiosis, G., Garrido, C., *Current Medicinal Chemistry*, **2007**, *14*, 2839-2847.

Dobson, C.M., *Nature*, **2004**, *432*, 824-828.

Duke, S.O., Oliva, A., *Allelopathy, chemistry and mode of action of allelochemicals*, J. M. G. Molinillo, H. G. Cutler, CRC press, **2004**, 201-216.

Eckenwalder, J.E., *Conifers of the world: the complete reference*, Timber Press, **2009**.

Erkan, N., Cetin, H., Ayranci, E., *Food Research International*, **2011**, *44*, 297-303.

Faiella, L., Dal Piaz, F., Bisio, A., Tosco, A., De Tommasi, N., *Molecular BioSystem*, **2012**, *8*, 2637-2644.

Faiella, L., Temraz, A., De Tommasi, N., Braca, A., *Phytochemistry*, **2012**, 76, 172-177.

Faiella, L., Temraz, A., Siciliano, T., De Tommasi, N., Braca, A., *Phytochemistry Letters*, **2012**, 5, 297-300.

Fang, S., Xu, Y., Li, Y., Chen, M., *Huaxue Xuebao*, **1990**, 48, 312-314.

Flaherty, K.M., DeLuca-Flaherty, C., McKay, D.B., *Nature*, **1990**, 346, 623-628.

Fraga, B.M., Alvarez, L., Suarez, S., *Journal of Natural Products*, **2003**, 66, 327-331.

Fraga, B.M., Hernandez, M.G., Fernandez, C., Arteaga, J.M., *Phytochemistry*, **1987**, 26, 775-777.

Frelek, J., Geiger, M., Voelter, W., *Current Organic Chemistry*, **1999**, 3, 117-146.

Gabai, Yaglom, J.A., Volloch, V., Meriin, A.B., Force, T., Koutroumanis, M., Massie, B., Mosser, D.D., Sherman, M.Y., *Molecular and Cellular Biology*, **2000**, 20, 6826-6836.

García, P.A., Braga de Oliveira, A., Batista, R., *Molecules*, **2007**, 12, 455-483.

Ghosh, J.C., Dohi, T., Kang, B.H., Altieri, D.C., *Journal of Biological Chemistry*, **2008**, 283, 5188-94.

Gonzalez, A.G., Fraga, B.M., Hernandez, M.G., Hanson JR, *Phytochemistry*, **1981**, *20*, 846-847.

Gonzalez-Burgos, E., Carretero, M.E., Gomez-Serranillos, M.P., *Journal of Ethnopharmacology*, **2011**, *135*, 209-225.

Gullo, V.P., McAlpine, J., Lam, K.S., Baker, D., Petersen, F., *Journal of Industrial Microbiology and Biotechnology*, **2006**, *33*, 523-531.

Guvenc, A., Okada, Y., Akkol, E.K., Duman, H., Okuyama, T., Calis, I., *Food Chemistry*, **2010**, *118*, 686-692.

Han, C., Demetris, A.J., Liu, Y., Shelhamer, J.H., Wu, T., *Journal of Biological Chemistry*, **2004**, *279*, 44344-44354.

Hanson, J. R., *Natural Products Reports*, **2005**, *22*, 594-602, and previous reviews in this series.

Hayashi, Y., Matsumoto T., Uemura, M., Koreeda M., *Organic Magnetic Resonance*, **1980**, *14*, 86-91.

Hayashi, Y., Kim, Y., Hayashi, Y., Chairul, T., *Bioscience, Biotechnology, Biochemistry*, **1992**, *56*, 1302-1303.

Hayashi, Y., Matsumoto, T., *Journal of Organic Chemistry*, **1982**, *47*, 3421-3428.

Hayashi, Y., Yokoi, J., Watanabe, Y., Sakan, T., *Chemistry Letters*, **1972**, *9*, 759-762.

- Hsiao, J.Y., Lin, M.L., *Botany Bulletin Sinica*, **1995**, *36*, 247-251.
- Iqbal, A., Khwaja, I., Ilyas, M., Rahman, W., *Indian Journal of Chemistry*, **1982**, *21B*, 898.
- Jannet, H.B., Chaari, A., Mighri, Z., Martin, M.T., Loukaci, A., *Phytochemistry*, **1999**, *52*, 1541-1545.
- Jeffery, D.A., Bogyo, M., *Current Opinion in Biotechnology*, **2003**, *14*, 87-95.
- Kanokmedhakul, S., Kanokmedhakul, K., Buayairaksa, M., *Journal of Natural Products*, **2007**, *70*, 1122-1126.
- Karioti, A., Skaltsa, H., Heilmann, J., Sticher, O., *Phytochemistry*, **2003**, *64*, 655-660.
- Kirkpatrick, P., *Nature Reviews Drug Discovery*, **2003**, *2*, 607.
- Kliwer, S.A., Forman, B.M., Blumberg, B., Ong, E.S., Borgmeyer, U., Mangelsdorf, D.J., Umesono, K., Evans, R.M., *Proceedings of National Academy of Science*, **1994**, *91*, 7355-7359.
- Koehn, F.E., Carter, G.T., *Nature Reviews Drug Discovery*, **2005**, *4*, 206-220.
- Krey, G., Braissant, O., L'Horsset, F., Kalkhoven, E., Perroud, M., Parker, M.G., Wahli, W., *Molecular Endocrinology*, **1997**, *11*, 779-791.
- Kubo, I, Ying, B-P., *Phytochemistry*, **1991**, *30*, 3476-3477.

Kubo, I., Klocke, J.A., Matsumoto, T., Naoki, H., *Revista Latinoamericana de Quimica*, **1983**, *14*, 59-61.

Kubo, I., Matsumoto, T., Klocke, J.A., *Journal of Chemical Ecology*, **1984**, *10*, 547-559.

Kubo, I., Muroi, H., Himejima, M., *Journal of Natural Products*, **1993**, *56*, 220-226.

Kuo, Y.J., Hwang, S.Y., Wu, M.D., Liao, C.C., Liang, Y.H., *Chemical and Pharmaceutical Bulletin*, **2008**, *56*, 585-588.

Kuono, I., Hashimoto, M., Enjoji, S., Takahashi, M., Kaneto H., Yang C.-S., *Chemical and Pharmaceutical Bulletin*, **1991**, *39*, 1773-1778.

Kupchan, S.M., Baxter, R.L., Ziegler, M.F., Smith, P.M., Bryan, R.F., *Experientia*, **1975**, *31*, 137-138.

Lee, C.A., Olson, P., Hevener, A., Mehl, I., Chong, L.W., Olefsky, J.M., Gonzalez F.J., Ham, J., Kang, H., Peters, J.M., Evans, R.M., *PNAS*, **2006**, *103*, 3444-3449.

Lelj-Garolla, B., Mauk, A.G., *Journal of Biological Chemistry*, **2006**, *281*, 8169-8174.

Lelj-Garolla, B.G., Mauk, A.G., *Journal of Molecular Biology*, **2005**, *345*, 631-642.

Markham, K.R., Sheppard, C., Geiger, H., *Phytochemistry*, **1987**, *26*, 3335-3337.

Markham, K.R., Webby, R.F., Whitehouse, L.A., *Journal of Botany*, **1985**, *23*, 1-13.

Matsuda, N., Kikuchi, M., *Chemical Pharmaceutical Bulletin*, **1996**, *44*, 1676-1679.

McGarvey, D.J., Croteau, R., *The Plant Cell*, **1995**, *7*, 1015-1026.

Miller, R.W., Clardy, J., Kozlowski, J., Mikolajczak, K.L., Plattner, R.D., Powell, R.G., Smith, C.R., Weisleder, D., Qi-Tai, Z., *Planta Medica*, **1985**, *51*, 40-42.

Moldenke H.N., *Phytologia*, **1985**, *57*, 334-365.

Mora, F.D., Jones, D.K., Desai, P.V., Patny, A., Avery, M.A., Feller, D.R., Smillie, T., Zhou, Y.D., Nagle, D.G., *Journal of Natural Products*, **2006**, *69*, 547-552.

Mosser, D.D., Morimoto, R.I., *Oncogene*, **2004**, *23*, 2907-2918.

Mymrikov, C.M., Seit-Nebi, A.S., Gusev, N.B., *Physiological Reviews*, **2011**, *91*, 1123-1159.

Nakanishi, K., Koreeda, M., Sasaki, S., Chang, M.L., Hsu, H.Y., *Chemical Communications*, **1966**, *24*, 915-917.

Nishiya, K., Kimura, T., Takeya, K., Itokawa, H., Lee, S.R., *Phytochemistry*, **1991**, *30*, 2410-2411.

Nurmukhamedova, M.R., Sidyakin, G.T., *Chemistry of Natural Compounds*, **1987**, *23*, 137-140.

Ohno, A. K., Kizu, H., Tomimori, T., *Chemical and Pharmaceutical Bulletin*, **1996**, *44*, 1540-1545.

Okuda, T., *WFCC Newsletter*, **2002**, *35*.

Okwu, D.E., Iroabuchi, F., *Indian Journal of Chemistry Science*, **2009**, *6*, 631-63.

Okwu, D.E., Uchenna, N.F, *African Journal of Biotechnology*, **2009**, *8*, 7271-7282.

Ortholand, J.Y., Ganesan, A., *Current Opinion in Chemical Biology*, **2004**, *8*, 271-280.

Osterloh, A., Veit, A., Gessner, A., Fleischer, B., Breloer, M., *International Immunology*, **2008**, *20*, 433-43.

Otsuka, H., Yao, M., Kamada, K., Takeda, Y., *Chemical and Pharmaceutical Bulletin*, **1995**, *43*, 754-759.

Otsuka, H., *Phytochemistry*, **1994**, *37*, 461-465.

Pabst, A., Barron, D., Semon, E., Schreier, P., *Phytochemistry*, **1992**, *31*, 1649-1652.

Pandey, R., Verma R.K., Gupta, M.M., *Phytochemistry*, **2005**, *66*, 643-648.

Parcellier, A., Schmitt, E., Gurbuxani, S., Seigneurin-Berny, D., Pance, A., Chantome, A., Plenchette, S., Khochbin, S., Solary, E., Garrido, C., *Molecular and Cellular Biology*, **2003**, *23*, 5790-5802.

Park, H.-S., Yoda, N., Fukaya, H., Aoyagi, Y., Takeya, K., *Tetrahedron*, **2004**, *60*, 171-177.

Paul, C., Simon, S., Gibert, B., Virost, S., Manero, F., Arrigo, A., P., *Experimental Cell Research*, **2010**, *316*, 1535-1552.

Pauli, G.F., Junior, P., *Phytochemistry*, **1995**, *38*, 1245-1250.

Perkins, N.D., Pappin, D.J., Creasy, D.M., Cottrell, J.S., *Electrophoresis*, **1999**, *20*, 3551-3567.

Politi, M., De Tommasi, N., Pescitelli, G., Di Bari, L., Morelli, I., Braca, A., *Journal of Natural Products*, **2002**, *65*, 1742-1745.

Prasad, J.S., Krishnamurty, H., *Indian Journal of Chemistry, section B*, **1976**, *14B*, 727-728.

Raida M., *Current Opinion in Chemical Biology*, **2011**, *15*, 570-575.

Rastrelli, L., Aquino, R.P., Abdo, S., Proto, M., De Simone, F., De Tommasi, N., *Journal of Agricultural and Food Chemistry*, **1998**, *46*, 1797-1804.

Rix, U., Hantschel, O., Durnberger, G., Rensing, L., Rix, L., Planyavsky, M., Fernbach, N. V., Kaup, I., Bennett, K. L., Valent, P., Colinge, J., Kocher, T., Superti-Furga, G., *Blood*, **2007**, *110*, 4055-4063.

Rix, U., Superti-Furga, G., *Nature Chemical Biology*, **2009**, *5*, 616-624.

Rodriguez-Hahn, L., Esquivel, B., Cardenas, J., *Trends in Organic Chemistry*, **1992**, *3*, 99-111.

Rogalla, T., Ehrnsperger, M., Preville, X., Kotlyarov, A., Lutsch, G., Ducasse, C., Paul, C., Wieske, M., Arrigo, A.P., Buchner, J., Gaestel, M., *Journal of Biological Chemistry*, **1999**, *274*, 18947-18956.

Rosén, J., Gottfries J., Muresan S., Backlund A., Oprea, T.I., *Journal of Medicinal Chemistry*, **2009**, *52*, 1953-1962.

Rosselli, S., Bruno, M., Maggio, A., Bellone, G., Chen, T.H., Bastow, K.F. and Lee, K.H., *Journal of Natural Products*, **2007**, *70*, 347-352.

Rueda, R.N., *Annals of the Missouri Botanical Garden*, **1993**, *80*, 870-890.

Sadaghiani, A.M., Verhelst, S.H.L., Bogyo, M., *Current Opinion in Chemical Biology*, **2007**, *11*, 1-9.

Samali, A., Cai, J., Zhivotovsky, B., Jones, D.P., Orrenius, S., *The EMBO journal*, **1999**, *18*, 2040-2048.

Schmitt, E., Gehrman, M., Brunet, M., Multhoff, G., Garrido, C., *Journal of Leukocyte Biology*, **2007**, *81*, 15-27.

Shan, Y.X., Liu, T.J., Su, H.F., Samsamshariat, A., Mestril, R., Wang, P.H., *Journal of Molecular and Cellular Cardiology*, **2003**, *35*, 1135-1143.

Shevchenko, A., Tomas, H., Havlis, J., Olsen, J.V., Mann, M., *Nature Protocols*, **2006**, *1*, 2856-2860.

Shiraki, T., Kamiya, N., Shiki, S., Kodama, T.S., Kakizuka, A., Jingami, H., *Journal of Biological Chemistry*, **2005**, *280*, 14145-14153.

Shrestha, K., Banskota, A.H., Kodata, S., Shrivastava, S.P., Strobel, G., Gewali, M.B., *Phytomedicine*, **2001**, *8*, 489-491.

Shrivastava, N., Patel, T., *Medicinal and Aromatic Plant Science and Biotechnology*, **2007**, *1*, 142-150.

Shu, Y.Z., *Journal of Natural Products*, **1998**, *61*, 1053-1060.

Steane, D.A., Scotland, R.W., Mabberty, D.J., Olmstead, R.G., *American Journal of Botany*, **1999**, *86*, 98-107.

Steinhoff, U., Brinkmann, V., Klemm, U., Aichele, P., Seiler, P., Brandt, U., Bland, P.W., Prinz, I., Zügel, U., Kaufmann, S.H., *Immunity*, **1999**, *11*, 349-58.

Takeda, Y., Mima, C., Masuda, T., Hirata, E., Takushi, A., Otsuka, H., *Phytochemistry*, **1998**, *49*, 2137-2139.

Taylor, D.A.H., *Journal of Chemical Society*, **1965**, 3495-3496.

Van Kley, H., Hale, S.M., *Analytical Biochemistry*, **1977**, *8*, 485-487.

Venturella P, Bellino A, Piozzi F, *Phytochemistry*, **1975**, *14*, 1451-1452

Vieira-Junior, G.M., Dutra, L.A., Ferreira, P.M., Moraes, M.O., Costa Lotufo, L.V., Pessoa Cdo, O., Torres, R.B., Boralle, N., Bolzani S., Cavalheiro, A.J., *Journal of Natural Products*, **2011**, *74*, 776-781.

Voss, O.H., Batra, S., Kolattukudy, S.J., Gonzalez-Mejia, M.E., Smith, J.B., Doseff, A.I., *Journal of Biological Chemistry*, **2007**, *282*, 25088-25099.

Waridel, P., Wolfender, J.L., Ndjoko, K., Hobby, K.R., Major, H.J., Hostettmann, K., *Journal of Chromatography*, **2001**, *A 926*, 29-41.

Whitson, L.H., Thomas, C., Henrich, C.J., Sayers, T.J., McMahon, J.B., McKee, T.C. J., *Journal of Natural Products*, **2010**, *73*, 2013-2018.

William, R.J.P., *Journal of Royal Society Interface*, **2007**, *4*, 1049-1070.

Xuan, L.-J., Xu, Y.-M., Fang, S.D., *Phytochemistry*, **1995**, *39*, 1143-1145.

Zhang, Y., Shen, X., *Clinical Cancer Research*, **2007**, *13*, 2855-2864.

Zhang, Y., *Proteins*, **2007**, *69*, 108-117.

Zhang, Z., Zhang, W., Ji, Y-P., Zhao, Y., Wang, C-G., Hu, J-F., *Phytochemistry*, **2010**, *71*, 693-700

.

List of abbreviations

μ M micromolar
15d-PGJ2 15-deoxy- Δ -12,14-prostaglandin J2
1D-2D mono e bidimensional
ABPP activity based protein profiling
Ac-DEVD-AMC *N*-acetyl-Asp-Glu-Val-Asp-7-amino-4-methylcoumarin
ACN acetonitril
AIF apoptosis-inducing factor
AKT protein kinase B
AMC 7-amido-4-methylcoumarin
Apaf-1 apoptosis proteases-activating factor
ARA arabinose
BAX Bcl-2-associated X protein
CD₃OD deuterate methanol
CH₂N₂ diazomethane
CH₃COONa sodium acetate
CHAPS 3-[(3-cholamidopropyl)dimethylammonio]-1-propansulphonate
CHCl₃ chloroform
C¹³-NMR carbon nuclear magnetic resonance
COSY correlation spectroscopy
CS citrate synthase
C-terminal carboxy-terminal
DAD diode array detector
DMSO dimethyl sulfoxide
DNA desossibonucleic acid
DQF double-quantum filtered
DTT dithiothreitol
EDTA ethylendiaminetetraacetic acid
ERK extracellular signal-regulated protein kinase
ESI-MS electrospray mass spectrometry

List of abbreviations

FPP farnesyl pyrophosphate
g gram
GGPP geranyl geranyl pyrophosphate
GLC glucose
GluC endoproteinase GluC
GPP geranyl pyrophosphate
HAA hardwickii acid
HCl chloridic acid
HEPES 4-(2-hydroxyethyl)piperazine-1-ethanesulfonic acid
HMBC heteronuclear multiple bond correlation
H¹-NMR proton nuclear magnetic resonance spectroscopy
HPLC high pressure liquid chromatography
HRESIMS high resolution electrospray mass spectrometry
HSP heat shock protein
HSQC heteronuclear single quantum correlation
Hz hertz
IC₅₀ inhibitory concentration half maxima
IL interleukin
IPP isopentenyl pyrophosphate
ITC isothermal titration calorimetry
J NMR coupling constant
JNK Jun amino-terminal kinases
K_D thermodynamic dissociation constant
KOH potassium hydroxide
LC-MS liquid chromatography coupled with mass spectrometry
m/z mass/ charge
MALDI matrix assisted laser desorption ionization
MeOH methanol
mg milligram

List of abbreviations

Mhz mega Hertz
MnO₂ manganese dioxide
MS mass spectrometry
MSn massspectroscopy tandem
NaCl sodium chlorode
NaHCO₃ sodium bicarbonate
NaOH sodium hydroxide
n-BuOH normal-buthanol
NFκβ nuclear factor kappa-light-chain-enhancer of activated B cells
n-HEXANE normal hexane
NHR nuclear hormone receptor
NMR nuclear magnetic resonance
N-terminal amminoterminal
PBS phosphate buffered saline
PPAR peroxisome proliferator activted receptor
ppm parts per million
PPRE peroxisome proliferator response element
Q-TOF quadrupole- time of flight
RHA rhamnose
ROESY rotating frame Overhause effect spectroscopy
RP reverse phase
RU response unit
SDS-PAGE sodium dodecylsulphate polyacrylamide gel electrophoresis
SER serine
SPR surface plasmon resonance
SR2017 15-keto-atractylgenin methyl ester
STD-NMR saturation transfer difference nuclear magnetic resonance
TLC thin layar chromatography
TNFα tumor necrosis factor α

List of abbreviations

TOCSY total correlation spectroscopy

TOF time of flight

t_R retention time

TRIZMA tris(hydroxymethyl)aminomethane

TZDs thiazolidinediones

ug microgramm

UPLC Ultra Performance Liquid Chromatography

XYL xylose

Figures index

- 1.1: *Screening of natural compounds* **p.3**
- 1.2: *Compounds isolation from plants and structural characterization scheme* **p.4**
- 1.3: *Kauranes and ent-kauranes skeleton* **p.7**
- 1.4: *Clerodane and labdane diterpenes skeleton* **p.8**
- 1.5: *Nagilactone C structure* **p.8**
- 1.6: *Fishing for partners strategy* **p.13**
- 2.1: *Podocarpus elongatus* (Aiton) L' Her. ex Pers. **p.20**
- 2.2: *Podocarpus gracilior* Pilger **p.21**
- 2.3: *New isolated compounds from P. elongatus* **p.28**
- 2.4: *New isolated compounds from P. gracilior* **p.28**
- 2.5: *Structure of known diterpenes isolated from P. elongatus* **p.39**
- 2.6: *Structure of the other known diterpenes isolated from P. gracilior* **p.39**
- 2.7: *Structure of the known compounds* **p.40**
- 3.1: *Flowers of Clerodendrum species* **p. 45**
- 3.2: *Clerodendrum splendens leaves and flowers* **p.46**
- 3.3: *Structure of compound I* **p.50**
- 3.4: *Structures of new diterpenes isolated from Clerodendrum splendens leaves* **p.50**
- 3.5: *Structure of a known diterpene isolated from C. splendens leaves* **p.56**
- 3.6: *Structures of known compounds* **p.56**
- 4.1: *Sideritis pullulans* Vent. **p. 61**
- 4.2: *New diterpenes isolated from S. pullulans* **p.66**
- 4.3: *Structures of compounds 7 and 8* **p.67**
- 4.4: *Structures of known diterpenes isolated from S. pullulans* **p.73**
- 4.5: *Structures of known compounds isolated from S. pullulans* **p.73**

- 5.1: *Structure of atractyligenin* **p.78**
- 5.2: *Reaction scheme of 15-ketoatractyligenin methyl ester synthesis* **p.79**
- 5.3: *Reaction's scheme of SR2017 with epoxy groups of swelled epoxy-activated Sepharose 6B resin* **p.82**
- 5.4: *Chromatographic peaks of SR2017* **p.83**
- 5.5: *SDS PAGE analysis of the affinity purified interactome* **p.84**
- 5.6: *Hsp70 ATPasic site* **p.86**
- 5.7: *Hsp70 involmnet in cell death; Hsp60 pathway, PPAR receptors pathway* **p.89**
- 5.8: *Sensorgrams obtained from immobilized Hsp 70 and PPAR γ* **p.90**
- 6.1: *Structure of compounds 1–16* **p.93**
- 6.2: *Preferential cleavage sites observed submitting to limited proteolysis Hsp27 or Hsp27/1 complex* **p.97**
- 6.3: *Aggregation kinetics of reduced insulin or CS at 43°C determined by light scattering* **p.99**
6. 4: *Apoptosis evaluation by analysis of hypodiploid nuclei percentage in U937* **p.100**
- 6.5: *Scheme of the Hsp27 protection from the proteolytic cleavage necessary for caspase-3 activation; apoptosis evaluation by analysis of caspase-3 activity measurements by fluorimetric assays in U937* **p.101**
- 7.1: *Flash chromatography column* **p.104**
- 7.2: *SPE chromatography parameters* **p.105**
- 7.3: *HPLC system* **p.106**
- 7.4: *Advance Bruker 250 NMR spectrometer* **p.107**
- 7.5: *LCQ Advantage ion trap mass spectrometer* **p.108**
- 8.1: *HPLC-DAD Agilent* **p. 111**
- 8.2: *Q-TOF instrument* **p.113**
- 8.3: *Sensor chip CM5* **p.115**
- 9.1: *MALDI-TOF instrument* **p.117**

- 10.1: Work scheme* **p.119**
- 10.2: New diterpenes isolated from Podocarpus spp.***p.120**
- 10.3: Structures of known diterpenes from Podocarpus spp* **p.121**
- 10.4: New clerodanes from C. splendens* **p.121**
- 10.5: Known clerodane from C. splendens* **p.122**
- 10.7: New diterpenes from S. pullulans* **p.122**
- 10.7: Known diterpenes from S. pullulans* **p.122**

Tables index

- 2.1: ^1H and ^{13}C NMR data of compounds 1-4 p.41
- 2.2: ^1H and ^{13}C NMR data of compounds 5-8 p.42
- 2.3: ^1H and ^{13}C NMR data of compounds 9-11 p.43
- 3.1: ^1H and ^{13}C NMR data of compound 1 p.57
- 3.2: ^1H and ^{13}C NMR data of compounds 2-3 p.58
- 3.3: ^1H and ^{13}C NMR data of compounds 4-5 p.59
- 4.1: ^1H -NMR data of compounds 1-3 p.74
- 4.2: ^1H -NMR data of compounds 4-6 p.75
- 4.3: ^{13}C NMR data of compounds 1-6 p.76
- 4.4: ^1H and ^{13}C NMR data of compounds 7-8 p.77
- 7.1: Flash chromatography parameter p.104
- 7.2: Biotage[®] Isolera[®] parameters p.105
- 8.1: HPLC gradient used to quantify SR2017 immobilization yield p.111

Acknowledgements

Under all point of view, this thesis period represented a challenge and was a great experience for me not only from the professional side. First of all, I'd like to thank my tutor Prof. Alessandra Braca since she gave me her support and guidance. I'd like to thank also Prof. Nunziatina De Tommasi who was for me a reference, Dr. Fabrizio Dal Piaz who believed in me since I was an undergraduate student and all the people of De Tommasi team of Dipartimento di Farmacia, Università di Salerno, with whom I spent much pleasant time

During these years I met so interesting people and I'd like to thank each of them, particularly all the students of my lab, some of which help me for this thesis work, the PhD students and undergraduate students with whom I shared pleasantly my lunch time. I'd like to thank especially Lorenzo, who is a good and funny friend and made me laugh a lot, Fulvia that I miss and I hope to see again, Silvia, Martina, Ileana.

A special thanks goes also to Mariela and Sara with whom it started a good friendship and I shared many fun evenings.

I'd like to thank also all the friends met in Pisa, especially Fabio who thanks to me is now an expert in the research for flats and Tito.

For my PhD I was so long divided between Salerno and Pisa but I met other reality and I saw interesting place, like the amazing Jordan. I learnt also a lot of new things, I changed companies and flats, but I learnt to change my lifestyle without changing the most important feelings. That's way I'd like to thank the following people.

I'd like to thank my old friends Rossella, Emilio, Fabio, Elia and Luana that I tried to see as much possible during these years.

It was also very important the support of the family and so a special thanks goes to Paola, Enrico, Nadia, Carmela, Maria, and Peppe's family.

I'd like to thank my parent that supported and stood me with their force and guidance in all the situations.

The most special thank goes finally to Peppe which supported me, understood me and approved my choices anyway. Despite the distance he was always close to me and despite the changes he never changed his mind.